THE UNIVERSITY
of EDINBURGH

A synthetic biology approach to monitoring transient interactions between cancer and immune cells

THE UNIVERSITY *of* EDINBURGH

Sofija Semeniuk

Thesis presented for the degree of

Doctor of Philosophy

Institute of Quantitative Biology, Biochemistry and Biotechnology

The University of Edinburgh

September 2022

Declaration

I declare that this thesis has been composed solely by myself and that it has not been submitted, either in whole or in part, in any previous application for a degree. Except where otherwise acknowledged, the work presented is entirely my own.

Sofija Semeniuk

30th September 2022

Abstract

Immune cells play an important role in tumour growth and progression, as well as establishment at metastatic sites. Although inherently, immune system is designed to locate, target and eliminate malignant cells, evolutionary processes within a host allow tumourigenic cells to develop mechanisms and pathways to avoid immune recognition. There is a substantial amount of knowledge on how particular immune cell subtypes contribute to cancer growth and progression. Specifically, macrophages play an important role in mitigating immune response and induction of anti-inflammatory response. Due to this reason, macrophages can become potential new therapeutic targets. However, the knowledge of underlying mechanisms is limited due to the absence of robust tools for studying transient cell-cell interactions between cancer cells and macrophages at tumour microenvironment. Recent advances in synthetic biology have introduced a vast array of tools, particularly synthetic receptors, which have reported a broad range of applications in biosensing. One of such tools is synNotch receptor, which is derived from the core of the Notch receptor and is activated by cell-cell contact. Both extracellular and intracellular domains of synNotch can be substituted with custom sensing and signal transduction domains to carry out custom input/output circuits. In this thesis, the aim is to repurpose synNotch to detect interactions between cancer cells and macrophages in aims to develop a robust tool to aid in studying the mechanisms of metastasis development and bring insights into potential therapeutic targets.

Lay summary

Cell growth and division are continual processes happening in human bodies throughout the course of life. Occasionally, mistakes that occur during these processes lead to appearance of malignant cells, which bear the potential to become tumours. Generally, the immune system is well equipped to detect and eliminate cells that behave erroneously; however, sometimes malignant cells evolve mechanisms that allow them to escape elimination. Eventually, this leads to the multiplication of defective cells and establishment of tumours.

While the processes by which malignant cells escape the immune system have been studied for decades, there are still substantial gaps in our knowledge. It is known, however, that communication between cancer cells and immune cells plays a crucial role in this process. In particular, this communication happens either through indirect interaction between the cells (e.g., through signal molecules) or through direct contact between neighbouring cells via receptor-ligand pairs (features present of the surface of cells). Because direct interactions are generally short-lived, studying them presents challenges for scientists due to the absence of robust tools, allowing to study communication between neighbouring cells in living organisms.

Therefore, this work was focused on developing a novel tool, which can potentially aid in studying short-lived interactions between cancer cells and immune cells. In particular, the work describes the development of a novel cellular receptor – an artificial molecular biosensor – which can detect and report interaction events between cells in close proximity. This receptor is intended to be used in mouse cancer models, and will hopefully provide useful insights into how intercellular communication between cancer cells and immune cells influences the establishment of tumours, their growth and progression to metastases.

Acknowledgements

First of all, I would like to thank my supervisor, Dr. Elise Cachat for providing me with the opportunity to undertake research in her lab. Your guidance, support, optimism and belief in me helped me to persevere despite the moments of desperation. Thank you for putting your trust in me, humouring me in my ideas and always being supportive in my endeavours in academia and beyond.

I would like to extend this gratitude to the rest of the Cachat lab and its previous members. Ugne, Weijia, Alex, Ish, Aleks, thank you for the good laughs and maintaining the collaborative spirit in the lab.

I would also like to express my gratitude to my thesis committee, in particular Dr. Binzhi Qian, Dr. Sara Buonomo and Dr. Andrew Free for valuable guidance and support throughout my project. Many thanks to Dr. Martin Waterfall for the help with flow cytometry and FACS, and Dr. David Kelly for the help at the COIL facilities.

This work would not have been possible without the help of my colleagues. In particular, many thanks to Vivek Senthivel and Dirk Jan Kleinjan for many hours of fruitful discussions and always being able to help with their knowledge or resources. Special thanks to Maryia Trubitsyna, Adam Mol and Mai-Britt Jensen for good humour and making my PhD experience a lot more enjoyable. I am very grateful to the whole of the Susan Rosser lab for helping me getting started and for continued support and company throughout the years.

None of this work would have been possible without my friends who have continuously supported me and shared both my success and frustration. First of all, Migle and Ieva Radvile, you have been instrumental in keeping my mental health in check by always finding the right words to say when I needed them. Ievaini, thank you for always keeping me down-to-earth and lifting my spirits at the same time. Many thanks to Lukas for sharing the journey and for the support.

During the course of my PhD I have developed new hobbies which allowed me to meet and make friends with incredible people. Ugne, Mantai, Ana, Vaidai, Ivo, Simo, Ieva, Sergio, Dima, Tadai – you have made it so much easier to

maintain a more or less healthy work-life balance, be it going to the pubs, spending evenings in the climbing gym or spending summer days at the local crags or camping. Ugne, thank you for always being there for me, for introducing me to a wonderful world of rock climbing and sharing lots of good memories. Ivo, thank you for encouraging me to pick up the bass, something that I always wanted to do but never had the courage to start.

Lastly, I would like to express special gratitude to my family: my parents, Irina and Michail, for continued support, my brother Konstantin for being a role model and my cousin Jevgenijus for good humour, therapeutic talks, entertainment and lasting encouragement.

Contents

DECLARATION **2**

ABSTRACT **3**

LAY SUMMARY **4**

ACKNOWLEDGEMENTS **5**

LIST OF TABLES **12**

LIST OF FIGURES **13**

ABBREVIATIONS **15**

CHAPTER 1 ..... **17**

INTRODUCTION **17**

Introduction **18**

1.1 Cancer and metastases **18**
1.1.1 Early cancer detection and treatment methods 19
1.1.2 Metastatic cascade 21
1.1.3 The role of immune cells in cancer progression and metastasis formation 23
1.1.4 The role of macrophages in tumour progression and metastasis formation 23

1.2 Challenges in studying transient cell-cell interactions **28**

1.3 Synthetic receptors **30**
1.3.1 Rewiring endogenous actuator systems 31
1.3.2 The use of orthogonal transcription factors in synthetic sensing systems 32
1.3.3 synNotch as an orthogonal and modular synthetic receptor system 33
1.3.4 Applications of synNotch in cancer research 37

Aims **39**

CHAPTER 2 ..... **41**

MATERIALS AND METHODS **41**

2.1 Materials **42**
2.1.1 Molecular biology materials 42
2.1.1.1 Antibiotics 42
2.1.1.2 Reagents and solutions 42
2.1.1.3 Buffers 43
2.1.1.4 Bacterial culture media 43
2.1.1.5 Molecular biology kits and enzymes 43
2.1.2 Cell culture materials 44
2.1.3 Other materials 45
2.1.3.1 Immunostaining reagents 45
2.1.4 List of key constructs 46
2.1.5 List of key primers 49

2.2 METHODS **51**
2.2.1 Bacterial cell culture methods 51
2.2.1.1 Preparation of competent cells 51
2.2.1.2 Transformation of chemically competent cells 51
2.2.2.2 DNA assembly methods 52

2.2.3 Cell culture **54**
2.2.4 Quantitative and qualitative procedures 57

CHAPTER 3 ..... **62**

INITIAL SYNNOTCH SYSTEM IMPLEMENTATION *IN VITRO* **62**

Outline **63**

3.1 Introduction **64**
3.1.1 Applications of synNotch systems in various mammalian cell chassis…. 64
3.1.2 The design of synNotch receptor-reporter system 65
3.1.3 Methods for assessing synNotch activity *in vitro* 69

3.2 Results **70**
3.2.1 αCD19-synNotch receptor-reporter system exhibits high background activation in HEK293 70
3.2.2 SynNotch is correctly targeted at cell plasma membrane in HEK293 and L929 cells 76
3.2.3 synNotch activity in mouse fibroblasts is ligand-independent 78
3.2.4 Clonal MetBo2 synNotch cell line exhibits efficient receptor activation with human $CD19^{+}$ cells 83

3.3 Discussion **85**

3.3.1 The importance of the cell chassis on receptor-reporter system function. ... 86
3.3.2 Speculations regarding the requirement for ligand overexpression for synNotch activation ... 88
3.3.3 Effective signalling of synNotch is restricted to isolating a clone with desired efficiency ... 88

3.4 Conclusions ... 89

CHAPTER 4 ... 90

DEVELOPMENT OF STABLE METBO2 SYNNOTCH CELL LINES ... 90

Outline ... 91

4.1 Introduction ... 92
4.1.1 Methods for genomic integration of synthetic constructs ... 92
4.1.1.1 Targeted genomic integration ... 92
4.1.1.2 Non-targeted genomic integration ... 93
4.1.2 Considerations for incorporating synNotch system into genomic DNA…. ... 94
4.1.2.1 ROSA26 safe harbour for reporter cassette integration ... 94
4.1.2.2 PiggyBac system for receptor cassette integration ... 96

4.2 Results ... 97
4.2.1 Development of a MetBo2^{RMCE} cell line ... 97
4.2.2 Development of synNotch clonal cell lines ... 102

4.3 Discussion ... 103
4.3.1 Off-target integrations of reporter cassette ... 104
4.3.2 The problem of non-functional αF4/80-synNotch ... 105

4.4 Conclusions ... 106

CHAPTER 5 ... 107

ASSESSING ACTIVITY OF CLONAL SYNNOTCH CELL LINES ... 107

Outline ... 108

5.1 Introduction ... 109
5.1.1 Considerations for the sender cells in further synNotch experiments ... 109
5.1.2 Important notes on methodology for assessing receptor activity *in vitro*… ... 110

5.2 Results ... 112

5.2.1 Development of recombinant sender cells 112
5.2.2 Evaluation of αCD19-synNotch and αCD206-synNotch receptor activity… 116
5.2.3 Both αCD19-synNotch and αCD206-synNotch exhibit unspecific activity… 118
5.2.4 synNotch ECDs demonstrate high levels of non-specific binding to multiple immune cell subsets 119

5.3 Discussion 123
5.3.1 synNotch receptor activity is non-reproducible and unspecific 124
5.3.2 The challenges of applying synNotch receptors for cell-cell contact monitoring *in vivo* 126

5.4 Conclusions 127

CHAPTER 6 129

SYNFP: SYNNOTCH RECEPTORS BASED ON DIMERISATION-DEPENDENT FLUORESCENT PROTEINS 129

Outline 130

6.1 Introduction 131
6.1.1 The utility of fluorescent proteins in biological research 131
6.1.2 Dimerisation-dependent fluorescent proteins 131
6.1.3 Incorporation of ddFPs in the synNotch system 134
6.1.4 Design considerations for synFP platform 134

6.2 Results 136
6.2.1 MetBo2-RANLS cells exhibit low fluorescence when transfected with B-NLS 136
6.2.2 Assessing αCD19-synFP activity *in vitro* 138

6.3 Discussion 139
6.3.1 Low efficiency of MetBo2-RANLS may be due to low RA-NLS expression 139
6.3.2 αCD19-synFP exhibits low activation in response to $CD19^{+}$ cells 140

6.4 Conclusions 140

CHAPTER 7 141

FINAL DISCUSSION 141

7.1 Overview of the project 142

7.2 System design and potential further improvements 143

7.2.1 Reducing synNotch background activation levels 144
7.2.2 Irreproducible receptor activation presents challenges for standardised receptor characterisation 146
7.2.3 synFP requires further improvements in the system design 146
7.2.4 Permanent recording of cell-cell contacts 147

7.3 Future application prospects for the developed synNotch system *in vivo* 148

7.4 Conclusions 150

REFERENCES 151

List of Tables

Table 1.1. Distinct functional subpopulations of TAMs.....26
Table 2.1. List of key constructs. 46
Table 2.2. List of the key primers used in this work. 49
Table 2.3. List of cell lines used in this thesis.....55
Table 3.1. List of constructs used in synNotch receptor system described in the chapter 3. 68
Table 3.2. The summary of all the receiver and sender cells used in chapter 3.....86
Table 5.1. The summary of the receiver and sender cells used in the chapter 4.....123

List of Figures

Figure 1.1. Cancer survivability rate by disease severity in the US (2016). . 21
Figure 1.2 Metastatic cascade. 22
Figure 1.3. Most common methods for studying cell-cell interactions. 29
Figure 1.4. Current scaffolds of existing synthetic receptors. 31
Figure 1.5. Canonical pathway of endogenous Notch signalling. 34
Figure 1.6. The architecture of synNotch receptors. 36
Figure 1.7. A schematic diagram of the project. 40
Figure 3.1. Synthetic Notch receptor system and published variants. 67
Figure 3.2. Validation of HEK293^{CD19} sender cells. 73
Figure 3.3. synNotch activity in HEK293 cells. 75
Figure 3.4. synNotch localisation validation. 77
Figure 3.5. Isolation of L929-UAS clone. 80
Figure 3.6. Assessing activity of synNotch in L929-UAS cells. 82
Figure 3.7. Activation of clonal MetBo2 αCD19-synNotch cells. 85
Figure 4.1. ROSA26 integration via homology-directed repair mechanism. . 95
Figure 4.2. The design of the constructs used in the generation of MetBo2-UAS cell line. 96
Figure 4.3. Development of MetBo2^{RMCE} cell line. 98
Figure 4.4. Development of MetBo2-UAS cell line. 100
Figure 4.5. Development of clonal synNotch cell lines. 103
Figure 5.1. Notes on experimental workflow. 111
Figure 5.2. Development of vectors for recombinant expression of F4/80 and CD206 on sender cells. 113
Figure 5.3. Validation of ligand expression on transiently-transfected sender cells. 115
Figure 5.4. Evaluation of synNotch receptor activity. 117
Figure 5.5. Evaluation of synNotch cross-reactivity with other ligands. 118
Figure 5.6. The experimental workflow of testing small antibody domains used as synNotch extracellular domains (ECDs) against diverse immune cell populations. 120

Figure 5.7. Investigating the binding of synNotch ECDs to various immune cell populations in mouse spleen extract. 122
Figure 6.1. Dimerisation-dependent fluorescent proteins. 132
Figure 6.2. Schematic representation of construct design for synFP system. 135
Figure 6.3. Development of MetBo2-RANLS cell line. 137
Figure 6.4. Evaluation of αCD19-synFP activity. 138
Figure 7.1. Schematic representation of esNotch[82]. 145
Figure 7.2. Potential incorsporation of Cre-loxP system in the synthetic Notch system. 148

Abbreviations

ADCs	Antibody-drug conjugates
CAR	Chimeric antigen receptor
CCL2	C-C motif chemokine ligand 2
CMV	Cytomegalovirus
CSF-1	Colony stimulating factor 1
CTC	Circulating tumour cell
ctDNA	Circulating tumour DNA
ECD	Extracellular domain
EpoR	Erythropoietin receptor
GEMS	Generalized extracellular molecule sensor
GPCR	G-protein coupled receptor
HA	Homology arm
ICD	Intracellular domain
IFN-TAM	Interferon-primed tumour-associated macrophages
ITR	Inverted terminal repeat
LCL	Lymphoblastoid cell line
MDCK	Madin-Darby canine kidney
MFI	Mean fluorescence intensity
MIP	Macrophage inflammatory protein
MMP	Matrix metalloprotease
minCMV	Minimal CMV promoter
MRC1	Macrophage mannose receptor
OD	Optical density
PGK	Phosphoglycerate kinase
RMCE	Recombinase-mediated cassette exchange
ROS	Reactive oxygen species
RTK	Receptor tyrosine kinase
RTM-like TAM	Resident tissue macrophage-like tumour-associated macrophages
SLB	Supported lipid bilayer

SRI	Super-resolution imaging
TA	Transcriptional activator
TAM	Tumour-associated macrophages
TCR	T-cell receptor
TME	Tumour microenvironment
VEGF	Vascular endothelial growth factor

Chapter 1

Introduction

Introduction

Cancer has been prevalent among humans and animals for thousands of years and was first mentioned in recorded history as early as 3000 BC[1]. Despite that, the advances in knowledge about cancer that led to improved diagnostics and treatment have been mostly made throughout the past few decades. This underlines the complexity of the disease as well as dependence of cancer research on the development of other research fields, such as immunology, pharmacology, foundational cell biology as well as medical imaging.

The introduction part of this thesis is aimed at highlighting the challenges in studying particular aspects of cancer development, in particular the involvement and the effect of host's immune cells on tumour establishment and metastasis formation. In the first part of the introduction to this thesis, the severity of oncological disease and its early detection and treatment methods will be discussed. Further, the importance of host's immune system on cancer growth and progression, as well as related research methods will be investigated. Lastly, but equally importantly, it will be demonstrated how modern synthetic biology can aid in studying the nature and effect of tumour-immune cell interactions.

1.1 Cancer and metastases

According to World Health Organisation statistics, cancer accounts for approximately one in six deaths globally[2]. Despite the 31% decline in global cancer rates throughout the past 30 years due to established preventative measures and early diagnostic techniques, it still remains a leading death cause worldwide[2,3]. In 2020, there were nearly 10 million deaths documented, primarily from lung, colon, liver, stomach and breast cancers[2]. Altogether, while this is a devastating human cost as well as a huge burden on worldwide economy, it is estimated that 30% to 50% of cancers could be prevented through correct preventative measures and timely diagnosis[2,4].

1.1.1 Early cancer detection and treatment methods

Unfortunately, even with rapidly improving quality of cancer diagnostic tests, early diagnosis still presents significant challenges. Current early cancer detection methods mostly include detecting traces of malignant cells in patient's blood. These include circulating tumour cells (CTCs), circulating tumour DNA (ctDNA) and specific cancer cell biomarkers[5]. However, these tests are not cancer-site specific and thus require further analysis to identify the locations and severity of the tumour. Additionally, most of the blood-based tests target ctDNA, which is a marker of cell apoptosis, and makes the tests subject to false negatives since inhibition of apoptosis is a common attribute of cancerous cells.

Another problem of early cancer detection lies within the limitations in the current knowledge of early tumour growth and progression dynamics. The efficacy of regular screening programmes is often biased as earlier detection does not necessarily increase patient's life expectancy, but rather increases the lead-time of diagnosis[5]. Additionally, early screenings are targeted at slowly-growing tumours and are limited by the variability of individual cancer growth rate. Tumours can metastasise as soon as they establish their own blood supply, which is already possible at the 1 mm in diameter size[5]. Regardless, at that stage metastases will remain largely undetected, which would likely result in inappropriate treatment allocation. In case of fast-growing tumours, screening intervals might simply be too long to be able to detect relatively small malignancies, which can progress to clinically detectable and potentially metastasis-competent tumours within one to two years[5]. Reducing screening intervals is usually a non-viable option, therefore, development of new robust techniques for early cancer detection is in demand[5].

Additionally, cancer screening programmes can cause undesirable consequences, associated with testing errors[4]. For example, false positives lead to extensive additional testing and often invasive procedures, which results in detrimental effects on patient's mental health. Additionally, screenings may sometimes lead to overdiagnosis of tumours that are non-malignant and do not require further treatment. Lastly, there are socio-economic barriers that decrease the effect of cancer screenings and early diagnosis, such as poor public health

awareness, social stigmas, logistical barriers and poor healthcare organisation systems[4].

In most cases, what makes cancer so deadly are metastases – secondary tumours that arise in distant organs (Fig. 1.1)[2]. For example, while non-metastatic breast and prostate cancers typically have very good survival rates, development of metastases can reduce it by roughly 75%. In recent decades there have been substantial improvements in cancer treatment strategies, which helped to some extent decrease the metastasis-associated mortality by either detecting cancer early enough, or developing anti-cancer treatments that successfully reduce proliferation of metastatic cancer cells[6]. This includes adjuvant therapies (i.e., prolonged anti-cancer treatment) that help to eliminate residual tumour cells; however, these have been associated with increased cytotoxicity against non-malignant cells and only effective in limited patient subgroups[7]. Another treatment strategy involves administration of antibody-drug conjugates (ADCs). Although ADCs allow for the targeted delivery of anti-cancer drugs, their efficacy has been proven only in a small subset if cancer types[7]. Recent advances in fundamental knowledge of cancer development shed light on the matrix metalloproteases (MMPs), which are involved in extracellular matrix degradation and hence increase cell detachment and motility[8]. Upregulation of MMPs was observed in many cancer types; therefore, there have been attempts to therapeutically inhibit MMPs. However, all of those resulted in failure due to non-specific nature of pro-metastatic cell shedding[7,8]. Metastases are also prone to developing therapeutic resistance which significantly reduces efficiency of any treatment option[7].

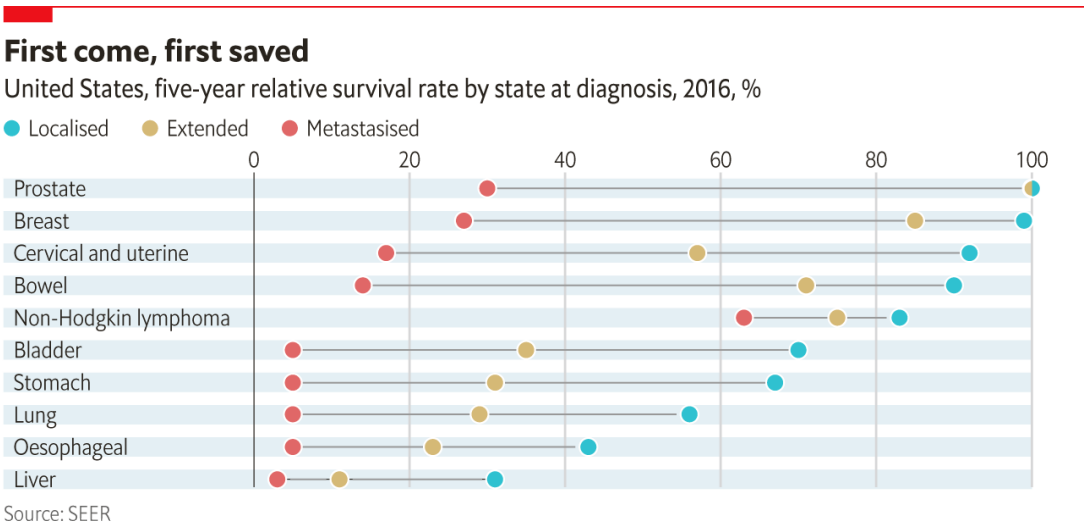

Figure 1.1. Cancer survivability rate by disease severity in the US (2016). *Metastases significantly reduce survival rates of various cancer patients. Taken from The Economist: Technology Quarterly*[9].

1.1.2 Metastatic cascade

Metastases are secondary tumours that appear in distant organs through a process called metastatic cascade. Throughout the growth of a primary tumour, cancer cells can detach, intravasate and extravasate at a site that is later defined as a metastatic niche (Fig. 1.2)[10]. At a primary tumour site, malignant cells are surrounded by a thick layer of interacting cells and extracellular matrix (ECM), such as fibroblasts and immune cells, which limit the influx of oxygen and nutrients to cancer cells. Consequently, cancer cells develop metabolic changes that help them to survive and proliferate, leading to immune escape, intravasation and, in a vast majority of cases, progression to metastases. [11,12]

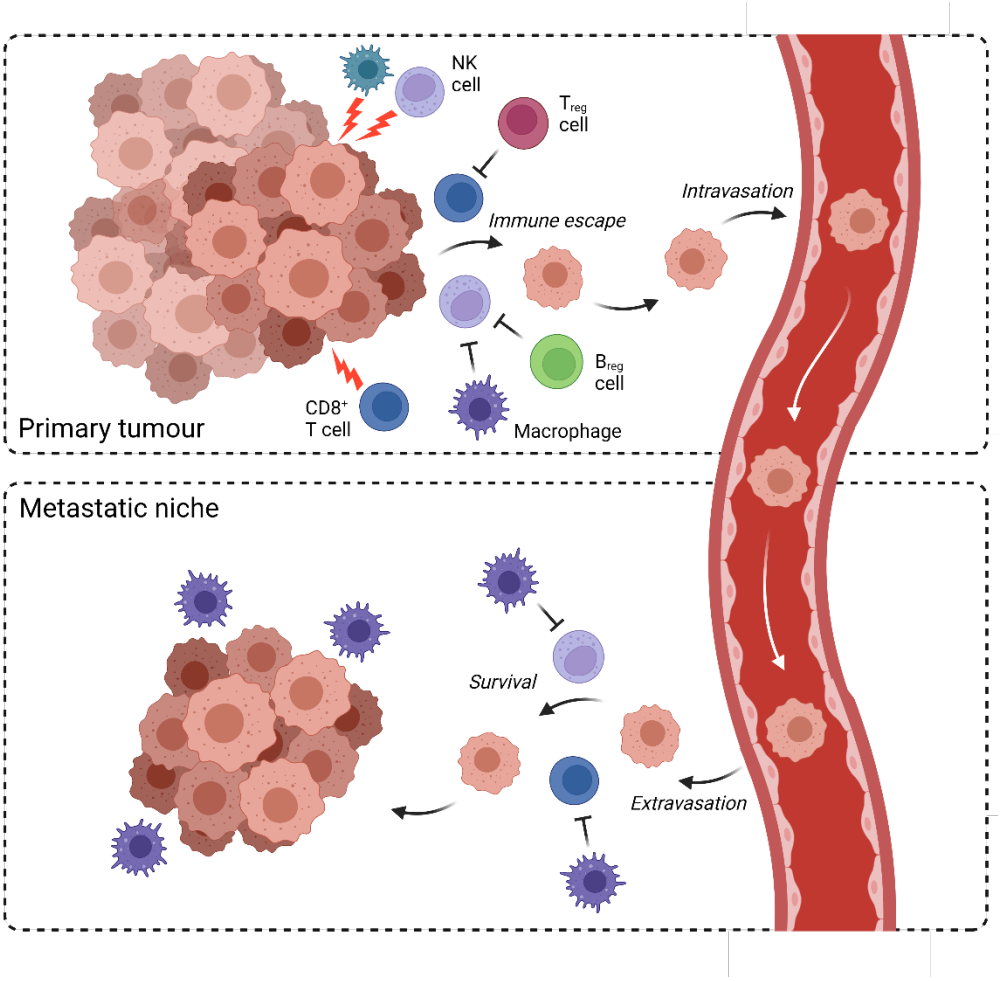

Figure 1.2. Metastatic cascade. *Cancer cells at the primary tumour site are surrounded by multiple populations of immune cells, both pro-inflammatory (e.g., NK cells, CD8+ T cells, specific macrophage subsets, etc.) and pro-tumorigenic (regulatory Treg and Breg cells, certain macrophage subsets, etc.). Eventually, successful tumour cells escape immune targeting, detach from primary tumours and intravasate. Intravasation allows metastasis-competent cells travel to distant organs, extravasate and establish secondary tumours at the pre-metastatic niche. Immune cells play an important role throughout the whole process of metastasis development.*

1.1.3 The role of immune cells in cancer progression and metastasis formation

The idea that immune cells can have a stimulating effect on tumour growth and development was first introduced in 1972[13]. This hypothesis was first based on the similarity between a tumour and a foetus, both being somewhat genetically foreign to the host body. At that time, it was known that foetal development and survival relies strongly on the foetus's ability to adapt to the maternal immune system; therefore, it was also speculated that similar processes might apply to tumour growth and progression[13,14].

It is also important to note that the general consensus is that cancer stems from chronic inflammation, which is caused by a plethora of external and internal factors[15,16]. Consequently, chronic inflammation creates an intricate localised immune cell ecosystem, enriched with pro-inflammatory chemokines and cytokines, growth factors and reactive oxygen species (ROS). Often referred to as chronic smouldering inflammation, this eventually leads to the establishment of a highly mutagenic environment and subsequent cancer initiation. Anti-inflammatory $CD8^+$ T cells and natural killer (NK) cells, as well as immunoregulatory T_{reg}, B_{reg}, T_H17 and myeloid cells are the densest immune cell populations that can be found at the primary tumour initiation site[10]. $CD8^+$ T cells and NK cells identify, supress and destroy tumour cells; however, their activity is downregulated by antagonistic immunoregulatory cells[10]. For example, T_{reg} cells are recruited to primary tumours through specific tumour-derived cytokines, where they decrease the anti-tumoral activity and increase apoptosis of $CD8^+$ T cells and NK cells[10].

1.1.4 The role of macrophages in tumour progression and metastasis formation

Myeloid cells, particularly macrophages, are known to be highly important in tumour development and progression. According to the original classification system, macrophages can be divided into two broad, functional subsets: M1 (anti-inflammatory, anti-tumorigenic) and M2 (pro-inflammatory, pro-

tumorigenic) macrophages[17,18]. The general concept is that in tumour microenvironment (TME), macrophages are polarized towards pro-tumorigenic M2 state, which makes them pivotal assets at every stage of the metastatic cascade[18]. The most prominent marker of M2 macrophage subset in humans is CD206, a macrophage mannose receptor (MRC1)[19]. Macrophage polarisation to anti-inflammatory M2 state is largely initiated through IL-4, IL-10 and IL-3 signalling from T_H2 cells[20].

Moreover, macrophages comprise distinct phenotypic subsets of tumour-associated macrophages (TAM), each being associated with a particular stage of tumour growth and progression: inflammation, immune regulation, tumour invasion, intravasation, angiogenesis or metastasis formation[16]. TAMs induce the formation of metastases through a number of processes: they supress immune responses by employing regulatory T_{reg} cells, which have a homeostatic effect and inhibit cytotoxic $CD8^+$ T cells[21] at the primary tumour site[22], and produce growth hormones and angiogenic factors[23] that induce tumour cell proliferation and propagation at distant organs. In particular, $CD4^+$ T cells were shown to be crucial for stimulation of various TAM phenotypes as they contribute to the invasive behaviour and metastatic potential of certain cancers[24].

A more recent review by Ma et al. suggested a far narrower classification of TAMs based on the data available from single-cell omics[25]. The proposed classification is largely based on the functional diversity of various macrophage subpopulations and can be identified by unique molecular markers (Table 1.1). Notably, these subsets are still mostly dominated by conventional M1 or M2-like characteristics, but they give a much deeper understanding of the metabolic profiles of TAMs and their effect on tumour growth and progression. For example, interferon-primed TAMs (IFN-TAMs) are marked by increased expression of IFN-regulated genes and exhibit a lot of M1 markers. However, unlike conventionally defined M1 macrophages, they are capable of inhibiting immune responses primarily through recruitment of T_{reg} cells. Additionally, three novel distinct subsets were identified: lipid-associated TAMs (LA-TAMs), resident tissue macrophage-like TAMs (RTM-TAMs) and proliferating TAMs (prolif-TAMs) which do not necessarily fall into traditional M1 or M2 categories but play important and distinct roles in TME.

Table 1.1. Distinct functional subpopulations of TAMs.

These populations can be defined by different functional and phenotypic markers, which makes them pivotal during specific stages of tumour progression and metastasis development. Interferon-primed TAMs (IFN-TAMs) exhibit M1 macrophage markers but act as immunosuppressive macrophages by recruiting T_{regs} to TME. Immune regulatory TAMs (Reg-TAMs) are marked by the expression of TREM2 receptor which is known to be important in modulating immunosuppressive functions of tumour-associated macrophages. Inflammatory cytokine-enriched TAMs (Inflam-TAMs) express inflammatory cytokines that regulate inflammatory immune response. Pro-angiogenic TAMs (Angio-TAMs), as the name suggests, are associated with expression of angiogenic factors and vascularisation. Lipid-associated TAMs (LA-TAMs) are thought to actively induce tumour progression as there is an association between pro-tumoral response and fatty acid accumulation in TAMs. Resident tissue macrophage-like TAMs (RTM-TAMs) and proliferating TAMs (Prolif-TAMs) require further investigation into their potential function in TME.

TAM subpopulation	Associated Biomarkers	Associated functions and properties
Inflam-TAMs	*CXCl1/2/3/5/8, CCL20, CCL3l1, IL1rn, IL1b, G0s2, Inhba, Spp1*	Production of inflammatory cytokines
IFN-TAMs	*CCL2/7/8, Cd274, CXCL9/10/11, Ifit1/2/3, Ifit3, Ifitm1/3, Il7r, Isg15, Nos2, Rsad2, Tnfsf10, Stat1*	Increased expression of IFN-regulated genes; Dominant in conventional M1 markers; Recruitment of T_{reg} cells
Reg-TAMs	*Apoe, Arg1, C1qa, CCL2, CD63, Clec4d, Cx3cr1, Gpnmb, Hilpda, Hmox1, Il7r, Mrc1, Pf4, Spp1, Trem2, Vegfa, Itga4;* Arg1^{+}, Cx3cr1^{+}, **CD206^{+}**, **F4/80^{hi}**, Gpnmb^{+}, Trem2^{+}	NK and CD8^{+} T cell suppression
Prolif-TAMs	*CDK1, Mki67, Stmn1, Top2a, Tubb*	Expression of proliferation markers and cell cycle genes
RTM-TAMs	Bin1, Cst7, CXCL13, Hexb, Nav3, P2ry12, Sall1, Siglech, Sparc, Krt79, Krt19, Car4	NK cell suppression
Angio-TAMs	*Arg1, Adam8, Bnip3, Mif, Slc2a1*	Expression of angiogenic factors, HIF signalling
LA-TAMs	*Acp5, Apoc1, Apoe, C1qa/B/C, CCL18, CCL8, CDD163,* ***CD206****, CD36, CD63, Ctsb/d/l, CXCL9, Fabp5, Folr2, Gpnmb, Lgals3, Macro,* ***Mrc1****, Trem2*	Fatty acid metabolism, phagocytosis, antigen processing and presentation

It is known that increased macrophage density is largely correlating with poor cancer prognosis in most cancers[16]. However, there are some exceptions, where increased macrophage density is, conversely, associated with higher survival rate[16]. This is particularly characteristic of leukaemia and liver cancers, where bone marrow macrophages or Kupffer cells, respectively, were shown to phagocytose malignant cells[16,26]. Nevertheless, it is speculated that transcriptomic profile of myeloid cells is just as an important marker of tumour malignancy level as is macrophage density. A recent study on a lung cancer model by Garrido-Martin et al. indicated that TAMs are enriched for both M1 and M2-like phenotypic macrophage populations, compared to non-TAMs[27]. However, although enrichment for M2 phenotype and associated expression of M2 signature genes involved in angiogenesis, metalloprotease activity and fibrosis were shown to be uniform among cancer patients, a much bigger variability of M1 phenotypes was observed. In particular, in patients with higher enrichment for M1 phenotypes, a better recruitment of $CD8^+$ T cells was observed, which led to a more efficient anti-tumour response and a two-fold increase in survival outcome at 10 years, compared to patients with M1-depleted phenotypes[27].

More broadly, the transcriptomic profile of a whole TME is also known to be an indicator of cancer prognosis. Since macrophages are recruited to TME by chemokines such as colony stimulating factor 1 (CSF-1), macrophage inflammatory proteins (MIPs), vascular endothelial growth factor (VEGF) and other interleukins and CC chemokine family proteins (e.g. CCL2)[28–30], overexpression of those markers, especially CSF-1 and CCL2, is strongly tied to poor prognosis for certain cancers. *In vivo* studies in mice revealed that ablation of CSF-1 factor reduced the rate of tumour progression and marginally decreased the formation of metastases[31]. Additionally, therapeutic targeting of CSF-1 was shown to have an inhibiting effect on tumour growth and metastasis formation[16,32,33].

1.2 Challenges in studying transient cell-cell interactions

As it was mentioned in the previous sections, intercellular interactions (both direct and indirect) play an important role in immune cell reprogramming and subsequent cancer growth and propagation. However, studying those interactions, in particular the direct cell-cell contacts presents certain challenges, mainly due to the transient nature of those interactions.

Cell-cell contact is an essential mechanism for many biological processes, including growth and development, signal transduction, immune modulation, metabolism, etc. However, the direct study of cell-cell interactions *in vivo* presents challenges often associated with spatiotemporal constrains. This has stimulated the development of diverse approaches to studying intercellular interactions, as well as led to the ability to exploit cell-cell contact mechanism in gene engineering and synthetic biology[34–36].

The most common methods for studying cell-cell interactions are based on fluorescent imaging. For example, one can use supported planar lipid bilayers (SLBs) (Fig. 1.3A)[37]. In SLBs, a lipid bilayer, which contains bioactive (and often fluorescently tagged) molecules, is attached to a coverslip. This allows tracking and visualizing of cell contact-induced molecular movement dynamics within the lipid bilayer. In addition, development of super-resolution imaging (SRI) techniques allowed to partially overcome spatiotemporal constrains by increasing the resolution of labelled biomolecules to a nanometre scale, as well as by providing a more targeted activation of quenched fluorescent biomolecules. Combined with chromobodies, developed to further increase the ability to tag confined epitopes, as well as protein complementarity methods (split fluorescent proteins, Halo Tag, etc.), SRI is a powerful method for detecting and tracking cell-cell interactions *in vitro*, but not in *in vivo* physiological settings due to low tissue penetrance by the wavelengths, which makes imaging challenging.

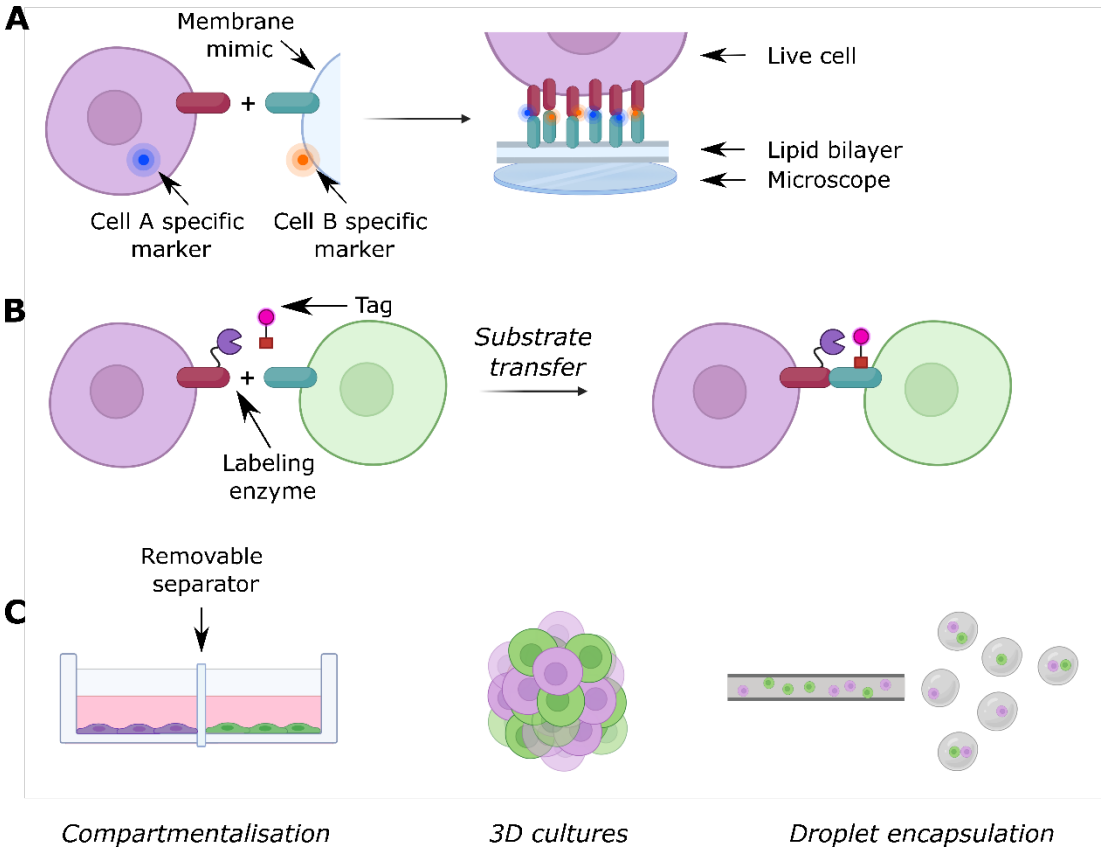

Figure 1.3. Most common methods for studying cell-cell interactions. *(A) Supported planar bilayers in cell-cell contact imaging. Contact visualisation is achieved when dynamic molecular movements are observed. (B) Chemical tagging methods for studying cell-cell contacts. A labelling enzyme transfers a tag (fluorescent tag, biotin, etc.) to a contacting cell. Tagged cells can be analysed by microscopy, Western blot, flow cytometry, etc. (C) Methods for studying cell contacts in vitro. Compartmentalisation allows controlled cell contact interface. 3D cultures and organs-on-chip provide near-natural environments for cell-cell interactions. Droplet encapsulation allows studying membrane fusion events.*

Chemical tagging of interacting protein partners is another approach to studying intercellular contacts[34]. This can be achieved through enzymatic labelling of interacting partners, where a labelling enzyme on one partner transfers the tag, usually biotin, to another partner when in close proximity (Fig. 1.3B). Biotinylated proteins are then visualised through gel imaging, microscopy, flow cytometry, etc.

Advances in bioengineering have expanded the toolkit for studying cell-cell contacts *in vitro* and *ex vivo* by providing novel engineered tools. Development of microengineered tools provided opportunities for tight control over the local

microenvironment. Such tools involve compartmentalisation devices, 3D cultures and droplet encapsulation (Fig. 1.3C). In particular, 3D cultures gained popularity due to their suitability to provide near-natural spatial cell organisation, which proved to be essential for viability of certain cells, in particular immune cells[38]. 3D cultures have also been evolved into the organs-on-chip technology, which allows to mimic mechanical forces and fluid shear stresses in microfluidics systems[39].

Although the list of methods for studying intercellular interactions seems to be quite extensive, there is still a limited number of methods that can be applied to *in vivo* settings. Current most common techniques include studying patient-derived tissues or tissues derived from animal models by immunohistochemistry or other means of histological analysis[40].

1.3 Synthetic receptors

In recent years, the emergence of synthetic biology provided receptor-based tools which allow us to study various fundamental biological processes, such as tissue development, morphological patterning[41], immune cell interactions, as well as contribute to applied biomedicine[42–44]. In particular, in the field of theranostics (diagnostics and therapeutics combined), synthetic receptors have been functionally exploited in order to meet the demand in cellular biosensors.

The scaffolds for synthetic receptors that will be described in this part of the thesis are summarised in figure 1.4. These receptors vary in their capacity to being reprogrammed, their ligand specificity and mode of action, as well as scaffold origin, as a lot of them are derived from existing cellular receptors. Additionally, receptors vary in their ability to detect either soluble or surface ligands. While a large fraction of existing receptors is targeted at soluble ligands, only few are capable of cell surface ligand recognition, which is a major caveat in receptor-based cell-cell contact studies.

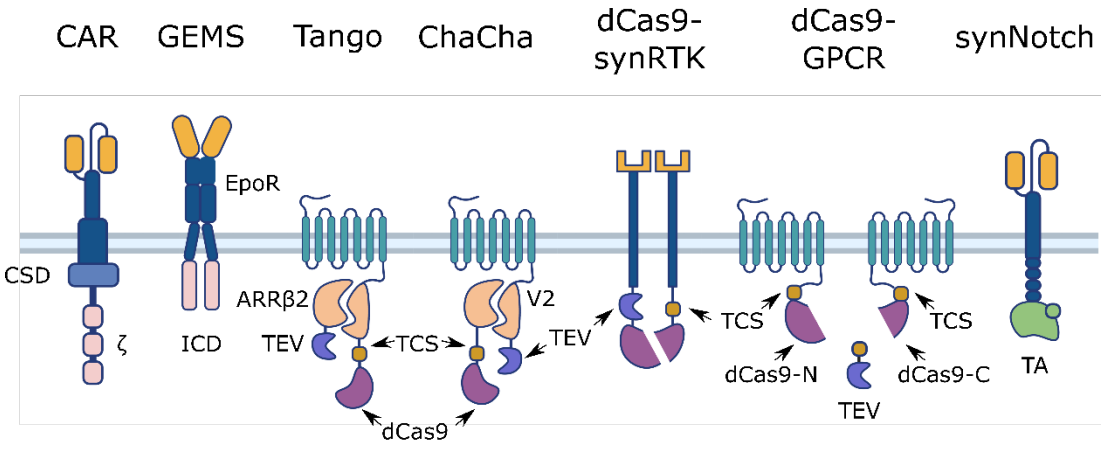

Figure 1.4. Current scaffolds of existing synthetic receptors. *Synthetic receptors differ in their capacity to modifications, nature of recognition target and signalling pathways they employ. CSD – Co-stimulatory domain; ICD – Intracellular domain; EpoR – erythropoietin receptor; ARRβ2 – β-Arrestin 2; TEV – TEV protease; TCS – TEV cleavage site; TA – Transcriptional activator.*

1.3.1 Rewiring endogenous actuator systems

Generally, early attempts at creating synthetic receptors were inspired by natural cell signalling systems, predominantly immune cell receptors and G-protein coupled receptors (GPCRs)[45]. Modifying the extracellular domains and rendering them specific to custom ligands allowed to repurpose natural signalling systems to produce a physiological response to novel environmental inputs. Chimeric Antigen Receptors (CARs) are one of the most prominent examples of such engineering[46–49]. While they have been modified to recognise CD19 on B cells, the downstream signal transduction is carried out through endogenous pathways, resulting in receptor activation and subsequent immune response. So far, CARs have been successfully applied in the treatment of B-cell acute lymphoblastic leukaemia, various subtypes of lymphoma and multiple myeloma in adults[50–55].

Generalized Extracellular Molecule Sensor (GEMS) is another example of how natural sensing systems can be repurposed to respond to custom cues[56]. GEMS are derived from erythropoietin receptor (EpoR) dimers, coupled with various

custom affinity domains. GEMS employ endogenous signal transduction pathways, such as JAK/STAT3, MAPK, NF-kB or NFAT, rewired to express a reporter gene from a responsive promoter.

However, it is important to note that harnessing endogenous response systems can potentially bring challenges in applying synthetic sensor systems *in vivo*. For example, off-target effects of immune cell-based systems can result in adverse immune reactions, such as cytokine storms from overactivated CARs.

1.3.2 The use of orthogonal transcription factors in synthetic sensing systems

Engineering synthetic transcription factors and downstream signalling components into natural receptor systems has been another approach aimed at generating synthetic sensing toolboxes[45]. Tango and ChaCha receptors are an example of how one can modify an existing system for tailored purposes[57,58]. Tango and ChaCha are derived from (GPCRs), natural receptors that employ downstream phosphorylation-mediated signalling cascade to induce a response. However, in the case of Tango and ChaCha the downstream signalling cascade has been rewired for phosphorylation to cause activation of orthogonal proteases, which release a transcription factor or a dCas9 which induce the expression of downstream genes.

Emergence of dCas9 caused significant advances in the development of synthetic receptor systems. Besides Tango and ChaCha, dCas9-synR receptors have been created[59]. These receptors employ either receptor tyrosine kinase (RTK) or GPCR receptor scaffolds for their core domains. dCas9-synRTK use receptor chain dimerisation in response to ligand binding and rely on TEV protease-mediated cleavage for the release of dCas9, while dCas9-GPCR relies on a phosphorylation-mediated actuator cascade.

1.3.3 synNotch as an orthogonal and modular synthetic receptor system

One of the synthetic receptors that uses completely synthetic input and output modules is the synthetic Notch (synNotch) receptor. Incidentally, synNotch is one of the few receptors able to detect membrane-tethered ligands[60].

synNotch originated from the Notch receptor, which participates in multiple developmental and homeostatic processes. It was shown that Notch has an evolutionarily conserved structure, which is divided in three main “modules”: (i) an extracellular domain (ECD; sensing domain), (ii) a transmembrane domain (membrane tether and signal transducer) and (iii) an intracellular domain (ICD; transcriptional activator)[61]. Signalling through Notch receptor is initiated by binding between the Notch ECD and its cognate ligands Jagged or Delta on a neighbouring cell, followed by mechanical pulling of Notch ECD via trans-endocytosis[62]. This exposes cleavage sites for ADAM family metalloproteases and the γ-secretase complex, which cleave the ICD, allowing its translocation into the nucleus and subsequent induction of target gene expression[63] (Fig. 1.5).

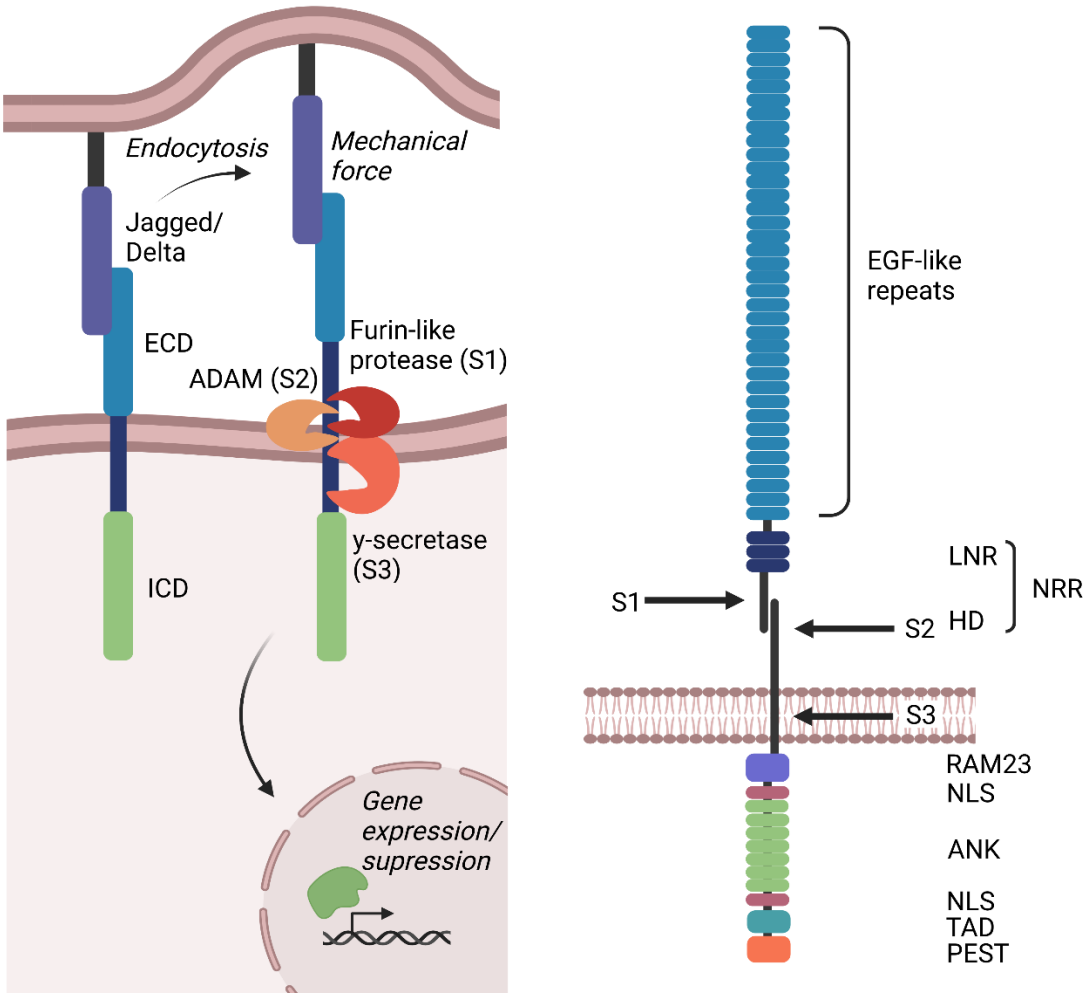

Figure 1.5. Canonical pathway of endogenous Notch signalling. *Following Notch extracellular domain (ECD) binding to its cognate ligands Jagged or Delta, the endocytosis by the ligand-presenting cell induces a mechanical pulling of the receptor. This exposes cleavage sites: S1 (for furin-like protease), S2 (for ADAM metalloprotease) and S3 (for γ-secretase complex). Cleaved intracellular domain (ICD) translocates to the nucleus and regulates expression of downstream genes. NRR – Notch regulatory region. LNR – cysteine-rich Lin12/Notch repeats. HD – heterodimerisation domain. RAM - recombination binding protein-Jκ-associated molecule. NLS – nuclear localisation sequence. ANK – ankyrin domain. TAD – transcriptional activation domain. PEST - proline (P), glutamic acid (E), serine (S), and threonine (T) sequence (proteolysis-associated).*

Previously, Notch ICD was successfully substituted with a custom orthogonal transcriptional activator, thus creating an efficient reporter system of Notch activity[64,65] (Fig. 1.6A). More recently, Morsut et al. showed that both ICD and ECD can be exchanged with a variety of orthogonal domains (Fig. 1.6B), which led to the development of synthetic Notch (synNotch) receptors[66.] Consequently, synNotch receptors were shown to have potential in therapeutics, diagnostics[42–44,60,67–72], tissue morphogenesis studies[41] and fundamental studies[73].

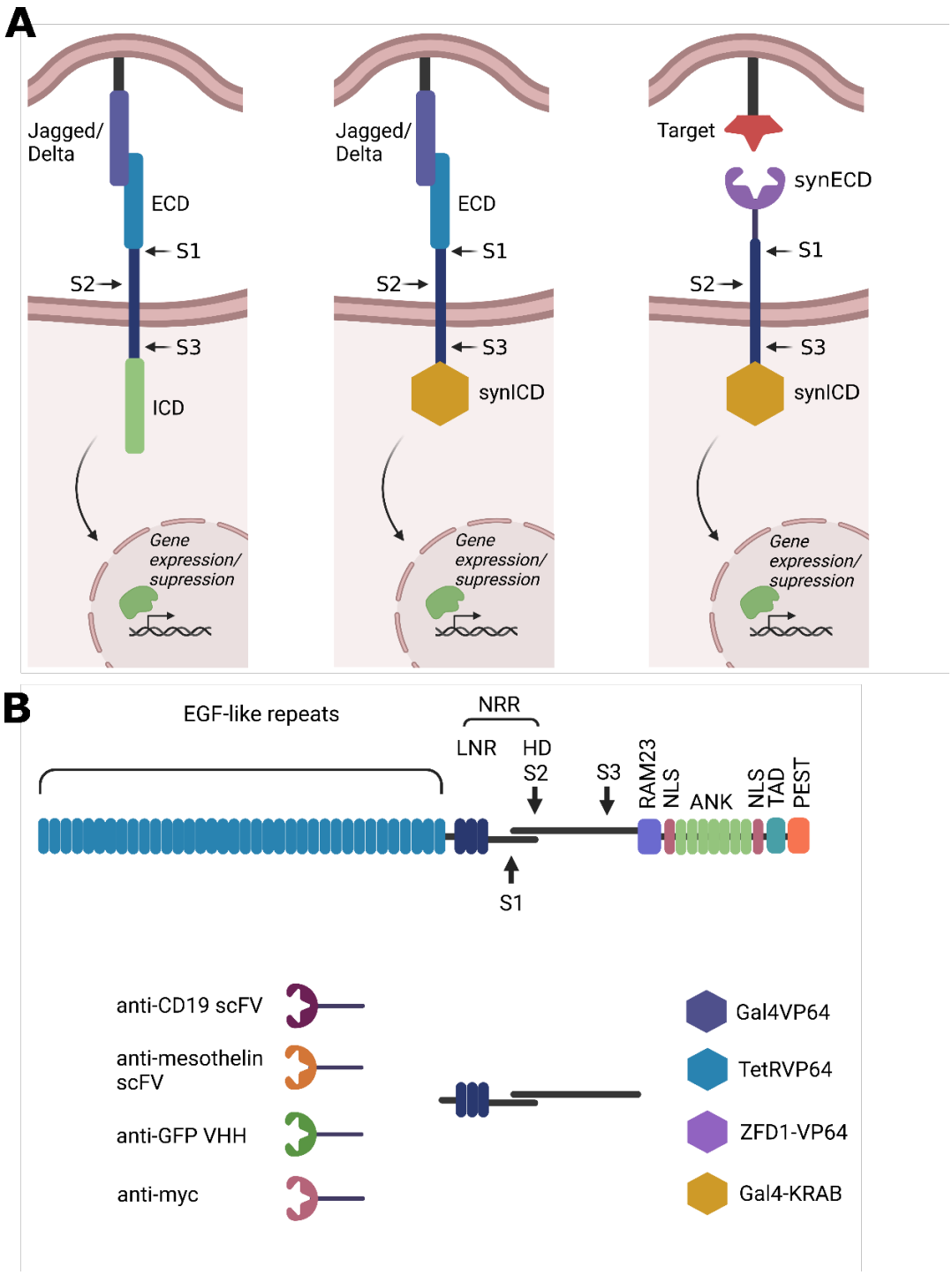

Figure 1.6. The architecture of synNotch receptors. *(A) Due to its modular structure, Notch receptor can be reengineered into various versions of synNotch receptors with orthogonal extracellular and intracellular domains. (B) Potential extracellular (ECD) and intracellular (ICD) domains for synNotch receptors. Figure from Morsut et al. 2016*[60].

1.3.4 Applications of synNotch in cancer research

Even the earliest applications of synNotch receptors centred around targeting tumours and eliminating malignant cells[42,43,66]. Similar to previous CAR-based attempts, these were T cells that were engineered with synNotch targeted against various cancer cell markers. The main advantage of using synNotch in favour to conventional CARs or T-cell receptors (TCRs) in T cells is the possibility to avoid T-cell specific endogenous immune response, which often results in cytokine storms and detrimental effects on host's body due to "on-target/off-tumour" effects, when a strong CAR receptor activation is achieved by epitopes present on non-malignant cells.

As a proof of concept, Roybal at al. demonstrated that T cells can be engineered with synNotch targeted against various markers, commonly overexpressed in tumours, and elicit a fluorescent response[42,43,60]. Among those markers were CD19, human epidermal growth factor receptor 2 (Her2) and mesothelin. SynNotch was shown to successfully recognise those antigens on both endogenous tumour cells and when expressed ectopically on orthogonal host cells, e.g., K562[42]. Moreover, synNotch efficiency has also been demonstrated in AND-gate circuits, where engineered Jurkat T cells were made to recognise CD19 and mesothelin double positive cells and produce inflammatory cytokines as a response[43]. What is more, in Jurkat T cells synNotch was used to induce expression of CAR upon target ligand recognition (e.g., CD19), which eventually resulted in a more specific CAR receptor activity and targeted tumour cell killing[43]. Incorporating CAR downstream from synNotch signalling also significantly reduced 'on-target/off-tumour' toxicity.

The approach of combining synNotch with CAR technology was further explored by several groups. For example, Hyrenius-Wittsten et al. exploited such circuit in mesothelioma (aggressive lung cancer) treatment. There, synNotch, specific to ALPPL2, a common tumour-specific marker, would drive the expression of a wide range of cancer-specific CAR receptors[72]. Similarly, Choe et al. demonstrated how, following synNotch activation with tumour-specific EGFRvIII antigen, tandem expression of CAR results in effective targeting of glioblastoma

tumour cells[71]. In another paper, researchers demonstrated effective tumour regression in hepatocellular carcinoma in response to anti-ROR1 CAR driven by synNotch activation[70].

In another approach to combining synNotch and CARs, researchers engineered NK cells with synNotch targeted against glypican-3 (GPC3), a hepatocellular carcinoma cell marker. Receptor activation would drive the expression of IL12, which, in turn, would activate nearby CAR-T cells. In this case, combination of synNotch and CAR T cells resulted in significantly higher but more spatially controlled production of inflammatory cytokines and subsequent tumour lysis[69].

SynNotch was also used on its own to target particular cancer cell biomarkers[44,66–68]. One of the examples of such application was demonstrated by Cho et al., who used synNotch to target Axl, a commonly overexpressed tyrosine kinase receptor in malignant cells, and induce production of IL10[44]. SynNotch was also used to target apelin (Apj), a tumour endothelium surface marker, in aims to be able to detect tumours that undergo vascularisation[44]. In another research, mesothelin-based synNotch was able to drive the expression of CXCL10, a pro-inflammatory anti-tumour cytokine and thus supress tumour growth in vivo[67].

Aims

The aim of this thesis is to develop a synNotch receptor system for monitoring transient interactions between cancer cells and immune cells.

A lot of research discussed in the previous sections was targeted at engineering immune cells for cancer cell targeting. In this project, on the contrary, the aim is to engineer cancer cells with macrophage-sensitive synNotch (Fig. 1.7). Two macrophage surface markers were chosen as targets: F4/80 and CD206. F4/80 is a widespread mouse macrophage marker, present on multiple macrophage subsets, while CD206 is unique to anti-inflammatory (M2) mouse macrophages, which are typically present in tumour microenvironment (TME).

Cancer cells will be engineered with macrophage-specific synNotch receptors and their ability to respond to stimulation with respective targets will be assessed *in vitro*.

Further applications *in vivo* would involve using engineered cancer cells to establish mouse cancer models and monitoring for fluorescent response as a read-out for macrophage contact. For this, intravital microscopy can be used. Intravital microscopy provides opportunity to image various cellular processes (e.g., migration, proliferation, intercellular signalling and behaviour, etc.) in live tissues and in real-time in live animals, removing the need to cull the animal in order to acquire organ or tissue of interest[74]. Despite it being an invasive method, it still allows to preserve the animal for continuous imaging over hours, days and weeks, which is an advantage for studying long-term dynamic processes, cancer development and progression being one of such.

Alternatively, tumours can be extracted and sorted into distinct populations of induced and non-induced cells. These populations can be subject to omics analysis in order to gain more insight into the outcomes of cell-cell interactions between tumour and immune cells.

The omics data derived from the *in vivo* research could provide useful insights into the changes that occur within cancer cells upon macrophage contact. For example, RNAseq data could reveal the changes of the transcriptomic profile of

affected cancer cells and highlight the genes or pathways that become up or downregulated. Further studies could be aimed at deciphering the impact of such gene expression changes on cancer cell survivability, isolating those that might be associated with the increased fitness of the malignant cells. Consequently, new potential cancer drug targets can be isolated.

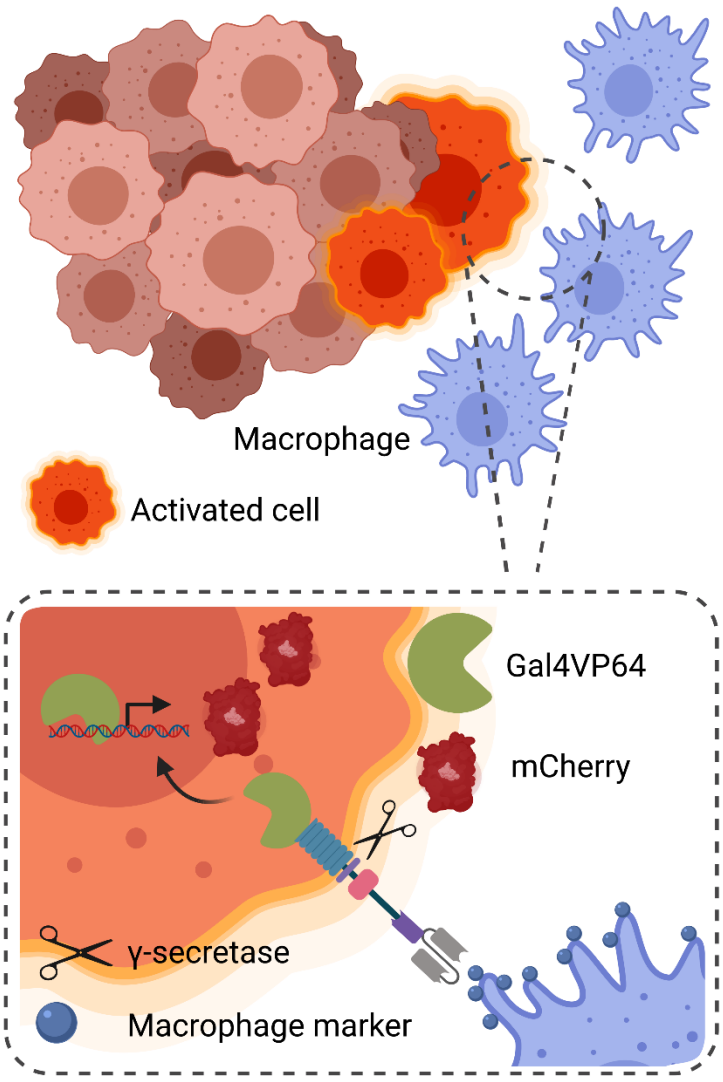

Figure 1.7. A schematic diagram of the project. *Cancer cells engineered with macrophage-specific synNotch detect macrophages within close proximity. Binding between macrophage surface marker (F4/80 or CD206 in this project) induces the cleavage of transmembrane domain by γ-secretase and, subsequently, releases a transcriptional activator, namely Gal4VP64. Gal4VP64 translocates to the nucleus and induces the expression of downstream mCherry reporter.*

Chapter 2

Materials and Methods

2.1 Materials

2.1.1 Molecular biology materials

2.1.1.1 Antibiotics

Ampicillin: 100 µg/ml working concentration.

Carbenicillin: 100 µg/ml working concentration.

Kanamycin: 50 µg/ml working concentration.

2.1.1.2 Reagents and solutions

Agarose (Ultra-Pure) (Invitrogen; Cat. No. 11553277).

Calcium chloride (NaCl) (Thermofisher scientific; Cat. No. 12685077).

Glycerol (Sigma Aldrich; Cat. No. G9012).

Manganese chloride (Sigma Aldrich; Cat. No. 1375127).

MOPS (Sigma Aldrich; Cat. No. M1254).

Potassium hydroxide (KOH) (Thermofisher scientific; Cat. No. 10575355).

Potassium acetate (CH_3COOK) (Sigma Aldrich; Cat. No. 236497).

Rubidium chloride (RbCl) (Sigma Aldrich; Cat. No. 215260).

Acetic acid (CH_3COOH) (Sigma Aldrich; Cat. No. A6283).

2.1.1.3 Buffers

PBS: 137 mM NaCl, 2.7 mM KCl, 8 mM Na_2HPO_4, 2 mM KH_2PO_4.

TAE 1X: 40 mM TRIS, 20 mM Acetate, 1 mM EDTA.

TBF1: 30 mM CH_3COOK, 100 mM RbCl, 10 mM $CaCl_2$, 50 mM $MnCl_2$, 15 % Glycerol. pH adjusted to 5.8 with CH_3COOH.

TBF2: 10 mM MOPS, 75 mM CaCl2, 10 mM RbCl, 15 % Glycerol. pH adjusted to 6.5 with KOH.

TE 1X: 10 mM Tris-Cl (pH 8.0), 1 mM EDTA.

2.1.1.4 Bacterial culture media

LB: 10 g/L Tryptone, 5 g/L Yeast Extract, 10 g/L NaCl.

LB agar: 10 g/L Tryptone, 5g/L Yeast Extract, 10 g/L NaCl, 20g/L agar.

2.1.1.5 Molecular biology kits and enzymes

Antarctic phosphatase (NEB; Cat. No. M0289).

E.Z.N.A.® Plasmid Mini Kit I (Qspin) (Omega Bio-Tek: Cat. No. D6942).

E.Z.N.A.® Total RNA Kit I (Omega Bio-Tek; Cat. No. R6834).

Gateway® BP Clonase™ II (Invitrogen; Cat. No. 11789020).

Gateway® LR Clonase™ II (Invitrogen; Cat. No. 11791020).

GoTaq® G2 DNA polymerase (Promega; Cat. No. M7841).

LunaScript® RT SuperMix Kit (NEB; Cat. No. E3010).

Monarch® DNA Gel Extraction Kit (NEB; Cat. No. T3010).

OneTaq® Quick-Load® 2X Master Mix with Standard Buffer (NEB; Cat. No. M0482).

Platinum™ Superfi II PCR Master Mix (Invitrogen; Cat. No. 12368010).

PureLink™ Genomic DNA Mini Kit (Invitrogen; Cat. No. K182002).

ReliaPrep™ DNA Clean-Up and Concentration System (Promega; Cat. No. A2893)

QIAquick PCR Purification Kit (Qiagen; Cat. No. 28104).

QIAquick Gel Extraction Kit (Qiagen; Cat. No. 28706).

Q5® DNA polymerase (NEB; Cat. No. M0491).

ReliaPrep™ DNA Clean-Up and Concentration System (Promega; Cat. No. A2893).

T4 DNA ligase (NEB; Cat. No. M0202).

T4 Polynucleotide Kinase (PNK) (NEB; Cat. No. M0201).

ZymoPURE™ II Plasmid Maxiprep Kit (Zymo Research; Cat. No. D4203).

2.1.2 Cell culture materials

Antibiotic-Antimycotic 100X (Thermofisher Scientific; Cat. No. 15240062).

Dimethyl Sulfoxide (DMSO) (Sigma Aldrich; Cat. No. 34869).

Dulbecco's Modified Eagle Medium (DMEM) (Thermofisher Scientific; Cat. No. 21969035)

Dulbecco's phosphate-buffered saline (DPBS) (Thermofisher Scientific; Cat. No. 14190144).

Fetal Bovine Serum (FBS) (Sigma Aldrich; Cat. No. F7524).

Geneticin™ (G418 Sulfate) 50 mg/ml (Thermofisher Scientific; Cat. No. 10131027).

GlutaMAX™ Supplement (Invitrogen; Cat. No. 35050061).

Iscove's Modified Dulbecco's Medium (IMDM) (Thermofisher Scientific; Cat. No. 12440053)

Lipofectamine™ 3000 (Invitrogen; Cat. No. L30000).

Penicillin/Streptomycin 100X: Gibco (cat. No. 15140)

Puromycin dihydrochloride 10 g/ml (Thermofisher Scientific; Cat. No. ant-pr-1)

Recombinant Murine Interleukin-4 (PeproTech; Cat. No. 214-14).

Recombinant Murine M-CSF: (PeproTech; Cat. No. 315-02).

RPMI 1640 Medium (Thermofisher Scientific; Cat. No. 11875093).

StemPro™ Accutase™ Cell Dissociation Reagent (Thermofisher Scientific; Cat. No. A1110501).

TrypLE™ Express (1X) (Thermofisher Scientific; Cat. No. 12604013).

X-VIVO™ 20 Serum-Free Hematopoietic Cell Medium (Lonza; Cat. No. BE04-448Q).

2.1.3 Other materials

2.1.3.1 Immunostaining reagents

Alexa Fluor® 700 anti-mouse F4/80 Antibody (Biolegend; Cat. No. 123129).

Bovine Serum Albumin (Sigma-Aldrich; Cat. No. A9418).

CD19 Rabbit Recombinant Monoclonal (Abcam; Cat. No. ab134114).

DAPI (Invitrogen; Cat. No. D1306).

Donkey Anti-Rabbit IgG (H+L) Highly Cross-Adsorbed Secondary AlexaFluor® 594 (Invitrogen; Cat. No. A-21207).

Epredia™ Polysine Adhesion Slides (Thermofisher scientific; Cat. No. 10219280).

Goat Anti-Rabbit IgG H&L AlexaFluor® 488 preabsorbed (Abcam; Cat. No. ab150081).

ImmEdge™ Hydrophobic Barrier Pen (Vector Laboratories; Cat. No. 101098-065).

Myc-Tag Mouse Monoclonal AlexaFluor® 647 Conjugate (Biolegend; Cat. No. 2233S).

Paraformaldehyde, 96 %: (Acros Organics; Cat. No. AC416780250).

PE anti-mouse CD206 (MMR) Antibody (Biolegend; Cat. No. 141705)

PE/Cyanine5 anti-mouse/human CD45R/B220 Antibody (Biolegend; Cat. No. 103209).

PE/Dazzle™ 594 anti-mouse CD3 Antibody (Biolegend; Cat. No. 100245).

PerCP/Cyanine5.5 anti-mouse/human CD11b Antibody (Biolegend; Cat. No. 101227).

ProLong™ Diamond Antifade Mountant (Invitrogen; Cat. No. P36965).

Triton X-100: (Alfa Aesar; Cat. No. A16046AP).

2.1.4 List of key constructs

Table 2.1. List of key constructs.

Code	Description	Construct	Notes
Addgene plasmid #79125	αCD19-synNotch	PGK→IgKleader→myc→aCD19→synNotch→Gal4VP64→WPRE	A gift from Wendell Lim[66].
Addgene plasmid #79130	UAS-BFP cassette used in early MetBo2 αCD19-synNotch clones.	5xGal4-UAS→minCMV→BFP→pA→PGK→mCherry→pA	A gift from Wendell Lim[66].
BNLS (Addgene plasmid #50836)	B-NLS monomer	CMV→B-3xNLS→pA	A gift from Robert Campbell[75].
KPL155	Φc31 recombinase	CMV→Φc31→pA	A gift from Sally Lowell lab[76].

pGB35	ROSA26 landing pad for creation of MetBo2^{RMCE}	ROSA HA 5'→Splice Acc→Kan/NeoR→pA←pA←3xNLS-mKate2←CAG←ROSA HA 3'	A gift from Sally Lowell lab[76].
pHWu1	αCD206-synNotch	PGK→IgKleader→6xHis→aCD206→synNotch→Gal4VP64→WPRE	
pHWu5	αF4/80-synNotch	PGK→IgKleader→myc→aF4/80→synNotch→Gal4VP64→WPRE	
pSSe3	CD19 ligand for engineering of MetBo2 CD19^{+} cells	CMV→IgKleader→HA→CD19→myc→PDGFRβ→pA	
pSSe13	F4/80 ligand for engineering of MetBo2 CD19^{+} cells	CMV→F4/80→pA	
pSSe14	CD206 ligand for engineering of MetBo2 CD19^{+} cells	CMV→CD206→myc→PDGFRβ→pA	
pSSe16	RA-NLS cassette for RMCE	attB53→Pac→pA→pA←RA-3xNLS←CMV←attB53	
pSSe22	αCD19-synNotch	PB 5'→PGK→IgKleader→myc→aCD19→synNotch→Gal4VP64→pA→PGK→H2B-TagBFP→pA→3' PB	PiggyBac backbone
pSSe23	αF4/80-synNotch	PB 5'→PGK→IgKleader→myc→aF4/80→synNotch→Gal4VP64→pA→PGK→H2B-TagBFP→pA→3' PB	

pSSe24	αCD206-synNotch	PB 5'→PGK→IgKleader→myc→aCD206→synNotch→Gal4VP64→pA→PGK→H2B-TagBFP→pA→3' PB	PiggyBac backbone
pSSe40	UAS-mCherry cassette for RMCE	attB53→Pac→pA→pA←mCherry←minCMV←5xGal4-UAS←attB53	
pSSe50	CD19 ligand used for engineering of HEK293^{CD19} cells	CMV→IgKleader→HA→CD19→myc→PDGFRβ→pA→PGK→emGFP-BlaR→pA	pcDNA6.2 backbone
pSSe56	B-NLS monomer with *VLLSRKR* residue at N terminal	CMV→VLLSRKR-B-3xNLS→pA	
pSSe59	ROSA26 gRNA and Cas9 vector	U6→gRNA→CMV→3xFLAG-Cas9-T2A-GFP→pA	
pWLi4	UAS-mCherry cassette used for transient expression of the synNotch system	5xGal4-UAS→minCMV→mCherry→pA→PGK→H2B-TagBFP→pA	
UBa1002	Anti-F4/80 scFV fused to sfGFP	EF1α→IgKleader→aF480-sfGFP→pA	Engineered by Ugne Baronaite (Cachat lab)
UBa1004	Anti-F4/80 scFV fused to mNeonGreen	EF1α→IgKleader→aF480-mNeonGreen→pA	Engineered by Ugne Baronaite (Cachat lab)

UBa0003	Anti-CD206 VHH fused to sfGFP	EF1α→IgKleader→aCD206-sfGFP→pA	Engineered by Ugne Baronaite (Cachat lab)
UBa1006	Anti-CD206 VHH fused to mNeonGreen	EF1α→IgKleader→aCD206-mNeonGreen→pA	Engineered by Ugne Baronaite (Cachat lab)
UBa0007	Anti-CD19 scFV fused to sfGFP	EF1α→IgKleader→6xHis-TCS→aCD19-sfGFP→pA	Engineered by Ugne Baronaite (Cachat lab)
UBa1007	Anti-CD19 scFV fused to mNeonGreen	EF1α→IgKleader→aCD19-mNeonGreen→TCS-6xHis→pA	Engineered by Ugne Baronaite (Cachat lab)

2.1.5 List of key primers

Table 2.2. List of of the key primers used in this work.

The list only includes the list of primers relevant to the results mentioned in the following chapters.

Primer name	Sequence	Notes
mROSAwt_F	GGCGGACTGGCGGGACTA	Wild-type ROSA26 locus fwd primer; Used for confirming integration with gRNA PCR;
BNLS/mCherry_R	CTTGGTCACYTTCAGCTTGG	Specific to B-NLS, RA-NLS and mCherry; Used as a reverse primer for confirming the integration of RA-NLS cassette with gDNA PCR;

Puro_R	CTTCCATCTGTTGCTGCG	Specific to puromycin resistance gene; Used as a reverse primer for confirming the integration of UAS-mCherry cassette with gDNA PCR;
mKate_R	TACGAAGACGGGGGCGTGC	mKate2 reverse primer; Used for confirming integration with gDNA PCR;
mActB_F	CTGTCCCTGTATGCCTCTG	Murine β-actin primers used as control during extraction of ligands from cDNA;
mActB_R	ATGTCACGCACGATTTTC	
ADGRE1_F	GGAGACCCAAGCTTGGTACCTGAATGACTGCCACAGTACG	F4/80 Gibson primers for extraction from cDNA
ADGRE1_RfuII	GGCTGATCTCGAGCGGCCGCTTAACCCATCTTGGAAGTGG	
MRC_F	CCGCCAGTGTGCTGGAATTCGGAAGATCCACTCTGGGCC	CD206 Gibson primers for extraction from cDNA.
MRC_R	ATGAGTTTTTGTTCGTCGACGCCATAGAAAGGAATCCACGC	
Gibson_hCD19_F	CCCAGCCGGCCAGATCTCCCGAGGAACCTCTAGTG	CD19 Gibson primers for extraction from cDNA.
Gibson_hCD19_R	GATGAGTTTTTGTTCGTCGACCTTCCAGCCACCAG	

2.2 Methods

2.2.1 Bacterial cell culture methods

2.2.1.1 Preparation of competent cells

Escherichia coli cells were streaked out on LB agar plate and grown overnight at 37° C. On the following day, single colonies were inoculated in 5 ml of liquid LB medium and grown overnight at 37° C in a 200 rpm shaking incubator. The overnight bacterial culture was inoculated at 1:400 dilution in pre-warmed LB media, supplemented with 20 mM $MgSO_4$, and grown in a 200 rpm shaking incubator at 37 °C until OD_{600} reaches ~0.48. Upon reaching the required OD, the bacterial culture was incubated on ice for 10 min and pelleted by centrifugation at 3752 x g for 5 min at 4 °C. The supernatant was discarded and the pellet was resuspended in 40 ml of cold TFB1 buffer per 100 ml cell culture. Following incubation on ice for 5 min, cells were centrifuged at 1351 x g for 10 min at 4 °C. The supernatant was discarded and the pellet was resuspended in 4 ml of cold TFB2 buffer per 100 ml cell culture. The cells were then aliquoted in pre-chilled Eppendorf tubes and stored at -80 °C after snap freezing on dry ice.

2.2.1.2 Transformation of chemically competent cells

An aliquot of competent cells was thawed on ice. DNA was added to the cells and the cell-DNA mix was incubated on ice for 5 min, following heatshock at 42 °C for 30 s. The tube was then left on ice for 2 min, SOC media was added and the cells were recovered for 1 h at 37 °C in a shaking incubator. Cells were plated on LB agar selection plates.

2.2.2 Molecular biology methods

2.2.2.1 Plasmid preparation

All miniprep DNA extractions were carried out using E.Z.N.A.® DNA plasmid miniprep kit (Omega Bio-tek; Cat. No. D6942) from 3-5 ml of bacterial culture. Maxiprep extractions were done using ZymoPURE™ II Plasmid Maxiprep Kit (Zymo Research; Cat. No. D4203) from 150 ml of bacterial cell culture.

2.2.2.2 DNA assembly methods

Traditional copy-paste method

For traditional copy-paste cloning method, NEB T4 DNA ligase (NEB; Cat. No. M0202) was used to ligate pre-digested and purified DNA fragments following manufacturer's protocols. For phosphorylation or dephosphorylation of DNA ends, T4 Polynucleotide Kinase (NEB; Cat. No. M0201) or Antarctic phosphatase (NEB; Cat. No. M0289) were used.

Gibson assembly

For Gibson assembly cloning method, NEBuilder® HiFi DNA Assembly Cloning Kit (NEB; Cat. No. E5520) was used to assemble pre-digested and PCR amplified DNA fragments following manufacturer's protocols.

Gateway® assembly

For Gateway® assembly cloning, Gateway® BP clonase™ II (Invitrogen; Cat. No. 11789020) and Gateway® LR clonase™ II (Invitrogen; Cat. No. 11791020) were used. BP reaction was carried out using 50 fmol of both fragment plasmid and pENTRY plasmid. LR reaction was carried out using 10 fmol of both pENTRY and pDONR plasmids. Both reactions were carried out overnight

at RT and inactivated by the addition of 1 µl of Proteinase K (Sigma-Aldrich; Cat. No. 3115887001) and incubation at 37 °C for 10 min.

Golden Gate assembly

For Golden Gate assembly method, NEB T4 DNA ligase (NEB; Cat. No. M0202) and NEB BsaI-HFv2 (NEB; Cat. No. R3733) were used. Vector and insert were used at a 0.04 to 0.08 pmol ratio. Reaction mix was incubated at 37 °C for 5 min to overnight. Enzymes were inactivated by incubating at 60 °C for 5 min prior to transformation in competent *E. coli*.

EMMA

All EMMA assemblies were set up according to the Martella' et al protocol[77], using T4 ligase (NEB; Cat. No. M0202) and Esp3I (NEB; Cat. No. R0734).

2.2.2.3 Restriction enzyme digestion and gel extraction

For any restriction digestion reactions, New England Biolabs restriction enzymes were used according to manufacturer's protocols. All gel extraction procedures were carried out using either QIAquick QG buffer (Qiagen; Cat. No. 19063) and PCR extraction kit (Qiagen; Cat. No. 28104), ReliaPrep™ DNA Clean-Up and Concentration System (Promega; Cat. No. A2893) or Monarch® DNA Gel Extraction Kit (NEB; Cat. No. T3010).

2.2.2.4 PCR amplification

For PCR amplifications reactions, 50 ng of DNA was used. For the Gibson product amplification reactions either GoTaq (Promega; Cat. No. M7841) or Q5 (NEB; Cat. No. M0491) polymerase reactions were carried out. For screening of monoclonal cell lines, Platinum™ SuperFi II Green PCR Master Mix (Invitrogen; Cat. No. 12368010) was used following manufacturer's protocols.

2.2.3 Cell culture

2.2.3.1 Cell lines

HEK293, HEK293T, L929, MetBo2, RAW264.7, bone marrow-derived macrophages (BMDM) and peritoneal macrophages (Table 2.3) were maintained in 1X Dulbecco's Modified Eagle Medium (DMEM) (Thermofisher Scientific; Cat. No. 11995065) with 10 % Fetal Bovine Serum (FBS) (Sigma-Aldrich; Cat. No. F2442) and 1 % Pen/Strep (Thermofisher Scientific; Cat. No. 15140122) or Antibiotic-Antimycotic (Thermofisher Scientific; Cat. No. 15240096). BL2 cells were maintained in 50 % RPMI (Sigma Aldrich; Cat. No. R8758) and 50 % X-vivo (Lonza; Cat. No. BE02-060F) cell culture medium. All cell cultures were kept at 37 °C with 5 % CO_2 (shaking at 90 rpm for BL2). BMDMs and peritoneal macrophage cultures were supplemented with 20 ng/ml of mouse M-CSF (PeproTech; Cat. No. 315-02).

Table 2.3. List of cell lines used in this thesis.

Name	Description	Source
HEK293	Human embryonic kidney cells	Susan Rosser lab, Mammalian Synthetic Biology Research Centre, University of Edinburgh
HEK293T	Human embryonic kidney cells, expresses mutant version of the SV40 large T antigen	Susan Rosser lab, Mammalian Synthetic Biology Research Centre, University of Edinburgh
L929	Mouse fibroblasts	Jamie Davies lab, Centre for Discovery Brain Sciences, University of Edinburgh
MetBo2	Bone homing clone of murine breast cancer cell line Met-1	Binzhi Qian lab, The Queen's Medical Research Institute, University of Edinburgh
RAW264.7	Mouse macrophage cell line	
BL2	Human Burkitt's lymphoma cell line	
BMDMs	Bone marrow-derived macrophages (extracted from C57BL/6 mice)	
Peritoneal macrophages	Extracted from C57BL/6 mice	Tovah Shaw lab, Institute of Immunology & Infection Research, University of Edinburgh

2.2.3.2 Mammalian cell transfections

Cells were seeded in 48- or 24-well plates 24 h prior to transfections. For transfections in HEK293 or MetBo2, Lipofectamine 3000® (Thermofisher Scientific; Cat. No. L3000001) was used. For transfection in L929 cells, GenJet™ pre-optimized L929 DNA transfection reagent (SignaGen® Laboratories; Cat. No. SL100489-L929) was used.

2.2.3.3 Co-cultures

For co-cultures, receptor and sender cells were mixed together at a 1:1 ratio and seeded in a cell culture plate. For a 24-well plate format, 0.5 x 10^5 of each cell type was used. For a 48-well format, 0.03 x 106 of each cell type was used. For suspension cells, a plate was then centrifuged at 400 x g for 1 min to induce cell-cell contact. Cells were grown in the 37 °C incubator for 24-72 hours prior to imaging/flow cytometry.

2.2.3.4 Production of small antibody fragment conjugates

For the production of the small antibody fragment conjugates, HEK293FT cells were seeded in a 6 well plate at the 0.4 x 10^6 cells/well density. Each well was transfected with 1 µg of plasmid encoding he small antibody fragment. Two days post-transfection cell media was collected form the wells, centrifuged at 1000 rpm for 3 min and supernatant was stored at 4 °C for up to two weeks.

2.2.4 Quantitative and qualitative procedures

2.2.4.1 Fluorescence-activated cell sorting (FACS)

In order to acquire heterogenous cell populations, cells were harvested from T75 flask on D10 after transfection using 3 ml of 1X Accutase® (Thermofisher Scientific; Cat. No. A1110501) and centrifuged at 1000 rpm for 5 min. The pellet was resuspended in 1 ml of sorting buffer (1X DPBS, 1 % FBS, 10 % penicillin/streptomycin) and centrifuged at 500 rpm for 5 min. The pellet was resuspended again in 0.5 ml of sorting buffer and kept on ice until the sorting. FACS sorting was carried out using BD FACS Aria IIIu 4-laser/11 detector Cell Sorter (The University of Edinburgh Institute of Immunology & Infection research Flow Cytometry Core Facility). Sorted cells were seeded in a recovery medium (1X DMEM, 20 % FBS, 5 % penicillin/streptomycin).

2.2.4.2 Flow Cytometry

All flow cytometry experiments were carried out using BD Fortessa instrument using FITC, PE, PE-Dazzle, PE-Cy5, PE-CY5.5, PE Texas Red, AlexaFluor700 and BV421 filters. Cells were washed using 1X DPBS and incubated for 5 min at 37 °C with 1X Accutase® (Thermofisher Scientific; Cat. No. A1110501). After that, cells were harvested using flow buffer (1X DPBS, 1 % FBS) and transferred to a 96 well plate for flow cytometry analysis.

In flow cytometry analysis, cells were first gated by size using forward and side scatters (SSC-A against FSC-A), and singlets were gated using forward scatters (FSC-A against FSC-W). Next, cells were further gated depending on the type of experiment and cells analysed.

For the assessment of synNotch activity in L929 cells (chapter 3), cells were gated by an H2B-TagBFP, therefore isolating only L929-UAS cells. Next, BFP^+ cells were evaluated for mCherry fluorescence. Mean fluorescence intensity (MFI)

of mCherry was then multiplied by the percentage of $mCherry^+$ cells from the parent population (BFP+) to get the total fluorescence of the cell population.

For the assessment of synNotch activity of early MetBo2 αCD19-synNotch clones (chapter 3), the cells were gated by mCherry fluorescence, therefore isolating only receptor cells. These cells were then analysed for BFP fluorescence. MFI of BFP was then multiplied by the percentage of BFP^+ cells from the parent population ($mCherry^+$) to get the total fluorescence of the cell population.

For the assessment of MetBo2-UAS and MetBo2-RANLS clones (chapter 4, 6), cells were analysed for mCherry/RFP fluorescence following singlet gating. MFI of mCherry/RFP was then multiplied by the percentage of $mCherry^+/RFP^+$ cells from the parent population (singlets) to get the total fluorescence of the cell population.

For the assessment of MetBo2 synNotch cell lines, as well as αCD19-synFP cell lines (chapter 4, 5, 6), cells were gated by TagBFP fluorescence, therefore isolating only receptor cells. These cells were then analysed for mCherry fluorescence. MFI of mCherry was then multiplied by the percentage of $mCherry^+$ cells from the parent population (BFP^+) to get the total fluorescence of the cell population.

All flow cytometry data analysis was carried out in FlowJo and GraphPad Prism.

2.2.4.3 Immunofluorescence staining of adherent cells

For adherent cells, cells were seeded in a 24 well plate on coverslips, cultured for 24 h and transfected with the plasmid of interest. After 48 h, medium was aspirated, and cells were washed with Ca^{2+} and Mg^{2+} PBS. All subsequent incubations were carried out at RT in the dark. For the fixing, 250 µl of 4 % paraformaldehyde (pH 6.9) were added and incubated for 20 min, following double washing with PBS for 5 min each. For permeabilization, 250 µl of 0.1 % Triton X-100 were added and incubated for 15 min. After that, cells were washed twice with

PBS for 5 min and 250 µl of blocking buffer (5 % BSA in 1X PBS was added). Following blocking for 1 h, 250 µl of primary antibody or conjugated fluorescent antibody (if single staining) diluted in 1 % BSA in 1X PBS were added and incubated for 1 h. Subsequently, cells were washed twice in PBS for 5 min and secondary antibody or conjugated fluorescent antibody (if double staining) diluted in 1 % BSA in 1X PBS were added. Following double washing with PBS for 5 min each, 250 µl of DAPI (Invitrogen; Cat. No. D1306) were added and incubated for 5 min. After that, two final washes with PBS for 5 min each were carried out and coverslips were mounted on glass slides using ProLong™ Diamond Antifade Mountant (Invitrogen; Cat. No. P36965).

2.2.4.4 Immunofluorescence staining of suspension cells

For suspension BL2 cells, 1.5 x 10^6 cells were resuspended in 1X PBS (Ca^{2+}, Mg^{2+}) and supplied with equal volume of 4 % paraformaldehyde (pH 6.9). All subsequent incubations were carried out at RT in the dark. Following 20 min incubation, cell suspension was centrifuged for 30 s, washed with 1 ml of dH_2O, centrifuged again and resuspended in 200 µl of dH_2O. Three drops of 5 µl were pipetted on the poly-l-lysine glass slide (Thermofisher Scientific; Cat. No. 10219280), smeared with a pipette tip and placed on a hot plate for 5 min, allowing the liquid to evaporate. A circle was drawn around a sample using a hydrophobic pen (Vector Laboratories; Cat. No. 101098-065). After washing the sample once with 200 µl of 1X PBS, 200 µl of blocking buffer was added and incubated for 1 h at RT. Following this, 200 µl of a primary antibody was added and incubated for 1 h. Prior to adding a secondary antibody, cells were washed twice with 200 µl of 1X PBS. Cells were incubated with a secondary antibody for 1 h. After this, the samples were washed twice with 1X PBS and 200 µl of DAPI (Invitrogen; Cat. No. D1306) was loaded and incubated for 5 min. After two final washes with 1X PBS and one wash with dH_2O, ProLong™ Diamond Antifade Mountant (Invitrogen; Cat. No. P36965) was added on the coverslip, which was then loaded on the slide.

2.2.4.5 Immunofluorescence staining with small antibody fragment conjugates

Immunostaining using small antibody fragment conjugates was carried out in a 24 well plate format. Transfected wells were washed with 500 µl of DPBS and 250 to 500 µl of supernatant, containing the small antibody fragment conjugates were loaded. Cells were incubated in the dark for 1h at 37 °C or overnight at 4 °C. Prior to imaging cells were washed twice with DPBS.

2.2.4.6 Immunostaining of C57BL/2 mouse spleen extract

Mouse spleen extract, pre-stained with immune-cell specific antibodies was acquired from the Binzhi Qian lab at the MRC Centre for Reproductive Health at The University of Edinburgh. The list of antibodies is provided in the Materials section. Following incubation with the antibody conjugates, the extract was centrifuged, washed with DPBS and 250 to 500 µl of supernatant, containing the small antibody domain conjugates was loaded on the extract. Following incubation in the dark for 1h at 4 °C, cells were washed with DPBS twice and analysed using flow cytometry. Compensation was carried out using UltraComp eBeads™ Compensation Beads (Invitrogen; Cat. No. 01-2222-42).

2.2.4.7 Fluorescent microscopy

Fluorescent imaging was carried out using Leica DMi8 fluorescent microscope with DAPI (Ex: 350/50, Em: 460/50), TexasRed (Ex: 560/40, Em: 630/75), GFP (Ex: 470/40, Em: 525/50) and Y5 (Ex: 620/60, Em: 700/75) filter cubes. Further image processing was carried out in FIJI software.

2.2.4.8 Confocal imaging

Confocal imaging was carried out using Zeiss Airyscan LSM800 confocal microscope at the University of Edinburgh Centre Optical Instrumentation Laboratory (COIL). Diode 405 nm and 633 nm lasers were used for DAPI and Cy5, respectively, Argon 488 nm laser was used for GFP, HeNe 594 nm laser was used for mCherry. Image processing was carried out in FIJI software.

Chapter 3

Initial synNotch system implementation *in vitro*

Outline

In this chapter early attempts at implementing the synNotch system will be described. These experiments were primarily targeted at learning how to use the synNotch system and how to apply it for the intended purpose. Initially, the synNotch architecture of choice was anti-CD19 synNotch receptor (αCD19-synNotch) since it is relatively well described in the published literature.

The following steps will be discussed:

a) Development of $CD19^+$ sender cells;
b) Transient expression of the αCD19-synNotch system in HEK293 cells and testing against $CD19^+$ cells;
c) Transient expression of αCD19-synNotch, αF4/80-synNotch, αCD206-synNotch receptors in L929 mouse fibroblast reporter cell line (L929-UAS) and testing against sender cells;
d) Testing of clonal αCD19-synNotch MetBo2 cell line against $CD19^+$ cells;

Importantly, in this chapter, only early conclusions about how to implement the synNotch system will be derived. The full implementation and characterisation will be covered in the following chapters.

3.1 Introduction

3.1.1 Applications of synNotch systems in various mammalian cell chassis

A lot of research demonstrated high potential of synNotch to detect and react to various ligand-presenting cells[41–44,60,67,69,71,72]. For example, Morsut et al. demonstrated synNotch capacity to function in L929 mouse fibroblasts, Madin-Darby canine kidney (MDCK) cells and even primary mouse fibroblasts CH3[66]. Roybal et al. expanded the portfolio by demonstrating synNotch capacity to be activated both *in vitro* and *in vivo* in engineered Jurkat T cells as well as primary $CD4^+$ and $CD8^+$ T cells[42,43]. Due to their application potential in immunotherapies, Jurkat T cells remain to be the most common chassis for synNotch receptor-reporter systems. Moreover, Jurkat T cells present opportunities to combine synNotch with CAR T cell technology in many cancer-targeting applications[69,71,72]. Several examples of this have been given in chapter one of this thesis.

However, in this research the aim is to engineer non-immune cells – cancer cells – which will be used as biosensors to report interactions between cancer and immune cells. Therefore, the intention is to implement the receptor-reporter system in a breast-to-bone metastasis cell line (MetBo2)[78], derived in the Qian lab at the MRC Centre for Reproductive Health at The University of Edinburgh. MetBo2 are a bone-homing clone of murine breast cancer cell line Met-1, previously derived from Polyoma Middle T Oncoprotein (PyMT) tumour[78]. When injected into mice, these cells establish primary breast tumours, which later metastasise into the bones. However, in order to demonstrate the feasibility of the system *in vitro*, early experiments were performed in commonly used cell lines like HEK293 due to their high transfection efficiency, high expression efficiency of recombinant proteins and moderate growth rate[79].

3.1.2 The design of synNotch receptor-reporter system

synNotch receptor system consists of two functional elements: a receptor and a reporter. Morsut et al. described a whole array of synNotch receptor architectures with multiple sensing and signal transduction modules, which was invaluable for demonstrating receptor modularity and versatility[66]. While the choice of the sensing domain depends on the target of interest and usually comprises a single chain variable fragment (scFV) or a nanobody (VHH), the choice of the appropriate signal transduction domain depends on the desired outcome of the system. For example, DNA-binding elements such as Gal4, TetR, dCas9 fused to transcriptional activator domain VP64 have been used to induce gene expression following receptor activation[41–44,66,67,69,71,72,80,] while Krüppel associated box (KRAB) domain fusions were used to silence constitutive expression of genes of interest[66].

In this work, the Gal4-UAS reporter system was chosen as a downstream signal transduction/reporter circuit, primarily due to its explicit use in the original synNotch research. A detailed construct schematic is illustrated in figure 3.1. A reporter cassette (Fig. 3.1A) consists of a 5 x Gal4 responsive element (UAS) which regulates a downstream minimal CMV promoter. Binding of the Gal4VP64 molecules induces expression of downstream mCherry ORF. Additionally, downstream from UAS-mCherry cassette, a PGK promoter-driven human histone 2B-TagBFP fusion (H2B-TagBFP) cassette is integrated. This cassette is used for lineage-tracking purposes and can be used for FACS sorting in the future in synNotch cell line development pipeline.

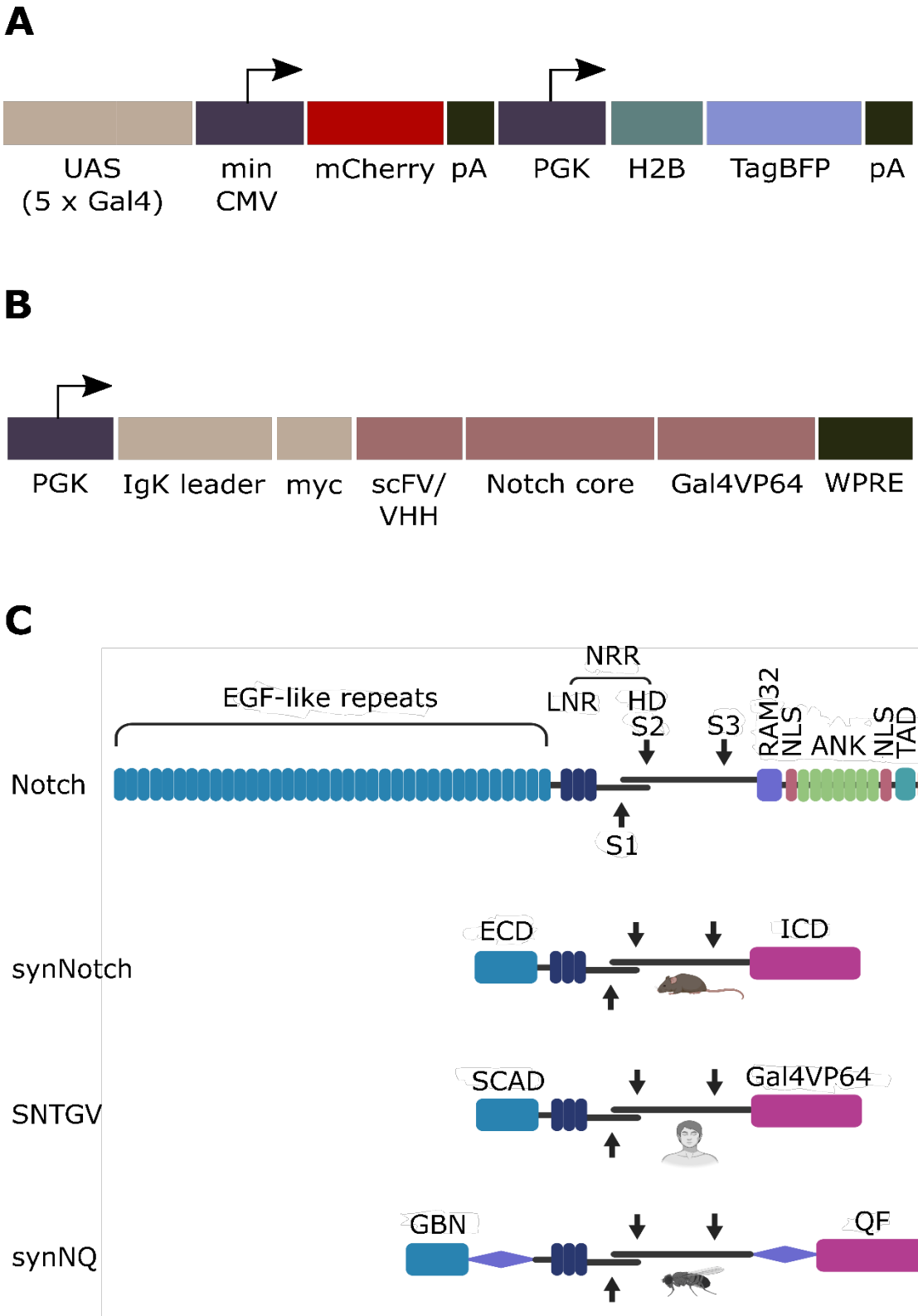
A
UAS
(5 x Gal4)
min
CMV
mCherry
pA
PGK
H2B
TagBFP
pA
B
PGK
IgK leader
myc
scFV/
VHH
Notch core
Gal4VP64
WPRE
C
NRR
EGF-like repeats
LNR
HD
S2
S3
RAM32
NLS
ANK
NLS
TAD
PEST
Notch
S1
ECD
ICD
synNotch
SCAD
Gal4VP64
SNTGV
GBN
QF
synNQ

Figure 3.1. Synthetic Notch receptor system and published variants. *(A) Structure of the UAS reporter element. Binding of the Gal4 proteins induces expression of mCherry fluorescent protein. A downstream cassette encoding nuclear BFP is used for lineage tracking purpose. min CMV – minimal Cytomegalovirus mammalian promoter, pA – polyadenylation sequence, PGK – phosphoglycerate kinase mammalian promoter, H2B – human histone 2B. (B) Structure of a synNotch receptor construct. Receptor is driven by a PGK promoter. scFV – single chain variable fragment, WPRE - Woodchuck Hepatitis Virus Posttranscriptional Regulatory Element. (C) Different synthetic Notch receptor versions available in published literature. synNotch, SNTGV and synNQ contain a minimal Notch Regulatory Region (NRR) and differ in their core domain host origin – mouse, human and fruit fly, respectively. SCAD – single chain antibody domain, GBN – GFP binding nanobody, QF – transcription factor.*

Regarding the receptor design, anti-CD19-synNotch-Gal4VP64 (αCD19-synNotch) construct was obtained from the original publication, where the whole construct is driven by a PGK promoter (Fig. 3.1B)[66]. Macrophage specific synNotch variants - anti-F4/80-synNotch-Gal4VP64 (αF4/80-synNotch) and anti-CD206-synNotch-Gal4VP64 (αCD206-synNotch) were designed in the Cachat lab. Detailed descriptions of the constructs can be found in the Table 3.1.

Table 3.1. List of constructs used in synNotch receptor system described in the chapter 3. *minCMV – minimal Cytomegalovirus mammalian promoter, polyA – polyadenylation sequence, PGK – phosphoglycerate kinase mammalian promoter, scFV – single chain variable fragment, NNR – Notch Regulatory Region, WPRE - Woodchuck Hepatitis Virus Posttranscriptional Regulatory Element, IRES – Internal ribosome entry site.*

Construct name	**Structure**	**References/ Notes**
UAS-mCherry	UAS(5xGal4)→minCMV→mCherry→polyA→PGK→H2B-TagBFP→polyA	[66], engineered
αCD19-synNotch	PGK→IgKleader→myc→antiCD19-scFV→NNR→Gal4VP64→WPRE	[66]
αF4/80-synNotch	PGK→IgKleader→myc→antiF4/80-scFV→NNR→Gal4VP64→WPRE	[66], engineered
αCD206-synNotch	PGK→IgKleader→6xHis→antiCD206-VHH→NNR→Gal4VP64→WPRE	[66], engineered
Gal4VP64	CMV→Gal4VP64→IRES→TGFP→polyA	[66]

Several alternative synthetic Notch receptor versions have also been published recently: SNTGV[81] and synNQ[82]. The main distinction between these receptors lies within the transmembrane (core) domain, since it plays the most essential role in regulation of Notch and, therefore, synthetic Notch activity (Fig. 3.1C). While synNotch core domain is of mouse Notch core origin, SNTGV incorporates human Notch and synNQ – fly Notch core domains. synNQ also has additional linkers spanning the core domain, which are commonly speculated to increase the signal-to-noise ratio[66,83]. Both SNTGV and synNQ have been utilised to monitor interaction between neurons and glia cells *in vivo* in *Drosophila* and provided some new insight into the wiring of neuronal circuits and interactions between neurons and neighbouring cells[81,82]. Despite that synNotch, SNTGV and synNQ haven't been compared directly, synNotch remains to be the most commonly used and referred to version.

3.1.3 Methods for assessing synNotch activity *in vitro*

The methodology behind assessment of synNotch activity *in vitro* strongly depends on whether suspension or adherent cells are used in the assay. Commonly, when synNotch cells are adherent cells and sender cells are suspension cells, sender cells can be loaded onto synNotch cells and incubated in co-culture for the desired amount of time. Due to the inability of suspension cells to adhere to the cell culture dish surface, they can be easily removed and remaining adherent cells can be analysed. Additionally, this allows performing time point experiments quite easily because sender cells can be removed at any time. In case of both synNotch cells and sender cells being adherent or in suspension, synNotch cells need to be isolated from the heterogenous co-culture. This can be achieved either by using fluorescent markers to track lineage, or by isolating the cells in different ways, e.g., immunostaining.

Some researchers used surface bound ligand proteins instead of the membrane-tethered ones, which allows to omit the isolation of relevant cell populations, meaning that receptor cells can be relatively easily collected from coated culture plates and analysed[44].

Receptor activation can be assessed by either qualitative methods (e.g., fluorescent microscopy) or quantitative methods (e.g., flow cytometry or chemiluminescence assays[84]). While most synNotch applications in theranostics utilise flow cytometry to assess receptor activation[42–44,66,67,69,71,72,80], synNotch applications in patterning demonstrate that receptor activity is strong enough to be detected with microscopy[41,66,85]. In the research described in this thesis it was sought to achieve such receptor performance, which would allow visualising receptor activation primarily with fluorescent microscopy and, in later stages of application, intra-vital microscopy.

3.2 Results

3.2.1 αCD19-synNotch receptor-reporter system exhibits high background activation in HEK293

In the early proof-of-concept experiments the aim was to test αCD19-synNotch for activation with $CD19^+$ cells and establish a working experimental pipeline for receptor activity experiments in HEK293. αCD19-synNotch was selected due to its extensive use in the published literature; therefore, it was considered a reliable scaffold for developing and adapting the experimental workflow. The overview of the experimental procedures included transiently co-transfecting cells with both receptor and reporter plasmids, presenting them to $CD19^+$ sender cells by co-culturing 24 hours post-transfection and evaluating mCherry fluorescence 48 hours post-transfection.

The extracellular domain (ECD) of αCD19-synNotch contained an anti-CD19 scFV, specific to human CD19. Therefore, as sender cells, we engineered HEK293 to express human CD19. To do this, CD19 coding sequence was extracted from cDNA of human lymphoblastoid cells (LCLs) and cloned into a modified pcDNA6.2™ mammalian expression vector with an emGFP fluorescent marker downstream from the CD19 cassette (Fig. 3.2A). These cells ($HEK293^{CD19}$) were then sorted by FACS into a heterogenous population of $emGFP^+$ cells and CD19 expression as well as membrane localisation was confirmed via

immunofluorescence (Fig. 3.2B, C). Interestingly, confocal images of membrane localisation experiments also show fluorescent signal in the cell cytosol (Fig. 3.2C-b), which might have occurred due to ligand overexpression, during transportation to the plasma membrane or mislocalisation of a fraction of overexpressed ligands. However, it is important to note that testing the ligand for expression and positive staining relying solely on fluorescent microscopy is insufficient and using quantitative methods like flow cytometry could give better insights into expression efficiency. Additionally, using plasma membrane counterstains, as well as control constructs lacking membrane targeting sequences could provide more solid evidence of correct membrane localisation of CD19 ligand.

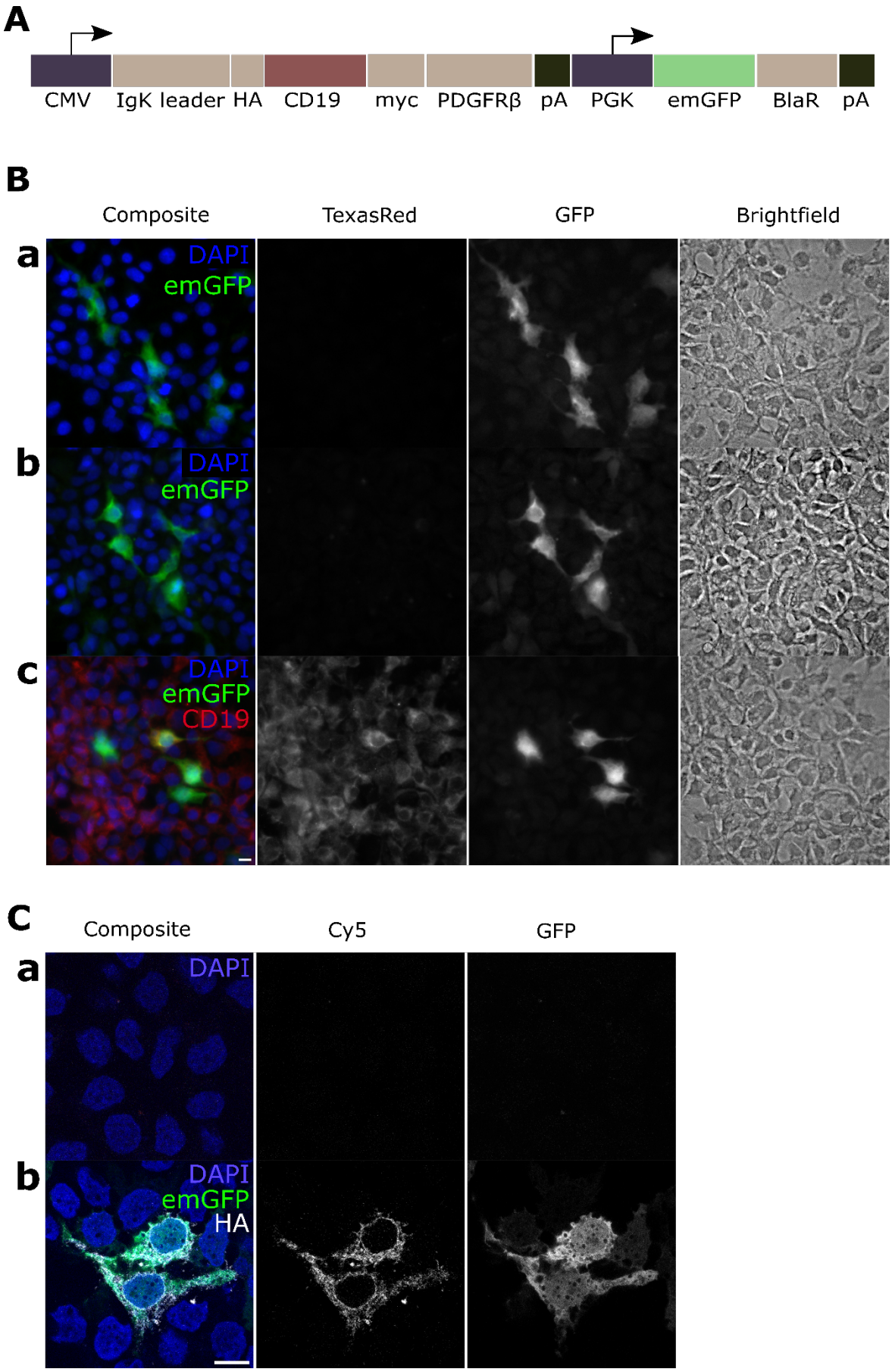
A
CMV
IgK leader
HA
CD19
myc
PDGFRβ
pA
PGK
emGFP
BlaR
pA
B
Composite
TexasRed
GFP
Brightfield
a
DAPI
emGFP
b
DAPI
emGFP
c
DAPI
emGFP
CD19
C
Composite
Cy5
GFP
a
DAPI
b
DAPI
emGFP
HA

Figure 3.2. Validation of HEK293^{CD19} sender cells. *(A) The schematic representation of CD19 construct. (B) Immunostaining of HEK293^{CD19} cells: (B-a) negative staining control (no antibodies), (B-b) secondary antibody control, (B-c) positive staining confirming the expression of CD19. Scale bar 10 µm. (C) Confocal microscopy images: (C-a) negative control (wild-type HEK293 stained with anti-HA antibody), (C-b) positive staining confirming the membrane localisation of CD19 using the HA tag upstream the CD19 ORF. Scale bar 10 µm . CMV – Cytomegalovirus mammalian promoter. HA - Human influenza hemagglutinin tag. Myc – c-myc tag. PDGFRβ - Platelet-derived growth factor receptor beta transmembrane domain. pA – polyadenylation sequence. PGK - phosphoglycerate kinase mammalian promoter. BlaR – Blasticidin resistance gene.*

After confirming CD19 expression, co-culture experiments were performed, which revealed high background fluorescence level from UAS-mCherry reporter alone (Fig. 3.3B), as well as high background activation level in receptor cells without exposure to HEK293^{CD19} cells (Fig. 3.3C). Interestingly, co-culture image (Fig. 3.3D) exhibits lower fluorescence levels than the well without sender cells (Fig. 3.3C). Although the microscopy images shown here are representative images from the testing well of a cell culture dish, flow cytometry analysis could provide better understanding of fluorescent reporter levels across various experimental conditions, especially when transient transfection is used, as it is in these experiments.

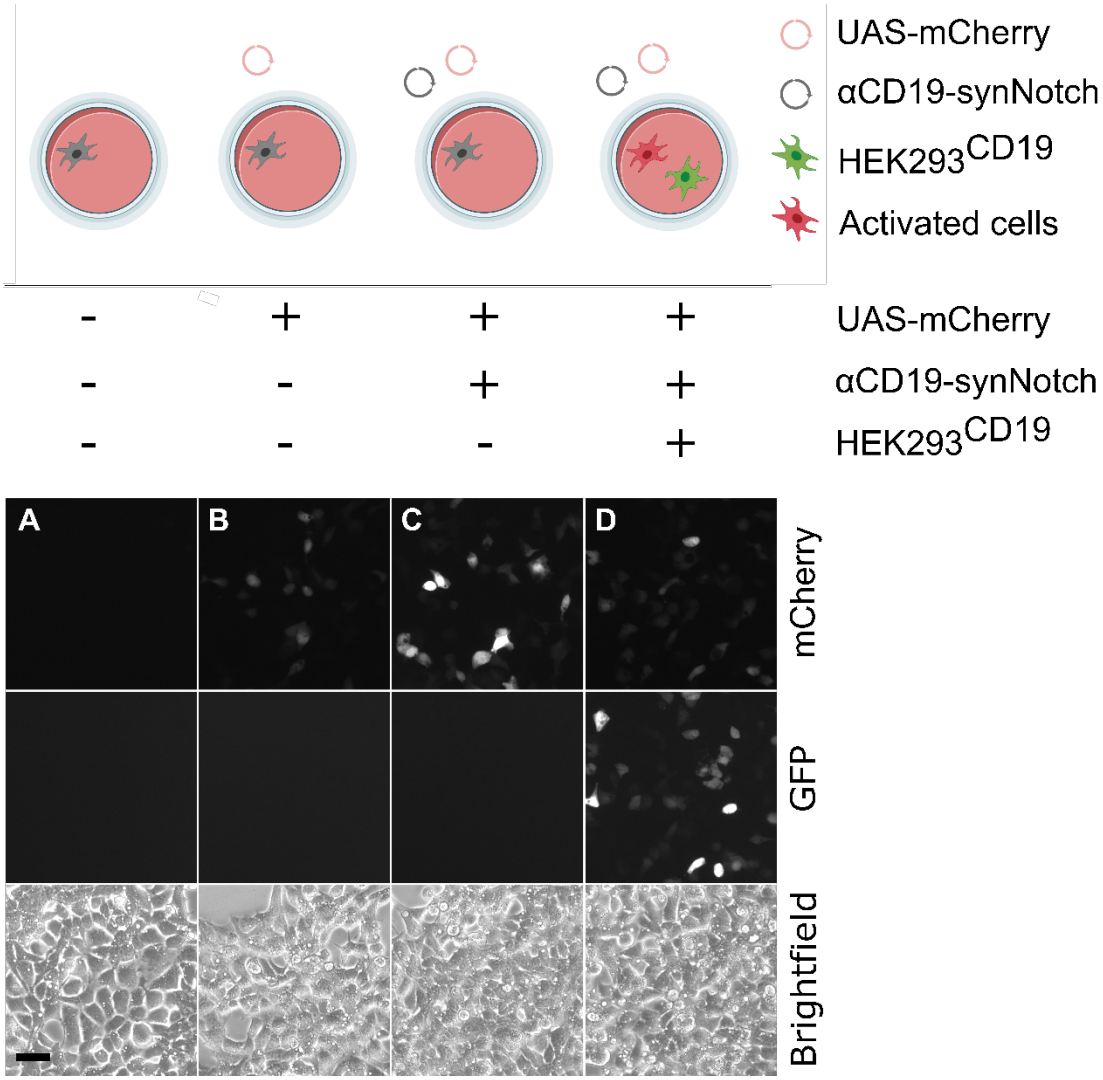

Figure 3.3. synNotch activity in HEK293 cells. *αCD19-synNotch activity in HEK293 cells. (A) Wild-type HEK293 cells. (B) HEK293 transfected with UAS-mCherry construct. High mCherry fluorescence from leaky UAS promoter is observed. (C) HEK293 transfected with UAS-mCherry and αCD19-synNotch constructs. High background activation level is observed. (D) HEK293 transfected with UAS-mCherry and αCD19-synNotch constructs, presented to HEK293^{CD19} cells. Low activation level is observed in co-culture. Scale bar 10 μm.*

3.2.2 SynNotch is correctly targeted at cell plasma membrane in HEK293 and L929 cells

While a lot of background in the synNotch system comes from the leaky reporter cassette, the reasons for high background activation levels in absence of sender cells are unclear. One of the possible reasons was incorrect or poor synNotch receptor targeting at the cell membrane and resulting ligand-independent activation of a reporter cassette. In order to assess whether receptor is correctly displayed on the cell plasma membrane, immunostaining of the receptor N-terminal myc-tag was performed on cells transiently transfected with αCD19-synNotch. Both permeabilised and non-permeabilised cells were used to allow for better discrimination between membrane and cytoplasmic staining, i.e., only membrane epitopes are expected to be stained in non-permeabilised cells, and both internal and external epitopes in permeabilised cells. Despite fluorescent signal present in cytoplasmic compartments of cells, omitting cell permeabilization step during immunofluorescence staining allowed to confirm that synNotch is correctly localised on the plasma membrane of HEK293 (Fig. 3.4A, B).

There is a lack of solid evidence of HEK293 being used in synNotch applications in the published literature. Therefore, it was speculated that HEK293 might be a suboptimal chassis for this receptor-reporter system. Therefore, after confirming correct receptor localisation (Fig. 3.4C), the system was moved in L929 mouse fibroblasts.

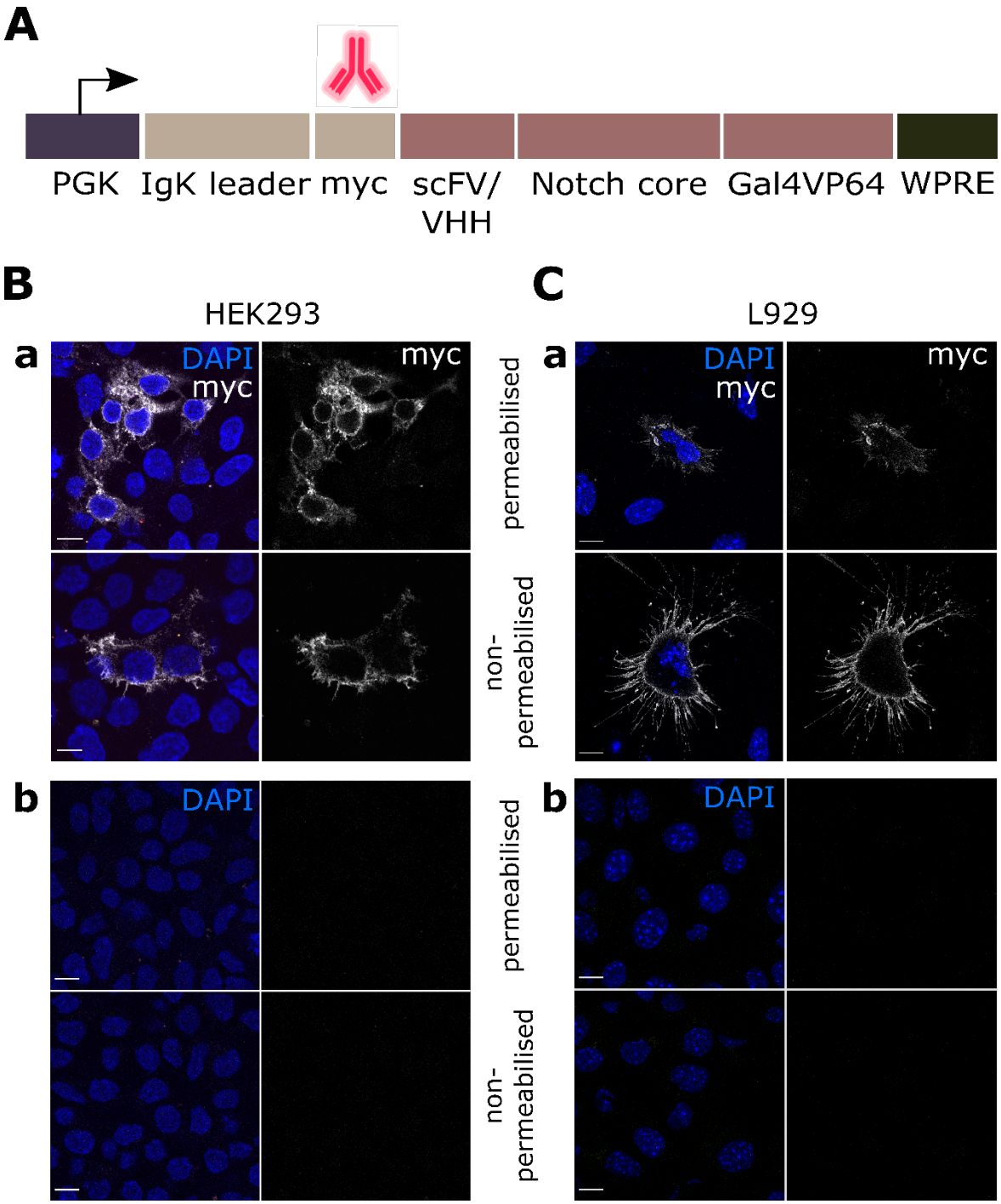

Figure 3.4. synNotch localisation validation. *(A) Schematic representation of a synNotch construct, highlighting the myc-tag upstream from receptor ECD. Myc-tag was stained with a AlexaFluor647 conjugate. Membrane localisation was confirmed in both HEK293 cells (B-a) and L929 cells (C-a). Wild-type HEK293 (B-b) and L929 (C-b) cells were used as negative control. DAPI was used a counterstain. Scale bar 10 µm. PGK - phosphoglycerate kinase mammalian promoter. Myc – c-myc tag. WPRE - Woodchuck hepatitis virus (WHV) posttranscriptional regulatory element.*

3.2.3 synNotch activity in mouse fibroblasts is ligand-independent

High background activation in transient receptor-reporter system expression can also be attributed to the leakiness of a UAS reporter cassette. Meaning, that mCherry expression is independent from Gal4VP64 binding. In order to derive cells with reduced UAS-minCMV promoter leakiness, genomic integration and monoclonal selection of L929-UAS cells was carried out. L929 cells were transfected with the reporter plasmid, expanded and sorted into single cells by H2B-TagBFP fluorescence (Fig. 3.5A). A successful clone eliciting a good level of mCherry fluorescence tested by transfecting with transactivator plasmid was isolated (Fig. 3.5B).

L929-UAS cells were then transiently transfected with receptor plasmids and presented to sender cells. Receptor activation was evaluated using flow cytometry. The gating strategy is depicted in figure 3.5C. A 1.7-fold activation of αCD19-synNotch L929 cells was observed when stimulated with $BL2^{CD19}$ sender cells, using flow cytometry (Fig. 3.5D). In contrast to previous experiments where fluorescent microscopy was used to assess receptor activity, flow cytometry was able to reveal low-fold activation of the synNotch receptor. However, it is important to take into account that the use of two consecutive ORFs within a reporter cassette might mutually impact the expression levels of each other due to the effects of promoter interference or the metabolic burden, i.e., the increased expression of one will cause the decrease of the expression of another. This will be discussed in more detail in the Discussion section in Chapter 5.

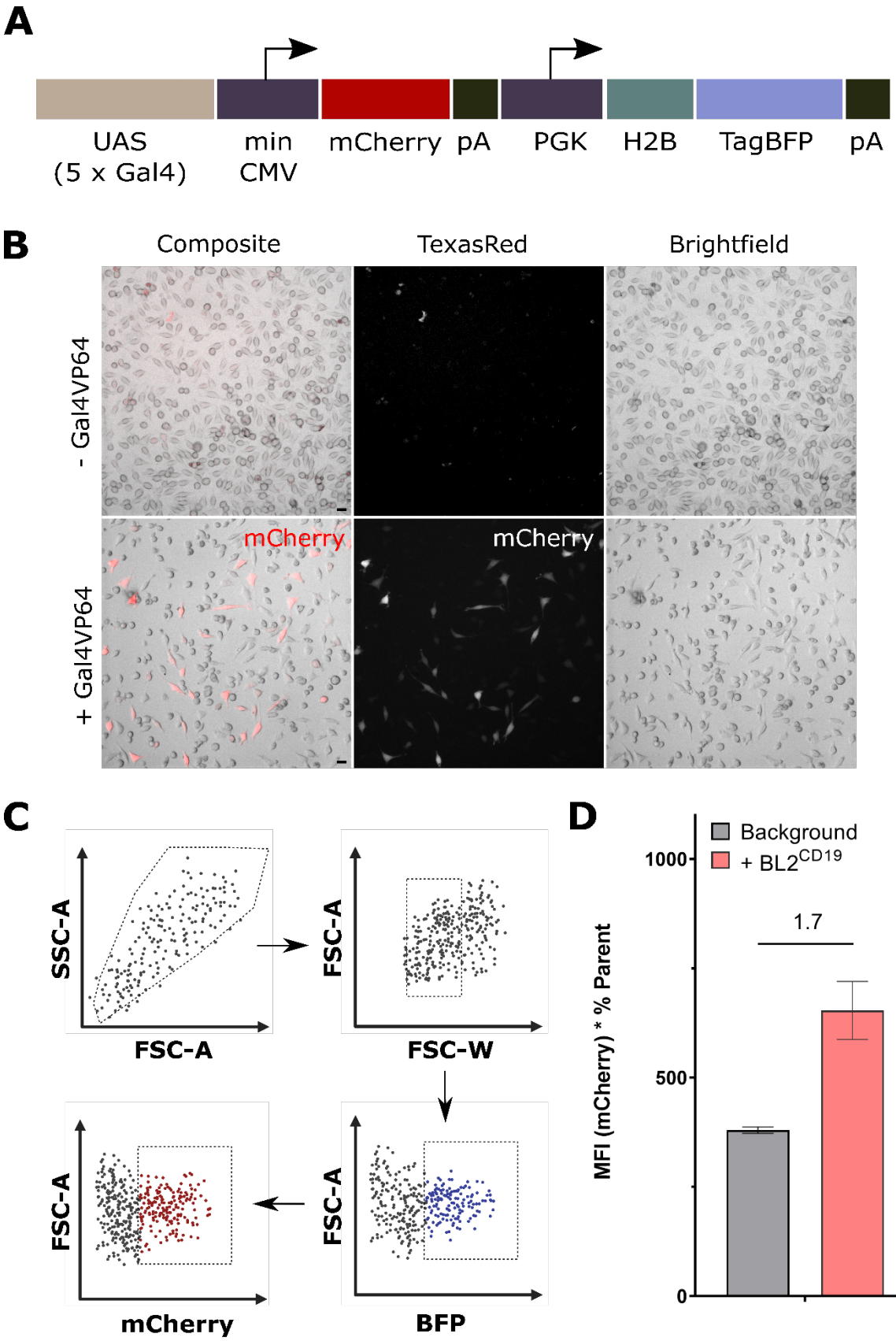
A
UAS
(5 x Gal4)
min
CMV
mCherry
pA
PGK
H2B
TagBFP
pA
B
Composite
TexasRed
Brightfield
- Gal4VP64
+ Gal4VP64
mCherry
mCherry
C
SSC-A
FSC-A
FSC-A
FSC-W
FSC-A
mCherry
FSC-A
BFP
D
Background
+ BL2CD19
1.7
MFI (mCherry) * % Parent
1000
500
0

Figure 3.5. Isolation of L929-UAS monoclonal cell line and reporter expression with the αCD19 synNotch. *(A) A schematic of the construct that was randomly integrated into L929 genomic DNA. (B) Successful clone, which elicited mCherry fluorescence upon transfection with Gal4VP64 transcriptional activator, was isolated. Scale bar 10 μm. (C) Flow cytometry gating strategy for the evaluation of αCD19-synNotch activation with BL2^{CD19} cells. First, the cells were gated by size using forward and side scatters, following singlet isolation. L929-UAS cells in co-culture were isolated by TagBFP and mCherry fluorescence of TagBFP^{+} cell population was analysed. Total fluorescence of the reporter cell line population was calculated by multiplying the mean fluorescence intensity (MFI) of mCherry by the percentage of mCherry^{+} cells in a parent TagBFP^{+} cell population. Due to the fact that (i) transient transfection was used and (ii) there was no way to ensure that every receptor cell contacts a CD19^{+} cell, total fluorescence allowed to more reliably quantify the change in fluorescence intensity of a whole cell population. (D) αCD19-synNotch activation with BL2^{CD19} cells. minCMV – minimal Cytomegalovirus mammalian promoter. pA – polyadenylation sequence. PGK - phosphoglycerate kinase mammalian promoter. H2B – human 2B histone tag.*

Next, macrophage-specific synNotch receptors - αF4/80-synNotch and αCD206-synNotch - were tested for activation in L929-UAS cells. These novel receptor architectures were constructed by engineering existing synNotch variants with F4/80 and CD206-specific extracellular domains[86,87]. Both anti-F4/80 and anti-CD206 binding domain sequences were ordered as gBlocks® and used to replace the anti-CD19 scFV in the original αCD19 synNotch receptor. In αF4/80 synNotch, the myc-tag was preserved; however, in αCD206 synNotch, the myc-tag was replaced by a 6xHis-tag. This was done in order to enable the use of both of these receptors together in the future, for example, in the logic AND gate settings, where the synNotch cell would elicit a fluorescent response only in the presence of both F4/80 and CD206 epitopes on a neighbouring cell. The idea behind this rationale is discussed in more detail in the Chapter 7 of this thesis. The schematic representations of the novel receptor constructs are illustrated in figure 3.6A.

Similar to αCD19-synNotch L929 cells, αF4/80-synNotch and αCD206-synNotch L929 cells elicited a 1.3- and 1.4-fold activation, respectively, when presented to RAW264.7 cells (Fig. 3.6B), an immortalised mouse macrophage cell line that endogenously display F4/80 and CD206. The gating strategy in these experiments was identical to the gating strategy described in Figure 3.5C.

However, when we expanded the experimental set up with additional controls, it was revealed that the fluorescent response was independent of synNotch activity, as L929-UAS cells alone elicited a fluorescent response when presented to RAW264.7 macrophages (Fig. 3.6C). Literature analysis revealed that L929 are common producers of macrophage colony-stimulating factor (M-CSF), which is a macrophage M2 polarisation factor[88]. Consequently, the observed behaviour might be associated with the change in macrophage activity, and the following effect on mouse fibroblasts. For example, the increased fluorescence could be a result of the cell death-associated processes within L929 cells – in order to test this hypothesis, cell cycle or cell viability assays must be performed. However, investigating this further was beyond the scope of this project and, despite L929 cells being a functional chassis for the implementation of the αCD19-synNotch system, a decision was made to move the system into the final application chassis, breast-to-bone metastasis cell line (MetBo2).

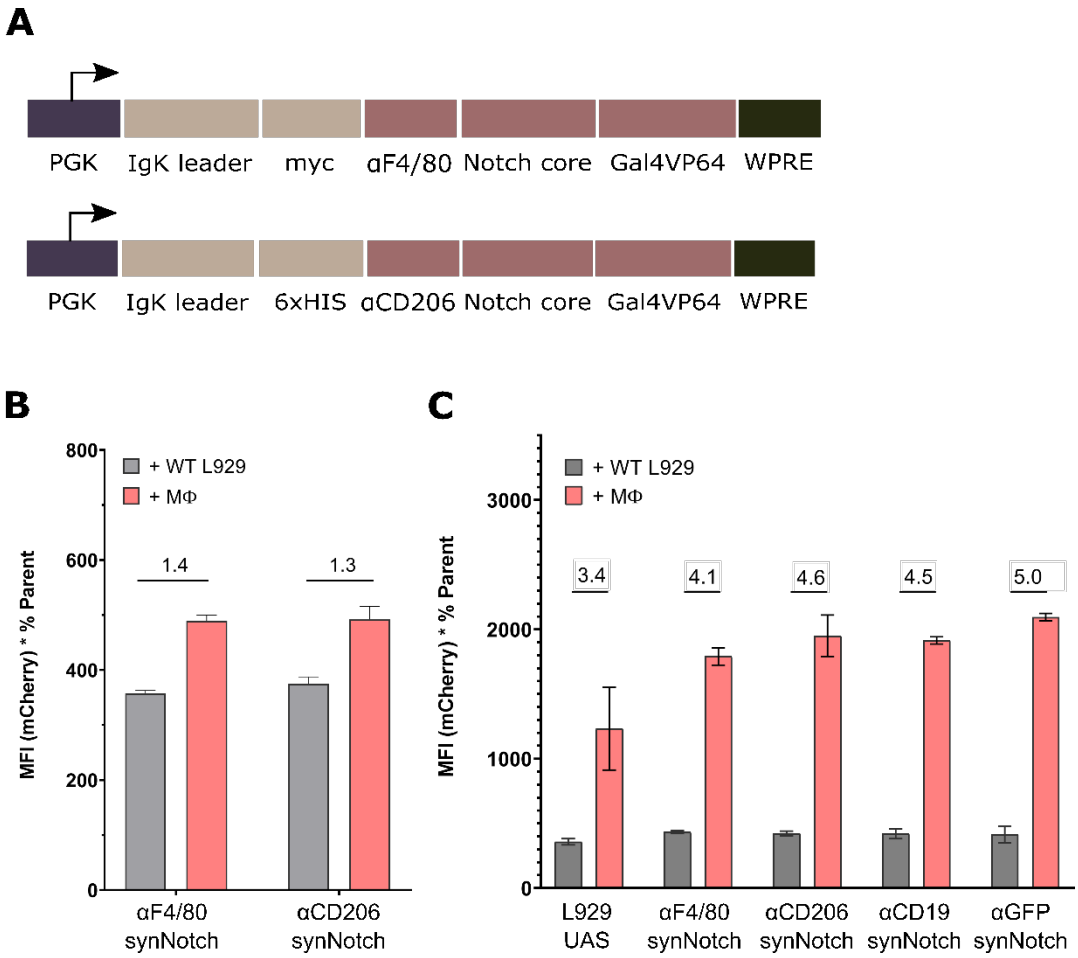

Figure 3.6. Assessing activity of synNotch in L929-UAS cells. *(A) Schematic representation of αF4/80-synNotch and αCD206-synNotch constructs. (B) αF4/80-synNotch and αCD206-synNotch activation with RAW264.7 macrophage cell line. (B) Unspecific and synNotch-independent induction of mCherry in L929-UAS cells. PGK - phosphoglycerate kinase mammalian promoter. pA – polyadenylation sequence. WPRE - Woodchuck hepatitis virus (WHV) posttranscriptional regulatory element.*

3.2.4 Clonal MetBo2 synNotch cell line exhibits efficient receptor activation with human CD19^{+} cells

Monoclonal αCD19-synNotch cell line was derived by project collaborators in Binzhi Qian lab at the MRC Centre for Reproductive Health at The University of Edinburgh. The Qian lab was supplied with the αCD19-synNotch system plasmids to derive a monoclonal MetBo2 αCD19-synNotch cell line, with genomic integration of both reporter and receptor cassettes. In this cell line, a reporter cassette was designed in a way that TagBFP was expressed under a 5 x Gal4 UAS inducible minimal CMV promoter, with a downstream mCherry cassette for the lineage tracking purposes, and a receptor cassette was identical to the one developed by Morsut et al[66] (Fig. 3.7A). These cells demonstrated an 87.3-fold activation in co-culture with human CD19^{+} cells (Burkitt's lymphoma BL2), compared to receptor cells with no exposure to CD19^{+} cells. However, activation fold dropped to 46.2-fold after the clonal cell line was passaged 4 times and retested in the same conditions (Fig. 3.7B, C). Similarly, the percentage of activated cells within a population reduced by approximately 4-fold (from a 124.9-fold activation to a 30.2-fold activation after retesting 2 weeks later) (Fig. 3.7D) meaning that a lower fraction of cells got activated by sender cells. These observations suggest that receptor cells might have been subjected to epigenetic silencing of integrated transgenes and a more robust method of deriving stable cell lines is required.

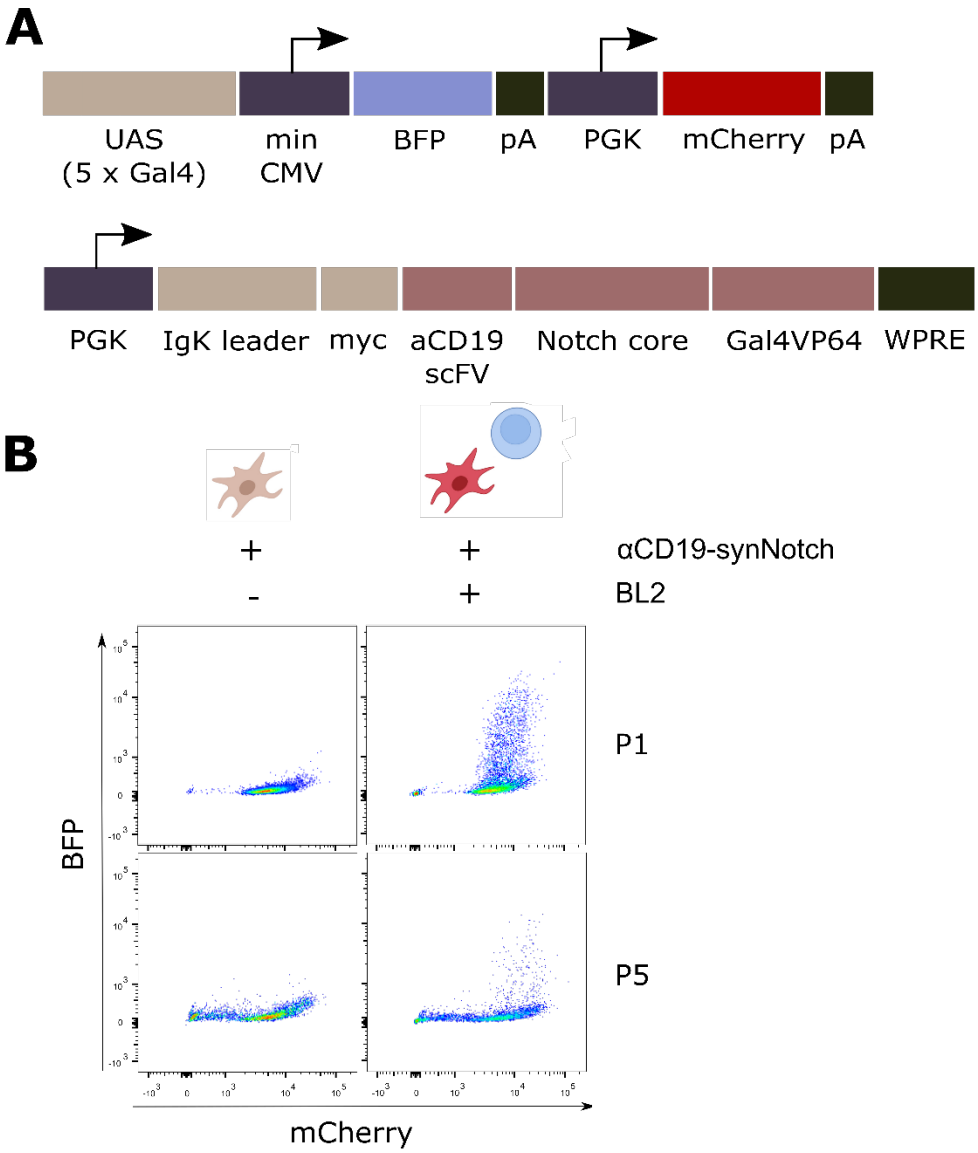
A
UAS
(5 x Gal4)
min
CMV
BFP
pA
PGK
mCherry
pA
PGK
IgK leader
myc
aCD19
scFV
Notch core
Gal4VP64
WPRE
B
+
+
αCD19-synNotch
-
+
BL2
P1
P5
BFP
mCherry
C
87.3
46.2
Background
+ BL2CD19
MFI (BFP) * %Parent
7.5×10⁴
5×10⁴
2.5×10⁴
8×10²
4×10²
0
P1
P5
D
124.9
30.2
Background
+ BL2CD19
% Parent
20
15
10
5
0.1
0.0
P1
P5

Figure 3.7. Activation of monoclonal MetBo2 αCD19-synNotch cells. *(A) The schematics of genetic constructs that were integrated into genomic DNA of MetBo2 cells. (B) Flow cytometry charts demonstrating a drop in synNotch activation from passage one to passage five. (C) Total fluorescence upon αCD19-synNotch activation with BL2 cells. (D) Population percentage of activated cells upon co-culture with BL2 cells. P1 – relative passage one. P5 – relative passage five. minCMV – minimal Cytomegalovirus mammalian promoter. pA – polyadenylation sequence. PGK - phosphoglycerate kinase mammalian promoter. WPRE - Woodchuck hepatitis virus (WHV) posttranscriptional regulatory element.*

3.3 Discussion

The primary aim of the work described in this chapter was to establish a working experimental pipeline and design framework for synNotch receptor-reporter system. In order to achieve this, synNotch was expressed in different host cell lines (HEK293, L929 and MetBo2) transiently, semi-transiently (i.e., genomic integration of a reporter cassette and transient expression of a receptor cassette) and following genomic integration of both reporter and receptor cassettes. The summary of all receiver and sender cells used in this chapter is given in the Table 3.2. Transient expression of both receptor and reporter cassettes in HEK239 cells resulted in high background activation levels and low ligand-dependent activation levels. Interestingly, high background fluorescence levels from the reporter cassette might be associated with the use of a lentiviral vector in transient transfection. Lentiviral expression vectors contain long terminal repeats (LTRs) that were shown to be capable of exhibiting promoter activity[89], and, therefore, cause leaky expression of the mCherry reporter. In L929 cells, genomic integration of a reporter cassette reduced its leakiness, as well as ligand-independent activation, as cells transfected with a reporter cassette exhibited similarly low levels of fluorescence as non-transfected L929-UAS cells (Fig. 3.6C). Interestingly, L929-UAS cells exhibited unexpected fluorescent response in co-culture with macrophages, the ultimate sender cell type in this project. In MetBo2, isolating functional reporter-receptor clones allowed to reduce background levels and increase actual activation fold in response to $CD19^{+}$ cells.

Table 3.2. The summary of all the receiver and sender cells used in chapter 3.

Receiver cells	Sender cells	Surface ligand	Notes
HEK293 (αCD19 synNotch)	HEK293	CD19 (human)	Transient transfection of the synNotch system; Anti-CD19 scFV[66] (human CD19); Genomic integration of CD19;
L929 (αCD19 synNotch)	BL2	CD19 (human)	Genomic integration of a reporter cassette; Transient expression of a receptor cassette; Anti-CD19 scFV[66] (human CD19); Endogenous expression of CD19;
L929 (αF4/80 synNotch)	RAW264.7	F4/80 (mouse)	Genomic integration of a reporter cassette; Transient expression of a receptor cassette; Anti-F4/80 scFV[86] (mouse F4/80); Endogenous expression of F4/80;
L929 (αCD206 synNotch)	RAW264.7	CD206 (mouse)	Genomic integration of a reporter cassette; Transient expression of a receptor cassette; Anti-CD206 VHH[87] (mouse CD206); Endogenous expression of CD206;
MetBo2 (αCD19 synNotch)	BL2	CD19 (mouse)	Genomic integration of the synNotch system; Anti-CD19 scFV[66] (human CD19); Endogenous expression of CD19;

3.3.1 The importance of the cell chassis on receptor-reporter system function

The diversity of cell lines that have been engineered to express synNotch in the last decade spans both immortalized and primary cell lines, with most common host cells being MDCK[66], L929[41,66] and Jurkat T[42–44,66,71,72,85] cells. MDCK cells are a frequent host choice in multicellular patterning applications due

to their retained properties of epithelial cells, and therefore their ability to form cell-cell junctions and self-arrange into both monolayers and 3D cultures[90]. Jurkat T, being immortalized T lymphocytes, also retain T cell endogenous signalling pathways, and therefore can be used in diverse therapeutic applications[91]. The utility of L929 mouse fibroblasts as engineering chassis, however, doesn't have obvious basis besides the long history of use in cancer and cytotoxicity research[92].

HEK293 cells, on the other hand, have been used in biological research for many years due to their relatively fast growth, easy manipulation and simple growth conditions. Moreover, HEK293 are extremely efficient at producing recombinant proteins, biologics as well as viruses for gene therapy applications. Engineered versions of HEK293, e.g., HEK293T cells, have been modified with a T antigen, which allows sustained propagation of vectors with SV40 origin of replication. Although, collectively, these properties make HEK293 a favourable chassis for biotechnology and synthetic biology applications, it has been reported that expression of recombinant membrane proteins can present certain challenges[93,94] and optimisation is often required in terms of vector choice, transfection method, growth and media conditions, codon usage, etc[94]. Despite that, HEK293 have been used in several published research on synthetic receptors, but with a relatively limited coverage in synNotch publications. For example, Morsut et al. listed HEK293 cells among the confirmed receptor chassis; however, there is no solid evidence of their use in the published materials[66]. Alternatively, other receptor systems report unequivocal evidence of HEK293 suitability for reporting both cell-cell contact events[84], as well as binding of soluble ligands[56,95].

While L929 cells have been explicitly used in several synNotch-related publications, there are no records to date of their co-culture with macrophages in receptor-reporter systems. On the other hand, L929 cell culture supernatant can be used to differentiate primary monocytes or bone marrow-derived macrophages (BMDMs)[88,96]. Additionally, it has been reported that macrophages are able to induce apoptosis of co-cultured cell lines, L929 included[97,98]. Hence, it is important to take these macrophage properties into account when performing synNotch activation assays and include appropriate controls in experimental setups.

3.3.2 Speculations regarding the requirement for ligand overexpression for synNotch activation

In the experiments described in this chapter, engineered HEK293^{CD19} were used as sender cells primarily due to the restricted availability of immortalized or primary CD19^{+} cell lines. Additionally, the majority of published literature on synNotch, similarly, reports using engineered cell lines as sender cells, such as K562 (human immortalised myelogenous leukaemia cell line)[44,66,71] or cancer cells, for their respective surface biomarkers[42,43,72] (e.g., CD19^{+} BL2 cells in this chapter). However, it is unclear why engineered ligand cell lines are usually preferential. Possibly, synthetic receptor systems require overexpression of ligands on the surface of sender cells, following the principle of CAR T cell technology, where CAR T more efficiently target overexpressed cancer cell markers[99]. However, there is no solid evidence to support this assumption.

3.3.3 Effective signalling of synNotch is restricted to isolating a clone with desired efficiency

In the last part of this chapter, synNotch activity was demonstrated in monoclonal MetBo2 cell line, which contained genomic integration of both receptor and reporter cassettes. Significant receptor activation was achieved, leading to establishing the pipeline for future synNotch experiments and confirming the requirement for stable genomic integration and isolation of functional clones.

Interestingly, the information on whether synNotch can be used in transient systems or exclusively in clonal cell lines is often omitted from synNotch publications. However, since the system was also reported to exhibit high background activation levels, as well as failed to perform in certain combinations of extracellular and intracellular domain combinations[66], it became clear that screening for functional clones is essential to isolate cell populations that exhibit desired activity.

In MetBo2 αCD19-synNotch clones, a drastic reduction in both the activation fold and percentage of activated population indicated the possibility for low stability of genomic integration and gene silencing. Epigenetic silencing of transgenes is a common challenge of recombinant gene expression in mammalian cells[100]. In particular, transgenes, that are expressed constitutively under strong promoters, or those regulated by synthetic transcription factors, are often subject to DNA methylation and chromatin remodelling[100,101]. Additional factors like genomic location[102] and promoters[103,104], as well as transcriptionally active/inactive state[105], have also been shown to play a role in long term expression of recombinant proteins. Therefore, it is important to take this into consideration in the synNotch cell line generation procedures. For example, future synNotch cell line engineering can be based on integrating gene cassettes into genomic safe harbours – well defined genomic locations with reduced epigenetic silencing activity[102].

3.4 Conclusions

Overall, experiments described in this chapter provide valuable insights into how synNotch receptor-reporter system operates and what considerations need to be undertaken in applying this system for its intended aims.

First of all, transient expression of the synNotch system results in high background fluorescence elicited from the reporter cassette, as well as high background activation associated with the transient expression of the receptor cassette. According to this, future efforts should involve genomic integration of both receptor and reporter cassettes. Secondly, it was revealed that certain chassis are suboptimal for the implementation of the synNotch system, specifically for the detection of macrophages. This is a crucial finding highlighting the importance of cell-cell interactions on changes of cell phenotype and behaviour.

To conclude, the following efforts will be focused on establishing stable monoclonal MetBo2 cell lines with genomic integration of both receptor and reporter cassettes. Specifically, genomic safe harbours will be considered for this purpose.

Chapter 4

Development of stable MetBo2 synNotch cell lines

Outline

In this chapter, the development of the stable synNotch MetBo2 cell lines will be covered. Primarily, this will be achieved through Cas9-mediated ROSA26 safe harbour engineering and genomic integration using the PiggyBac system. In general, this will be achieved through multiple steps:

a) Development of the MetBo2 landing pad cell line (MetBo2^{RMCE});
b) Development of a MetBo2 reporter cell line (MetBo2-UAS);
c) Development of monoclonal MetBo2 αCD19-synNotch, αF4/80-synNotch, αCD206-synNotch cell lines;
d) Testing of synNotch cell line candidate clones against sender cells;

The characterisation of the receptors developed in this chapter, as well as the development of sender cells will be covered in the following chapter.

4.1 Introduction

4.1.1 Methods for genomic integration of synthetic constructs

Previous attempts to implement a synNotch system in multiple types of mammalian cell lines revealed that transient and semi-transient expression of receptor-reporter system presents certain challenges such as high background activation levels and resulting low signal-to-noise ratios. One of the possible ways to overcome this problem is integrating genetic constructs into genomic DNA of host cells. This allows screening for clones with (i) non-leaky reporter expression and (ii) desired receptor activity. However, there are multiple ways and toolkits available for genomic integration of transgenes; therefore, careful consideration of the most optimal integration method was required.

4.1.1.1 Targeted genomic integration

Targeted integration implies incorporating a construct into a pre-defined place within the genomic DNA. This includes genomic safe harbours, for example AAVS1 or CCR5 loci in human cells[106,107], ROSA26[108] or Hipp11[109] in mouse cells, etc., which are notable for exhibiting low gene silencing potential. These safe harbours are typically well documented, and some of them have compatible commercial ready-to-use toolboxes available. Integration into these sites is usually mediated by DNA cleaving enzymes, such as Cas9, zinc finger nucleases (ZNFs) or TALEN[110,111]. Transgenes are then inserted by endogenous DNA repair mechanisms, for example homology-directed recombination (HDR) via homology arms present at 5' and 3' ends of the transgene cassette[111].

Alternatively, custom integration sites, usually referred to as landing pads, can be engineered into mammalian cell genomes. Landing pads allow highly efficient targeted integration of transgenes through recombination. Insulator sequences are often used to prevent heterochromatin spreading and subsequent

gene silencing. Recombination is achieved through recombinase-mediated cassette exchange (RMCE) through recombinase-specific *att* sites[112].

The main caveat of targeted genomic integration is a gene copy number limitation. In particular, without intentional cassette multiplication, insertion will be restricted to a single gene copy number (not taking into account potential off-target integration events). This can reduce the expression yield of transgenes, especially in the case of difficult-to-express proteins.

4.1.1.2 Non-targeted genomic integration

Non-targeted integration, on the contrary, results in integration of multiple cassette copies in numerous unspecified genomic locations. One of the simplest non-targeted genomic integration methods is transfecting mammalian cells with a plasmid vector containing a gene-of-interest (GOI) and selecting for clones with successful GOI expression. The efficiency of such method is low as it relies on spontaneous integration of plasmid DNA into the genome.

The efficiency of non-targeted genomic integration can be improved by using transposase-based methods like PiggyBac, Sleeping Beauty or Tc1/Mariner systems[113–115]. Transposase-based methods use plasmid vectors that have transposon sequences flanking the GOI. These sequences are used to incorporate the cassette into genomic DNA where the transposase recognises particular sequences within the genome. These are normally short, frequent sequences, which leads to high integration efficiency.

Another strategy for high-efficiency random integration is using lentiviral transduction. This involves producing lentivirus, that contains a GOI sequence and infecting the host cells. Lentivirus, in turn, co-expresses reverse transcriptase and integrase, which allows it to transcribe and integrate the GOI into favourable loci in genomic DNA[116].

Despite non-targeted genomic integration methods being highly efficient and resulting in multicopy insertions, their main caveat is a higher risk of

epigenetic silencing. Therefore, cell lines derived using non-targeted integration methods often need to be subjected to multiple rounds of selection and cell sorting.

4.1.2 Considerations for incorporating synNotch system into genomic DNA

4.1.2.1 ROSA26 safe harbour for reporter cassette integration

In synNotch systems, two GOIs must be integrated: a reporter cassette and a receptor cassette. For the reporter cassette integration, ROSA26 safe harbour was chosen. This way, a clonal reporter cell line (MetBo2-UAS) can be isolated, which exhibits a non-leaky inducible mCherry expression. Having reporter cassette integrated into a ROSA26 save harbour also allows to use the MetBo2-UAS cell line as a negative control in downstream experimental setup, as well as ensure stable reporter cassette long-term maintenance.

ROSA26 is a widely used genomic integration locus in mouse cells, which allows for stable expression of transgenes both *in vitro* and *in vivo*. Moreover, GOIs can be expressed under ROSA26 endogenous promoter. ROSA26 was first identified by Philippe M. Soriano and his group during a gene trap experiment, where researchers randomly integrated a promotor-free retroviral β-galactosidase cassette into the mouse genome aiming to discover and characterise previously unidentified genes[108]. The cassette landed into a previously undescribed locus, which resulted in ubiquitous expression of β-galactosidase in mouse embryos[108]. The locus was later called ROSA26 (reverse orientation splice acceptor) and is located on the chromosome 6 in the mouse genome. A ROSA26 homolog was also identified in the human genome[117].

Synthetic constructs can be integrated in ROSA26 locus through homologous recombination (HR) or homology-directed recombination (HDR). In this work, the CRISPR/Cas9 system was used, and therefore, cassette insertion was carried out via HDR through 5’ and 3’ ROSA26 homology arms flanking the cassette (Fig. 4.1).

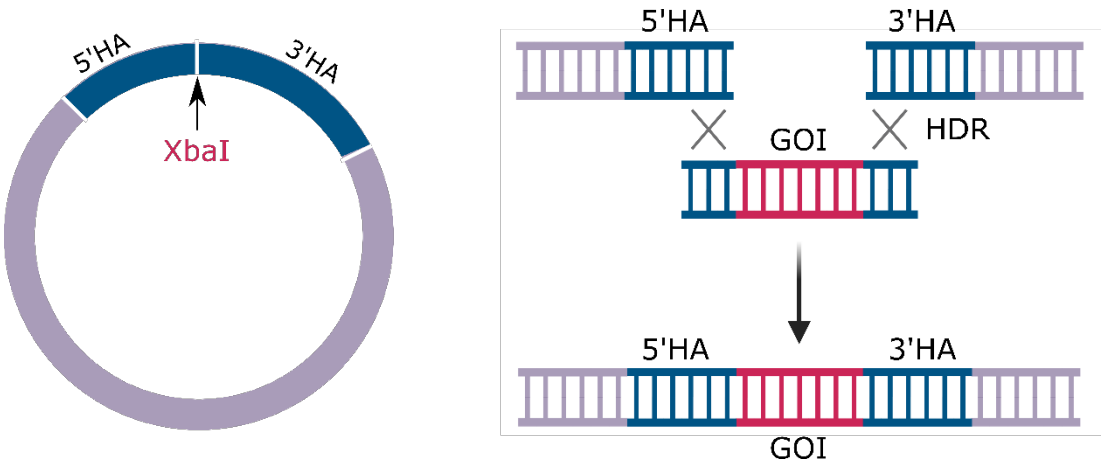

Figure 4.1. ROSA26 integration via homology-directed repair mechanism. *Vector design for ROSA26-targetting vector includes flanking the gene of interest (GOI) with 5‘ and 3‘ homology arms (HA). Vector used in the experiments performed in this thesis had an XbaI cutting site between the homology arms for GOI cassette integration. HA – homology arms. GOI – gene of interest. HDR – homology-directed repair.*

The development of a MetBo2-UAS cell line was carried out in two stages (Fig. 4.2). First, a landing pad was established in the ROSA26 locus to create a donor cell line (MetBo2^{RMCE}). Having a donor cell line allows fast and easy recombinase-based genomic integration in ROSA26 locus for future constructs. Second, a reporter cassette was integrated using Φc31 recombinase. The strategy was previously described in the context of creating TetO reporter cell line by Malaguti at al. [76].

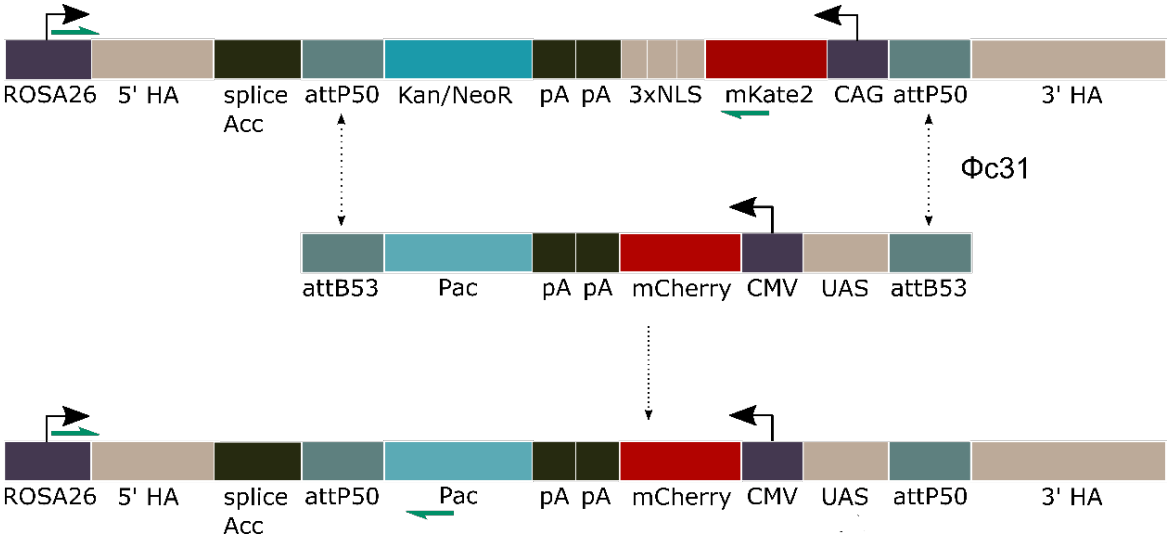

Figure 4.2. The design of the constructs used in the generation of MetBo2-UAS cell line. *First, a landing pad was established, which incorporated two selection markers – G418 resistance cassette, expressed from endogenous ROSA26 promoter upon successful integration, and a nuclear mKate2 fluorescence. Using Φc31 recombinase this cassette was exchanged to a UAS cassette, which conferred the cells to puromycin resistance (while losing G418 resistance). HA – homology arms. Kan/NeoR – Kanamycin/Neomycin (G418) resistance gene. pA – polyadenylation sequence. NLS – nuclear localisation sequence. CAG – Cytomegalvirus immediate enhancer/β-actin promoter. Pac – puromycin acetylase (puromycin resistance gene).*

4.1.2.2 PiggyBac system for receptor cassette integration

As it was discussed in section 4.1.1.2, introducing GOIs in safe harbours limits the number of genomic integrations. Therefore, the strategy for integrating synNotch into genomic DNA was based on using the PiggyBac transposon system.

Transposons, being mobile genetics elements, are DNA sequences of viral origins that are able to either move autonomously within or across genomes, or non-autonomously with the help of other transposons[118]. Transposons can be DNA-based or RNA-based[119]. The latter are called retrotransposons and require a reverse transcriptase to convert their RNA sequence into DNA sequence for further integration[119].

A PiggyBac system was isolated from cabbage looper moth *Trichoplusia ni*[120]. Its potential in gene engineering was soon realised and strengthened by unique PiggyBac properties: it is able to carry extremely large inserts (up to 100 kb)[121], has high integration efficiency in many different cell types and does not leave DNA footprints or scars upon excision[122]. PiggyBac transposase integrates constructs flanked by PiggyBac inverted terminal repeats (ITRs) into 5'-TTAA-3' locations in the genomic DNA[122]. Because of such short recognition sequence, PiggyBac integration results in a relatively high number of integrated gene copies. This property is highly favourable for the synNotch integrations, since it can potentially engineer cells with higher receptor expression, and therefore higher recognition capacity.

Therefore, in order to incorporate the receptor cassette into genomic DNA, the cassette must be cloned into a PiggyBac vector, where it is flanked by PiggyBac ITRs. In order for PiggyBac integration to happen, a carrier vector must be co-transfected with a plasmid coding for PiggyBac transposase. Here, an engineered high efficiency transposase – hyPBase – was used[123].

4.2 Results

4.2.1 Development of a MetBo2^{RMCE} cell line

The landing pad cassette consists of two selection markers: a neomycin (G418) resistance ORF with upstream splice acceptor for expression from ROSA26 endogenous promoter, and a CAG-mKate2_3xNLS cassette, which results in nuclear mKate2 fluorescence (Fig. 4.3A). A plasmid, containing this landing pad was co-transfected into wild-type MetBo2 cells along with a ROSA26 Cas9-gRNA plasmid at 2:1 ratio (500 : 250 ng) in a 12 well plate. Following selection with G418, subsequent expansion and single cell sorting with FACS, a monoclonal population of mKate2-positive cells was isolated (Fig. 4.3B). Importantly, prior to cell sorting, the cells were lifted using Accutase™ cell dissociation reagent, which allowed for a more efficient cell adherence and recovery post-sorting. This was applied

throughout all the cell sorting procedures discussed in this thesis. Targeted integration into ROSA26 was confirmed with PCR on genomic DNA (Fig. 4.3C).

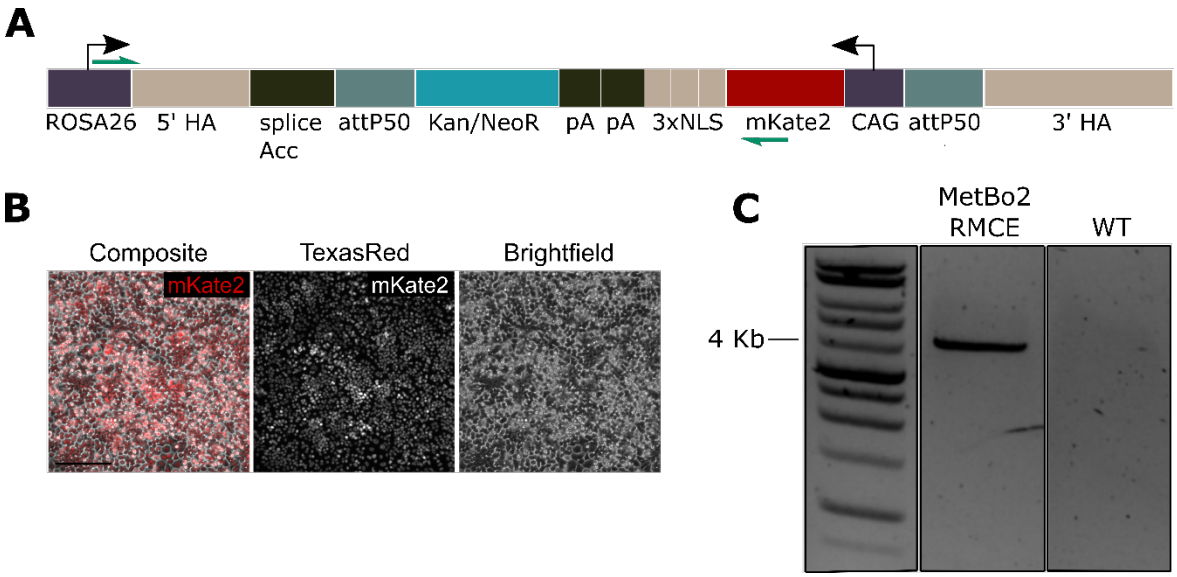

Figure 4.3. Development of MetBo2^{RMCE} cell line. *(A) Landing pad construct that was integrated into ROSA26 locus. Kan/NeoR conferred the cells to G418 resistance; mKate2-3xNLS exhibited red nuclear fluorescence. (B) Nuclear mKate2 expression in a selected clone. Scale bar 100 µm. (C) Targeted integration into ROSA26 locus was confirmed by PCR (4109 bp). Green arrows indicate primer binding sites. HA – homology arms. Kan/NeoR – Kanamycin/Neomycin (G418) resistance gene. pA – polyadenylation sequence. NLS – nuclear localisation sequence. CAG – Cytomegalovirus immediate enhancer/β-actin promoter.*

After clonal isolation of a MetBo2^{RMCE}, a RMCE was performed on a landing pad, inserting a UAS-mCherry cassette. UAS-mCherry cassette was designed as illustrated in figure 4.4A. The cassette includes a puromycin resistance ORF upstream the 5xGal4-UAS-minCMV-mCherry cassette. Upon successful integration, cells lose their resistance to G418 and acquire resistance to puromycin.

MetBo2^{RMCE} cells were co-transfected with UAS-mCherry reporter cassette plasmid and Φc31 encoding plasmid at a 1:1 ratio (250 : 250 ng) in a 12 well plate. Several monoclonal populations of puromycin-resistant cells were recovered after cell sorting with FACS and tested for activation with Gal4VP64 transcriptional activator. After identifying monoclonal populations that elicit an mCherry response upon transfection with Gal4VP64, a clone with the highest activation was selected (Fig. 4.4B). The clone exhibited a 317.1-fold increase in

mCherry fluorescence when transfected with Gal4VP64, compared to a 2.2-fold increase when both reporter and transactivator constructs were transiently expressed in MetBo2 cells (Fig. 4.4C-D). However, it is important to note that using transfection controls in these experiments would allow to acquire more reliable and quantitatively comparable data between transiently expressed and stably integrated UAS-mCherry cassettes. Successful integration into the landing pad was confirmed by PCR (Fig. 4.4E).

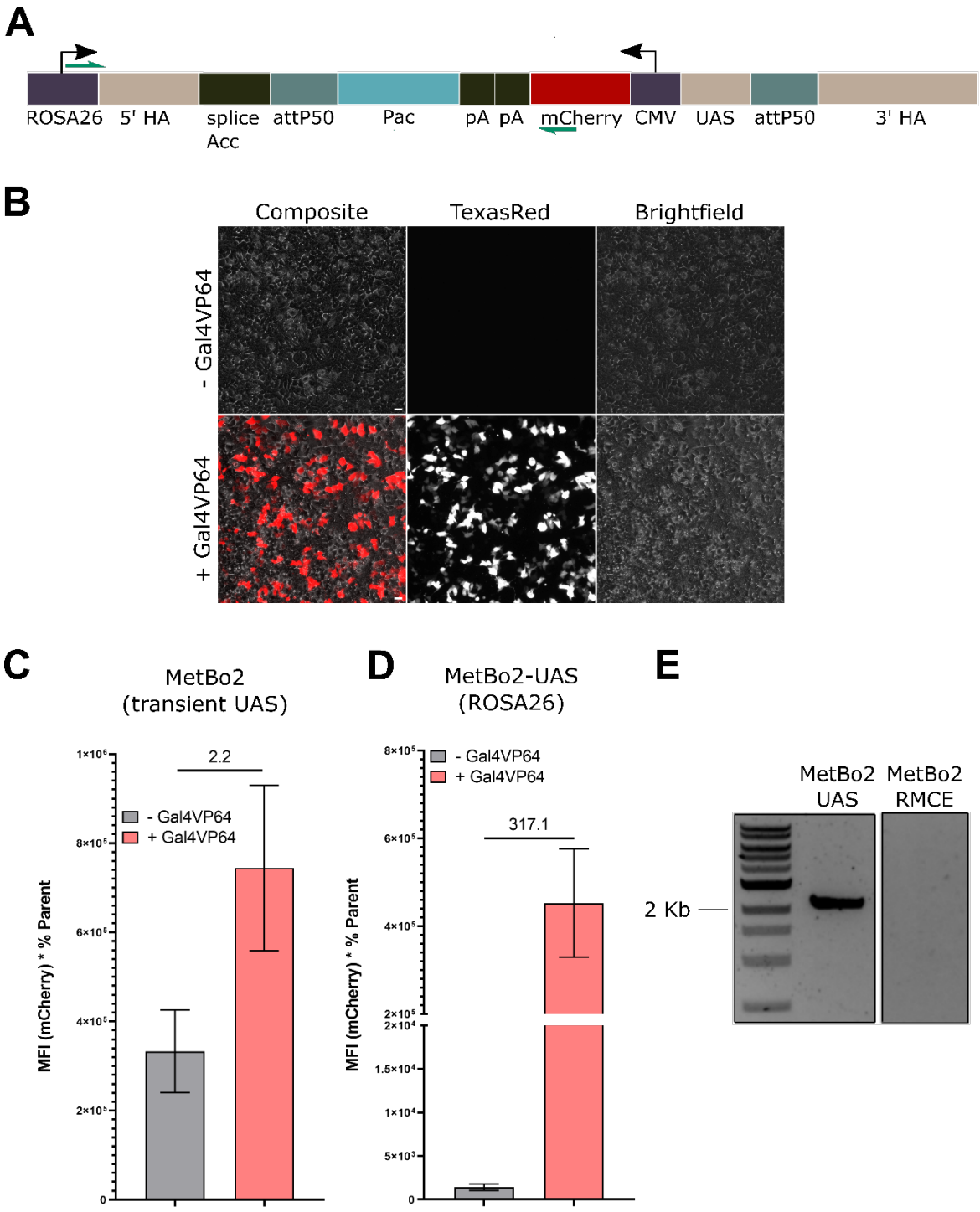

Figure 4.4. Development of MetBo2-UAS cell line. *(A) A UAS-mCherry construct schematic after integration into ROSA26 locus. Pac conferred the cells to puromycin resistance. (B) Selected clone exhibited no mCherry fluorescence in absence of Gal4VP64 transcriptional activator and high mCherry fluorescence when transfected with Gal4VP64. Scale bar 10 µm. (C) MetBo2 cells, transiently transfected a reporter UAS-mCherry cassette and tested for activation with Gal4VP64. (D) Monoclonal MetBo2-UAS cells tested for reporter cassette activation with Gal4VP64 transcriptional activator. (E) Targeted integration into ROSA26 locus was confirmed by PCR of genomic DNA (2175 bp). Green arrows indicate primer binding sites. HA – homology arms. Kan/NeoR – Kanamycin/Neomycin (G418)*

resistance gene. pA – polyadenylation sequence. NLS – nuclear localisation sequence. CMV – Cytomegalvirus promoter.

4.2.2 Development of synNotch monoclonal cell lines

Three synNotch architectures were engineered and integrated into MetBo2-UAS cells: αCD19-synNotch, αCD206-synNotch and αF4/80-synNotch. For αCD19-synNotch cassette, the original construct from Morsut et al. was used, while αCD206-synNotch and αF4/80-synNotch were engineered with novel ICDs[86,87]. The receptor cassette (PGK-scFV/VHH-synNotch-Gal4VP64) was followed by a downstream PGK-H2B-TagBFP cassette for lineage tracking purposes. The whole receptor cassette was flanked by PiggyBac ITRs (Fig. 4.5A).

MetBo2-UAS cells were co-transfected with the above-mentioned synNotch vectors and hyPBase vector at 2:1 ratio (500 : 250 ng). Cells were subjected to FACS sorting into heterogenous populations of TagBFP$^+$ cells 4 days post transfection to enrich for synNotch-positive candidates. After expansion, cells were co-cultured with respective sender cells for 24 hours and activated cells (mCherry$^+$) were sorted into single cells.

Expanded monoclonal populations were then tested by presenting them to respective sender cells and assessing activation using flow cytometry (Fig. 4.5B-C). The sender cells for these experiments were MetBo2 cells, transiently expressing recombinant ligands. The development of the sender cells will be described in chapter 5. Clones with the highest background to activation ratio were chosen for further work and characterisation. This way, αCD19-synNotch and αCD206-synNotch clones were isolated (Fig. 4.5B, C). However, attempts to isolate a αF4/80-synNotch clone were unsuccessful as no significant activation was observed when presenting either heterogenous or monoclonal αF4/80-synNotch cells to either recombinant F4/80$^+$ sender cells (data not shown) or F4/80$^+$ mouse peritoneal macrophages (Fig. 4.5D). Clones number two and four for αCD19-synNotch and αCD206-synNotch, respectively, were chosen for further experiments.

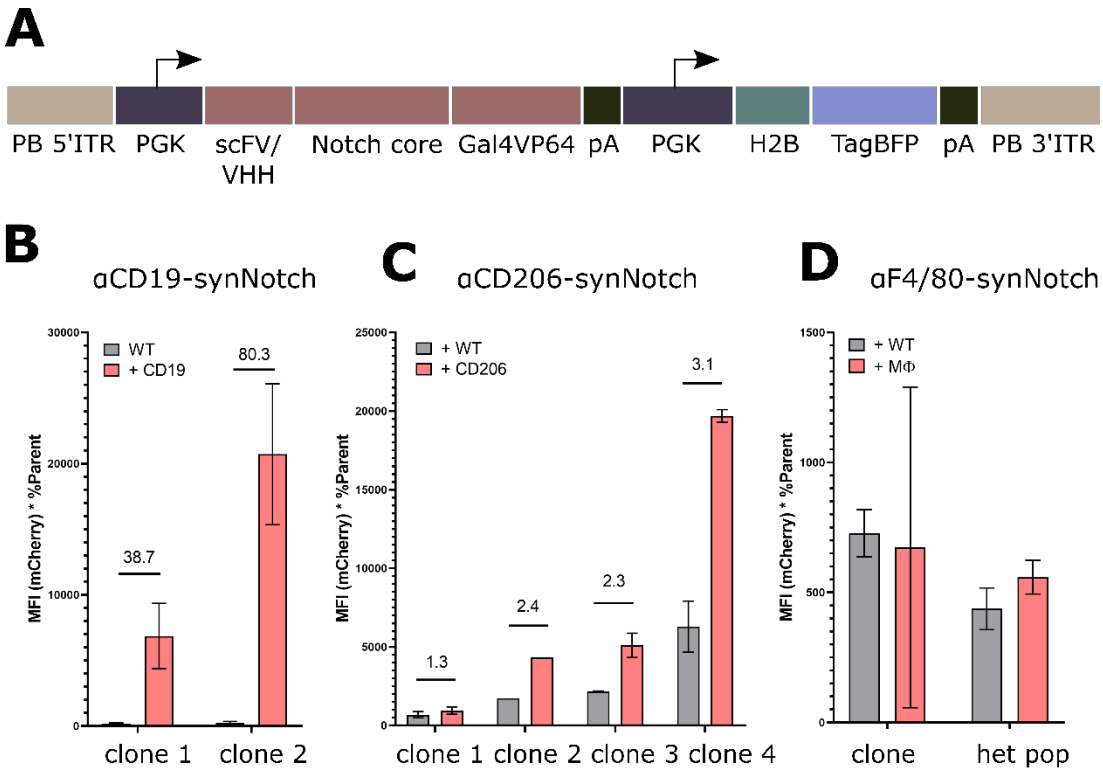

Figure 4.5. Development of monoclonal synNotch cell lines. *(A) Schematic representation of synNotch PiggyBac construct. (B) Two αCD19-synNotch clones were isolated and tested for activation with CD19⁺ cells. (C) 4 clones of αCD206-synNotch were isolated and tested for activation with CD206⁺ cells. (D) αF4/80-synNotch failed to achieve activation as both heterogenous population and monoclonal population when presented to F4/80+ cells. All clones were analysed in triplicates unless no error bars indicated. PGK – phosphoglycerate kinase promoter. scFV – single chain variable fragment. H2B – human histone 2B. pA – polyadenylation sequence.*

4.3 Discussion

The aims of this chapter involved developing monoclonal synNotch cell lines, which would exhibit receptor activation upon co-culture with respective sender cells. In order to achieve that, cells were engineered using genomic DNA manipulation tools such as CRISPR/Cas9 for reporter cassette integration and a PiggyBac transposon system for receptor cassette integration. Consequently, MetBo2-UAS, αCD19-synNotch and αCD206-synNotch cell lines were created.

However, the attempts at isolating monoclonal αF4/80-synNotch were unsuccessful.

4.3.1 Off-target integrations of reporter cassette

Despite the confirmation of targeted genomic integration of the reporter cassette in ROSA26 safe harbour, the possibility and frequency of off-target integration was never assessed in this research. Although multiple copy integration of UAS-mCherry reporter cassette might not have an effect on the function and efficiency of the receptor-reporter system, variability among different synNotch receptor cell lines severely restricts their direct comparison.

CRISPR/Cas9-guided genomic integration is not devoid of off-target integration effects. This can potentially happen in case of high sequence similarity of genomic sequences to the sequence of ROSA26 gRNA. Published prediction analysis indicated potential high similarity sequences in the mouse genome, however, only a few of them are expected to exert high risk of off-target integration[124]. Despite that, it would be beneficial to evaluate the transgene copy numbers for the purpose of cell line characterisation. This can be achieved using Southern blot, qPCR or digital droplet PCR (ddPCR)[125].

Conversely, a greater variability in the reporter-receptor system outcome can be caused by the varying numbers of receptor copies within a cell and a monoclonal population as a whole over generations. It has been reported that increased amount of transiently expressed synNotch resulted in higher receptor activation as well as high background activation levels[83]. This can potentially explain why certain clones exhibit higher background activation than others. Although quantifying the receptor copy number in those clones would be possible with commercial kits, due to the non-targeted nature of PiggyBac integration, monoclonal population can potentially become heterogenous in their level of receptor expression as well as in the response level due to epigenetic silencing. It has been demonstrated before that PiggyBac inserts are susceptible to transcriptomic silencing post-integration, although it is highly dependent on genetic context at the integration site[126]. Therefore, synNotch clones will require continuous re-sorting to

re-select the cells with high activation capacity. Alternatively, the system can be made more stable with the use of insulating sequences flanking the insert[127]. All in all, the need for ensuring stability and integrity of genomic integrations over generations is a major caveat in development of stable cell lines for diagnostic and therapeutic applications.

4.3.2 The problem of non-functional αF4/80-synNotch

Interestingly, the attempts at isolating a functional αF4/80-synNotch clone were unsuccessful. Although a small number of activated cells was detected during cell sorting of heterogenous αF4/80-synNotch population, none of the expanded clones exhibited sufficient activation level when presented to either recombinantly expressed F4/80 in MetBo2 cells, or F4/80$^+$ peritoneal macrophages.

The problem of certain receptor architectures being non-functional has not been explored in sufficient detail in the published literature. However, Morsut et al. reported that some of the receptor architectures they constructed were non-functional[66]. Among those were anti-GFP-synNotch-Gal4VP64, anti-GFP and anti-CD19-synNotch-Gal4-KRAB, anti-GFP and anti-CD19-synNotch-ZFHD/VP64, and anti-myc-synNotch-Gal4VP64[66]. Although the authors did not comment on these findings, they still provide valuable insight that certain functional domain combinations are incompatible.

One of the most crucial steps in the expression of transmembrane recombinant proteins is the correct protein folding in the cell plasma membrane. Naturally, incorrect folding is likely to prevent receptor from ligand binding and subsequent opening of transmembrane cleavage sites. One of the avenues that could be explored is extending synNotch transmembrane domain, since it was reported that additional linkers may result in a more robust receptor activity[66,82,83]. In these clones, however, synNotch was not tested for correct membrane localisation, which is one of the steps that must be undertaken in the future work. Nevertheless, exploring the problem of non-functional αF4/80-synNotch could provide valuable knowledge on not only receptor mode of action, but on future design considerations of transmembrane proteins.

4.4 Conclusions

Experiments presented in this chapter resulted in the development of two functional synNotch receptor cell lines: αCD19-synNotch and αCD206-synNotch. Further characterisation of these cell lines in regards to receptor activity relative to appropriate controls, as well as receptor specificity will be described in the following chapter.

Chapter 5

Assessing activity of clonal synNotch cell lines

Outline

In this chapter the testing and characterisation of the synNotch clones, developed in the chapter 4 will be carried out. This will be achieved in the following steps:

a) Development of recombinant sender cells: engineering recombinant CD19, F4/80 and CD206 vectors and their expression and validation in MetBo2 cells;
b) Testing of monoclonal MetBo2 αCD19 synNotch and αCD206 synNotch cell lines for activation against cognate sender cells;
c) Assessing synNotch receptors for cross-reactivity;

5.1 Introduction

In the previous chapter, functional αCD19-synNotch and αCD206-synNotch monoclonal cell populations were isolated. This chapter will aim at improving on synNotch receptor characterisation by quantitatively assessing synNotch receptor activity, its dependence on ligand availability and specificity towards cognate ligands.

5.1.1 Considerations for the sender cells in further synNotch experiments

In chapter 3 the importance of sender cells in receptor-reporter systems was discussed. Collectively, in the previous chapters, various sender cells have been used to assess synNotch activity: HEK293^{CD19}, BL2 (CD19^{+}), RAW264.7 (F4/80^{+} and CD206^{+}) and peritoneal macrophages. In order to have a more reliable and streamlined receptor testing platform, sender cells must be simplified and standardised. Experiments described in chapter 3 revealed that using sender cells that endogenously express ligands of interest introduces greater complexity in establishing synNotch cell lines, as observed in L929 αCD19-synNotch co-cultures with RAW264.7 cells, where macrophage's phenotype was potentially modified by L929 cells. In the published literature, sender cells which recombinantly express the ligand of interest are often used (e.g. L929^{CD19} [42,66], K562^{CD19} [44,66], L929^{GFP} [41,85]). Therefore, a similar approach was implemented in this work. In particular, MetBo2 sender cells were selected as sender cells in the following experiments in order to achieve relative homogeneity in activation co-cultures *in vitro*. While in the published literature the host cells for ligand expression are often a different cell type to the receptor cells[42–44,66], using the same cell chassis for both receiver and sender cells may allow to eliminate the possibility of receptor activation by endogenous ligands present on the surface of other cell types during selection of receptor cell clones.

Consequently, it was decided to express CD19, F4/80 and CD206 transiently in MetBo2 cells. Transient expression was selected as it allows high levels of transgene expression within the first days post-transfection. As described

in Chapter 3, CD19 sequence was already extracted from cDNA of human lymphoblastoid cells (LCLs). Similarly, coding sequence for F4/80 and CD206 were extracted from mouse macrophage cDNA.

5.1.2 Important notes on methodology for assessing receptor activity *in vitro*

The synNotch system is a complex and dynamic system, and its performance can be greatly influenced by a flawed experimental pipeline. Prior to characterising the different synNotch cell lines derived in this work, certain aspects of methodology were considered.

First of all, it was important to ensure normalised growth conditions among co-cultures. Co-cultures are carried out in cell culture dishes, and therefore cell growth is restricted by the available surface of the wells. Difference in cell growth dynamics, and so difference in cell function or behaviour can result in flawed data acquisition and subsequent data analysis. Therefore, along with co-culturing receptor cells with sender cells, receptor cells were also co-cultured with wild-type MetBo2 cells as a negative control (Fig. 5.1A). In addition to normalising growth conditions, this also contributed to achieving more reliable quantitative data.

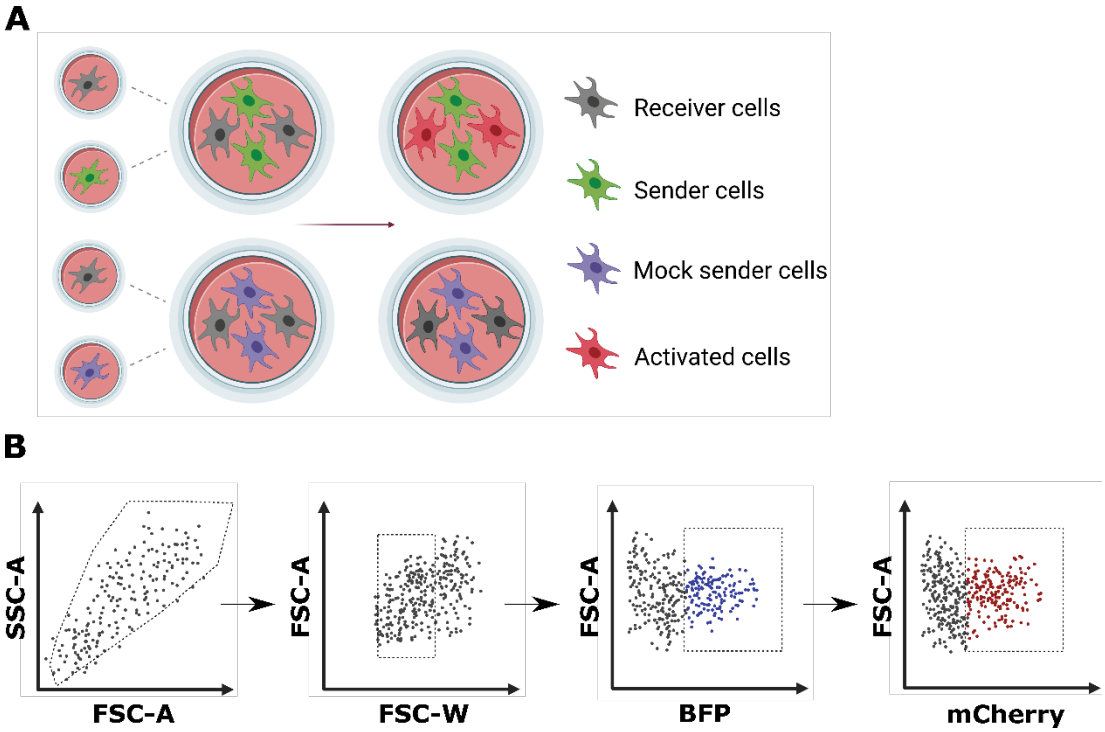

Figure 5.1. Notes on experimental workflow. *(A) Co-culture pipeline for normalisation of co-culture conditions among test and control wells. While test wells contained co-cultures of receptor and sender cells, control wells contained co-cultures of receptor and wild-type MetBo2 cells. (B) Flow cytometry gating strategy. First, cells were gated by size using forward and side scatters. Next, singlets were isolated by plotting width (FSC-W) against the area (FSC-A) of a forward scatter. Later cells were gated by TagBFP fluorescence and only TagBFP+ cells were analysed for mCherry expression.*

Additionally, receptor construct design involved using a H2B-TagBFP tag for lineage tracking purpose. In this experimental pipeline, BFP fluorescence was used for isolating synNotch cells during flow cytometry, i.e., only BFP^+ cells were analysed for mCherry fluorescence resulting from synNotch activation. Total fluorescence of activated cell population was quantified by multiplying mean fluorescence intensity (MFI) by the percentage of $mCherry^+$ cells in a total population of $TagBFP^+$ cells. The flow cytometry gating workflow is illustrated in figure 5.1B.

5.2 Results

5.2.1 Development of recombinant sender cells

Coding sequences for mouse F4/80 (NM_010130.4, 21 – 2836 nt) and mouse CD206 (NM_008625.2, 81 – 3835 nt) were determined from NCBI database. Notably, CD206 CDS was limited to only its putative extracellular domain (ECD) due to the large size of a full CD206 sequence (5322 bp).

F4/80 CDS was successfully extracted from the cDNA of RAW264.7 macrophages (Fig. 5.2A). Interestingly, attempts at acquiring CD206 CDS from RAW264.7 were unsuccessful. Since expression of CD206 is characteristic of M2 polarised macrophages, RAW264.7 were induced with interleukin-4 (IL-4). IL-4 is cytokine that contributes to the M2 macrophage phenotype *in vivo* and *in vitro*[20]. Again, no CD206 CDS was detected by PCR. Inducing bone marrow-derived macrophages (BMDMs) with IL-4, however, allowed successful isolation of CD206 ECD fragment (Fig. 5.2A). CD19, CD206 and F4/80 fragments were cloned into a mammalian expression vectors. Schematic representations of the constructs are shown in figure 5.2B. CD19 cassette comprised of a membrane-targeting signal peptide (IgK leader) and an HA tag upstream from CD19 coding sequence, and a myc-tag and PDGFRβ membrane anchor domain downstream. Since full F4/80 coding sequence was extracted from cDNA of RAW264.7 cells, the cassette did not include any additional membrane targeting peptides, membrane anchors or tags and relied on endogenous F4/80 membrane targeting sequence. Speaking of CD206, similarly, the membrane targeting relied on endogenous signal peptide. However, since only the putative ECD of CD206 was extracted, a myc-tag and a PDGFRβ domain were incorporated downstream in order to anchor the ECD at the cell surface (Fig. 5.2B). Consequently, these vectors were used to transiently transfect MetBo2 sender cells 24 hours prior to co-culture.

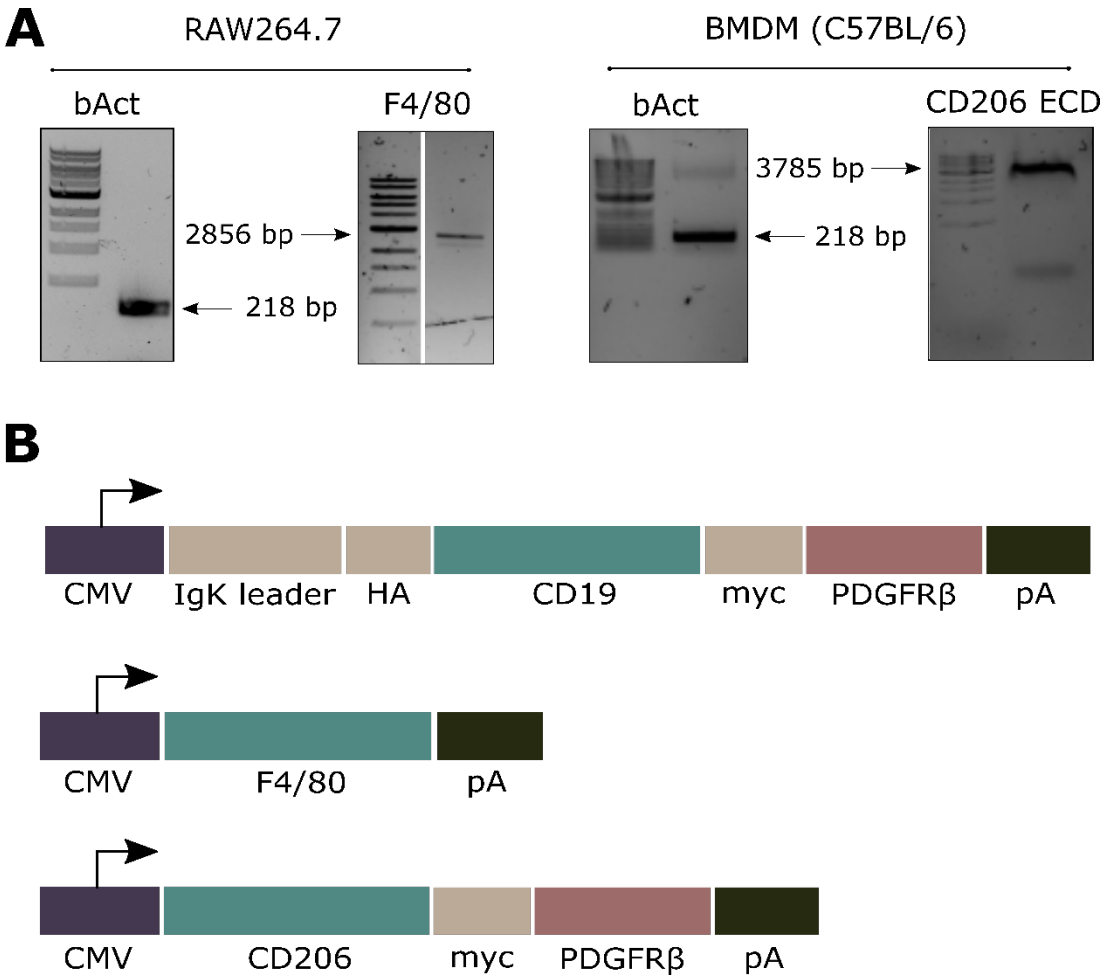

Figure 5.2. Development of vectors for recombinant expression of F4/80 and CD206 on sender cells. *(A) Extraction of F4/80 and CD206 ECD CDSs from cDNA of macrophages. F4/80 CDS was extracted from cDNA of RAW264.7 cells (left). CD206 ECD CDS was extracted from IL-4 stimulated bone marrow-derived macrophage cDNA. B-actin was used a housekeeping gene for validation of cDNA. (B) Final constructs for expression of three ligands: CD19, F4/80 and CD206. Both F4/80 and CD206 had native membrane-targeting sequences at the N-termini. CMV – Cytomegalovirus mammalian promoter. HA - Human influenza hemagglutinin tag. Myc – c-myc tag. PDGFRβ - Platelet-derived growth factor receptor beta transmembrane domain. pA – polyadenylation sequence.*

In order to assess the expression of recombinant ligands in sender cells and ensure that the small antibody domains (VHH or scFV) used as synNotch ECDs effectively bind their respective ligands, a platform developed by Ugne Baronaite in the Cachat lab was used. Vectors, containing anti-CD19 and anti-F4/80 scFV, as well as anti-CD206 VHH, fused to an exportation sequence at their 5' end and sfGFP at their 3' end, were transfected in HEK293T cells (Fig. 5.3A). This allowed production and exportation of soluble sfGFP-tagged ECDs, which were harvested as supernatant and used in fluorescent imaging experiments by applying the supernatants on transiently transfected MetBo2 sender cells. This approach was adopted due to the fact that commercial antibodies for CD19 and CD206 (for details see Methods) revealed unspecific staining on wild-type cells, which was not observed when small antibody domains were used instead. Consequently, the ability of the small antibody domains to recognise their cognate ligands was confirmed by fluorescent microscopy (Fig. 5.3B), where positive binding was indicated by GFP fluorescence. Therefore, it was concluded that recombinant ligands are being expressed in MetBo2 cells and the small antibody domains used as synNotch ECDs correctly interact with their sender cell targets. These results also demonstrate low numbers of stained cells, however, it is unclear whether this is due to the low expression or low transfection efficiency, since no transfection controls were used in these experiments.

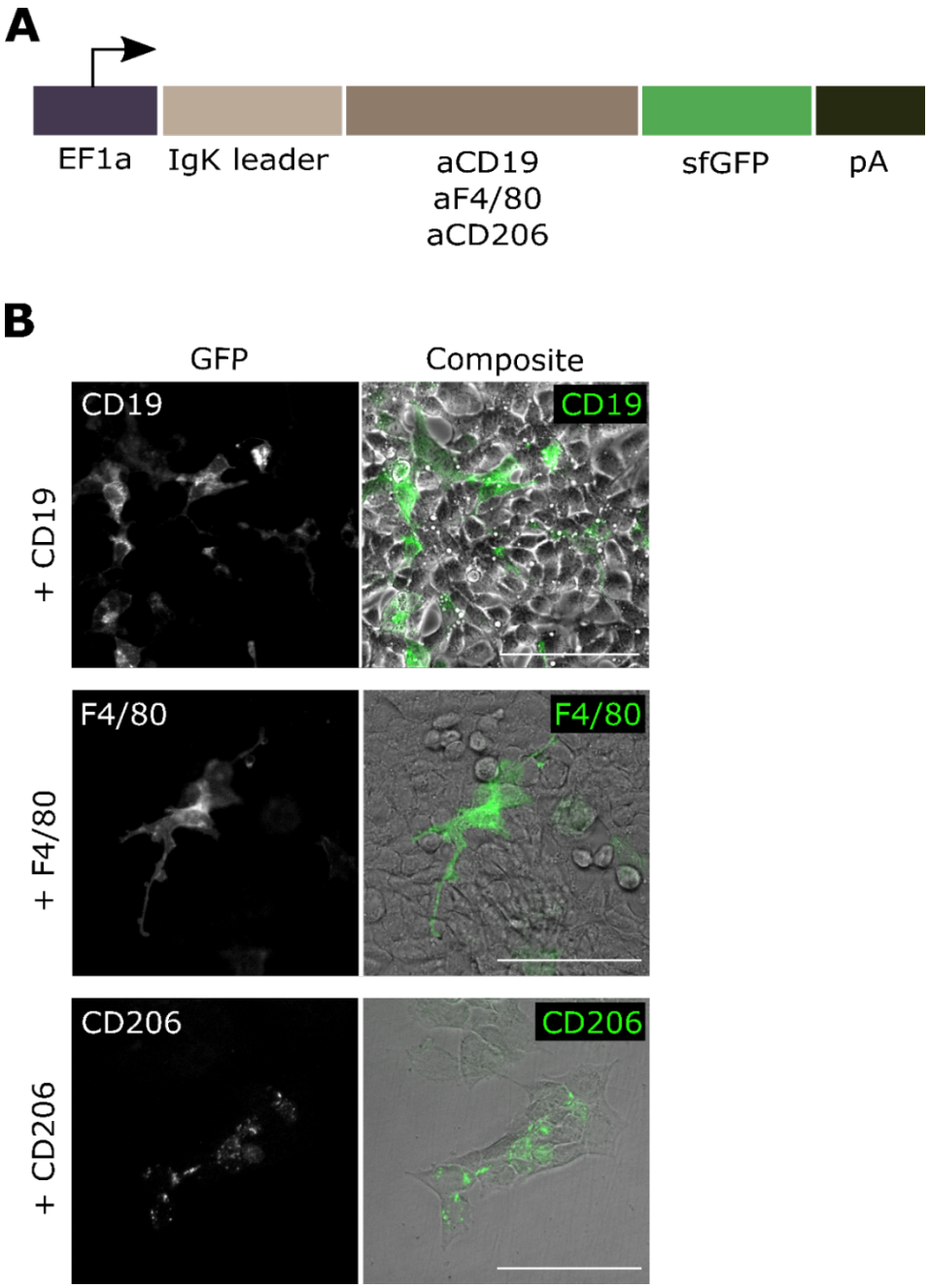

Figure 5.3. Validation of ligand expression on transiently transfected sender cells. *(A) The generalised scheme of a soluble scFV/VHH, fused to sfGFP, construct. (B) Immunostaining of MetBo2 cells, transiently transfected with respective ligands. Positive staining is indicated by GFP fluorescence. All recombinant ligands were successfully expressed on the surface of MetBo2 cells. Staining was performed on live cells. pA – polyadenylation site. Scale bar 100 µm.*

5.2.2 Evaluation of αCD19-synNotch and αCD206-synNotch receptor activity

Monoclonal populations of αCD19-synNotch and αCD206-synNotch were subjected to further testing against MetBo2 sender cells in order to isolate clones with the highest response activity. αF4/80-synNotch failed to respond to stimulation with MetBo2 F4/80$^+$ cells (data not shown). Among all three engineered receptors, only αCD19-synNotch demonstrated receptor activation high enough to be observed by fluorescent microscopy (Fig. 5.4A). Interestingly, compared to the initial screening conducted on MetBo2 CD19$^+$ cells, where αCD19-synNotch clone exhibited 80.3-fold activation, over the course of six generations the αCD19-synNotch clone exhibited 54.8-fold activation when presented to MetBo2 CD19$^+$ sender cells (Fig. 5.4B). Conversely, αCD206-synNotch exhibited sustained activation (2.9-fold) when stimulated with CD206$^+$ cells (Fig. 5.4C). Additionally, both clones demonstrated a dose-dependent activation pattern with increasing amount of ligand expression vector transfected in sender cells (Fig. 5.4D, E), with a sharp increase in activation when cells were transfected with 450 ng and 550 ng of plasmid for αCD19-synNotch and αCD206-synNotch, respectively.

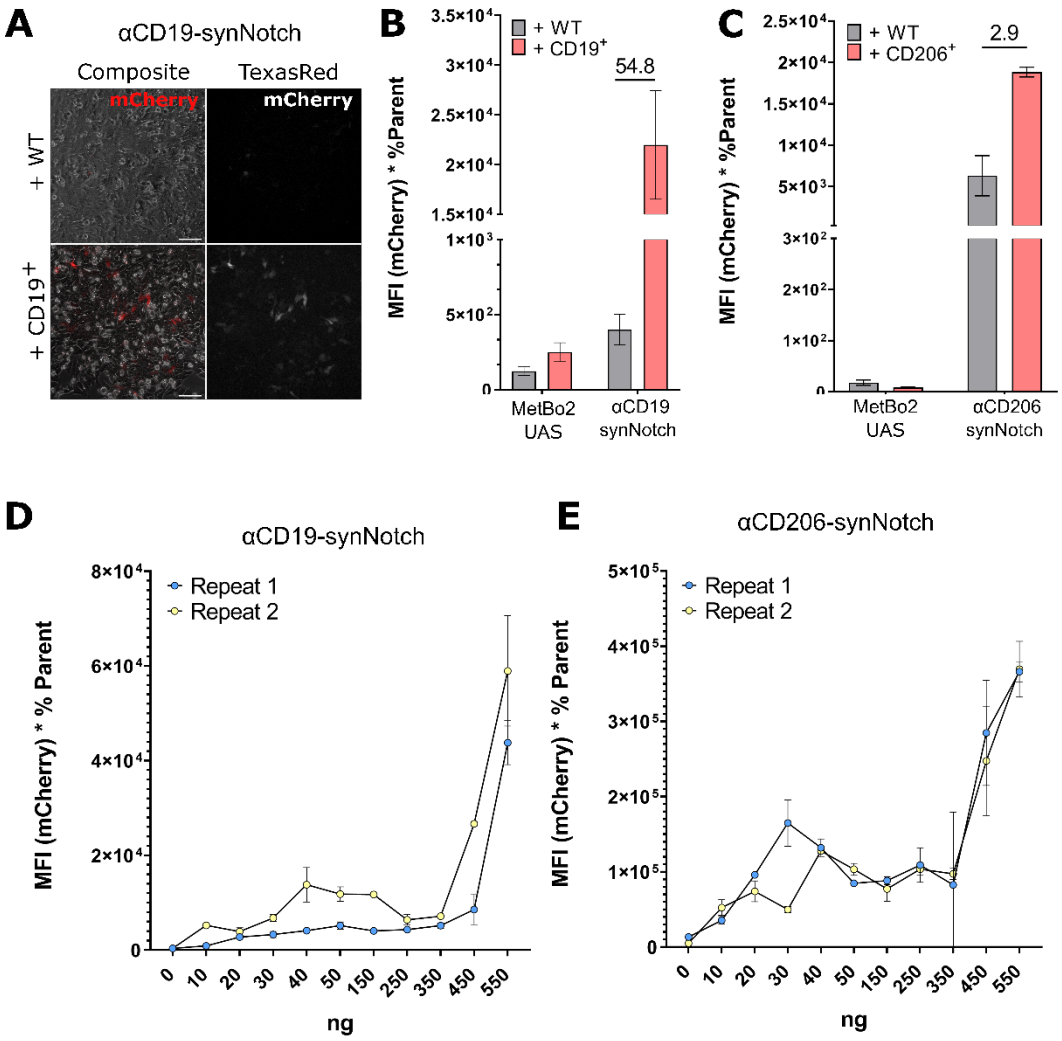

Figure 5.4. Evaluation of synNotch receptor activity. *(A) Microscopy images indicating αCD19-synNotch activation with MetBo2 CD19⁺ cells. Scale bar 10 μm. (B) 54.8-fold activation was observed when αCD19-synNotch cells were presented to CD19⁺ cells. (C) αCD206-synNotch exhibit a 2.9-fold increase in mCherry fluorescence in co-culture with CD206⁺ cells. (D) and (E) demonstrate increase in fluorescent response, proportional to the increase in ligand saturation on sender cells.*

5.2.3 Both αCD19-synNotch and αCD206-synNotch exhibit unspecific activity

In order to assess whether anti-CD19 and anti-CD206 receptors exhibit selectivity for their corresponding ligands, receptor cross-specificity was assessed. Receptor cells were co-cultured with various sender cells and receptor activation was assessed with flow cytometry. Interestingly, αCD19-synNotch demonstrated high activation fold when co-cultured with MetBo2 F4/80$^+$ sender cells (10.2-fold) while αCD206-synNotch exhibited unusually high fluorescence intensity when co-cultured with CD19$^+$ sender cells (22.2-fold) (Fig. 5.5). The reason for this in unclear as co-cultures with wild-type MetBo2 cells didn't exhibit elevated levels of fluorescence.

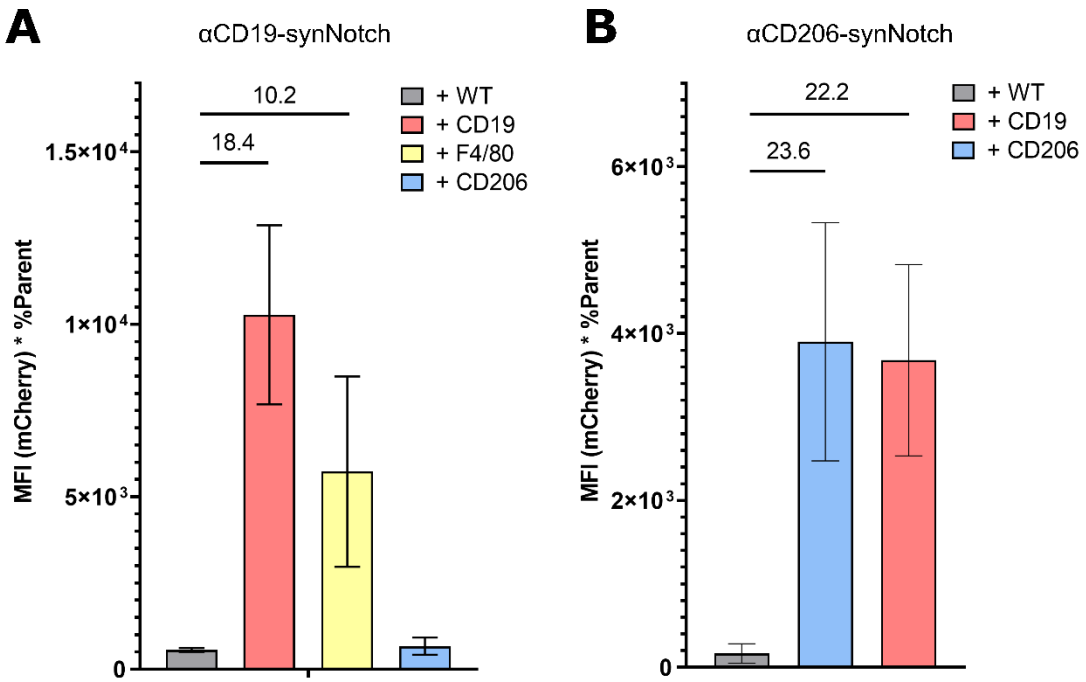

Figure 5.5. Evaluation of synNotch cross-reactivity with other ligands. *(A) αCD19-synNotch demonstrated 10.2-fold receptor activation when presented to F4/80$^+$ cells. (B) αCD206-synNotch exhibited a 22.2-fold increase in fluorescent response when presented to CD19$^+$ cells. Interestingly, both αCD19-synNotch and αCD206-synNotch demonstrated variability in receptor activation folds over generations with αCD19-synNotch reporting a significant drop in activation and αCD206-synNotch - an unusually high increase in mCherry fluorescent in co-cultures with respective ligands, compared to previous experiments.*

Moreover, these results repeatedly demonstrated the fluctuations in synNotch activity over generations. While αCD19-synNotch activation dropped significantly to 18.4-fold increase in mCherry fluorescence, αCD206-synNotch activation levels increased to 23.6-fold difference in reporter activity (Fig. 5.5).

5.2.4 synNotch ECDs demonstrate high levels of non-specific binding to multiple immune cell subsets

Next, in order to assess if unspecific receptor activation was caused by unspecific binding between synNotch ECD on receptor cells and ligands on sender cells, a testing platform against multiple endogenous immune cell subpopulations was developed. The idea behind this strategy was to perform an immunostaining assay using soluble small antibody domains used as synNotch ECDs on C57BL/6 mouse spleen extract in order to investigate whether they are capable of correctly binding endogenous epitopes on respective immune cell populations, as well as to assess them for cross-reactivity. Since mouse spleen is abundant with a wide range of immune cell subpopulations like leukocytes, granulocytes, macrophages and monocytes, T cells, B cells, etc., the extract provides a good substrate for the assessment of cross-reactivity of synNotch ECDs.

Mouse spleen extract was stained with five antibodies, specific to distinct immune cell markers, such as CD206, CD3, B220 (CD45), CD11b and F4/80 in order to distinguish five different immune cell populations: $CD206^+$ pro-inflammatory macrophages, T cells, B cells, leukocytes and $F4/80^+$ resident macrophages, respectively (Fig. 5.6A). Following the staining of the spleen extract with all five antibodies, the extract was separated into four equal parts and stained with mNeonGreen fusions of anti-CD19, anti-F4/80 and anti-CD206 separately, produced and secreted in HEK293FT supernatant. Co-staining was evaluated using flow cytometry to not only assess if the small antibody domains correctly detected cells that were positive for their respective antigen, but also if some cross-reactivity could be detected (Fig. 5.6B).

A

Epitope	FACS lazer	Cell population(s)
CD206	PE	Macrophages
CD3	PE-Dazzle	T cells
B220	PE-Cy5	B cells
CD11b	PE-CY5.5	Leukocytes
F4/80	AlexaFluor700	Resident tissue macrophages

B

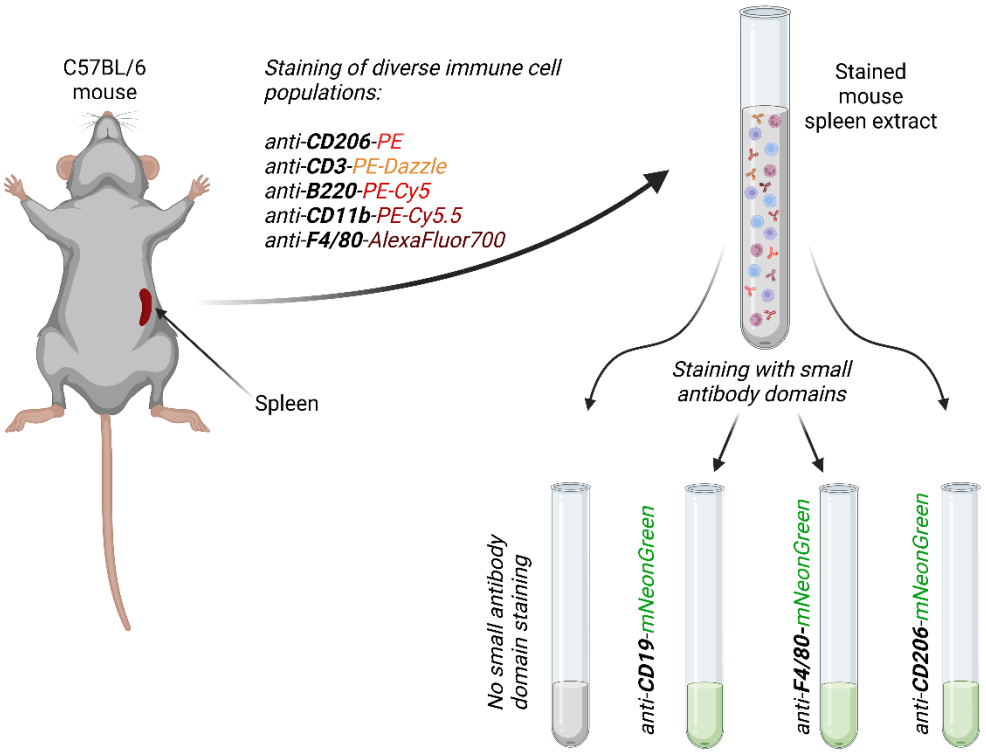

Figure 5.6. The experimental workflow of testing small antibody domains used as synNotch extracellular domains (ECDs) against diverse immune cell populations*. (A) The list of antibodies used to stain the C57BL/6 mouse spleen extract and respective immune cell subpopulations. (B) The schematic representation of the staining procedure. Mouse spleen extract was stained with a mix of conjugated antibodies in a one-pot reaction. The mix was then split into four equal parts and processed further by staining with small antibody domains fused to mNeonGreen.*

It was shown that both F4/80 and CD206 ECDs exhibit co-staining with different immune cell populations (Fig. 5.7). In particular, anti-F4/80-mNeonGreen demonstrated co-staining with $CD206^+$ macrophages (Fig. 5.7C-a) and $F4/80^+$ resident tissue macrophages (Fig. 5.7C-b), $CD11b^+$ leukocytes (Fig. 5.7C-d), as well as B cells ($B220^+$) (Fig. 5.7C-c). Anti-CD206-mNeonGreen, on the other hand, demonstrated significant co-staining with all present immune cell subpopulations (Fig. 5.7D). Interestingly, anti-CD19-mNeonGreen didn't show particularly increased co-staining with $F4/80^+$ resident tissue macrophages (Fig. 5.7B-b); however, it also didn't exhibit expected significant co-staining with $CD19^+$ B cell subpopulation (Fig. B-c).

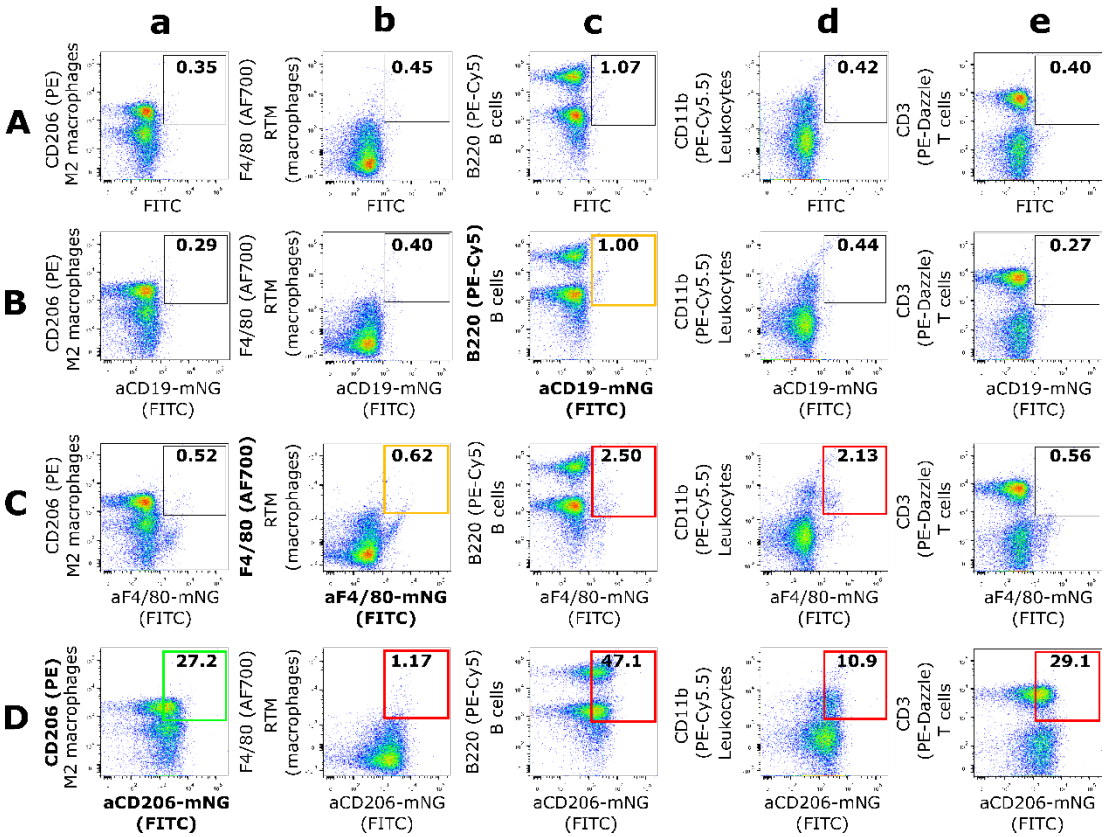

Figure 5.7. Investigating the binding of synNotch ECDs to various immune cell populations in mouse spleen extract. *Flow cytometry charts illustrating co-staining between mNeonGreen fusions of small antibody domains used as synNotch ECDs and various immune cell subpopulations. Numbers indicate percentage of the population that was co-stained. Highlighted in green is a correct staining between anti-CD206 VHH and CD206+ macrophages (D-a). Highlighted in yellow and is expected staining between small antibody domains and their respective immune cell subpopulations. Interestingly, both anti-CD19 and anti-F4/80 small antibody domains did not exhibit significant levels of binding to their corresponding ligands in mouse spleen extract (B-c, C-b). Highlighted in red are cases of cross-reactivity between small antibody domains and other immune cell populations. Anti-CD206 VHH illustrated highly unspecific binding to multiple immune cell subsets (D-b, D-c, D-d, D-e). Anti-F4/80 exhibited co-staining with B-cell markers and certain leukocyte subsets (C-c, C-d).*

5.3 Discussion

In this chapter, monoclonal MetBo2 αCD19-synNotch and αCD206-synNotch cell lines were assessed for their capacity to report interactions with their cognate ligands displayed on sender cells, as well as specificity for those ligands. The summary of the receiver and sender cells used in this chapter are given in the Table 5.1. The findings suggest that although both receptors report a detectable increase in fluorescent response to MetBo2 $CD19^+$ and $CD206^+$ cells, respectively, the response fold fluctuates among generations and is largely unspecific.

Table 5.1. The summary of the receiver and sender cells used in the chapter 4.

Receiver cells	Sender cells	Surface ligand	Notes
MetBo2	MetBo2	CD19	Genomic integration of the synNotch system (Cas9-mediated ROSA26 integration for the reporter cassette and PiggyBac for the receptor cassette); Transient expression of CD19;
MetBo2	MetBo2	CD206	Genomic integration of the synNotch system (Cas9-mediated ROSA26 integration for the reporter cassette and PiggyBac for the receptor cassette); Transient expression of CD206;
MetBo2	MetBo2	F4/80	Genomic integration of the synNotch system (Cas9-mediated ROSA26 integration for the reporter cassette and PiggyBac for the receptor cassette); Transient expression of F4/80;
MetBo2	Peritoneal macrophages	F4/80	Genomic integration of the synNotch system (Cas9-mediated ROSA26 integration for the reporter cassette and PiggyBac for the receptor cassette); Endogenous expression of F4/80;

5.3.1 synNotch receptor activity is non-reproducible and unspecific

Fluctuations in synNotch activation folds among different clonal populations (discussed in Chapter 4), as well as over cell line generations can be explained by the system being highly dynamic and containing many variables. Those variables are (i) stability of genomic integrations, (ii) consistency of co-culture conditions, (iii) integrity of ligand expression on transiently transfected sender cells, as well as (iv) appropriate experimental design and (v) data analysis protocols. All these factors greatly contribute to the outcome of the receptor-reporter system implementation and must be taken into consideration when reporting such findings.

The problem of quantifying genomic integrations and ensuring their stability over the generations has been discussed in the previous chapter. In the context of this chapter, however, performing quantitative analysis of synNotch expression over cell passages would have provided valuable insight into whether receptor activity is dependent on its expression levels and if so, the scope of this relationship could be evaluated. Such quantification could be achieved with standard laboratory methods such as RT-qPCR. It is unclear, however, if such receptor behaviour is specific to the designs in this work, since there are no reports of low synNotch system stability in the published literature.

Using transiently transfected sender cells can present certain challenges to the consistency of the synNotch system activity. First of all, consistent transfection efficiency must be ensured, which has not been evaluated in these experiments as no transfection controls have been used. Secondly, the synNotch system is dependent on direct interactions between neighbouring cells, therefore, co-cultures must ensure those contacts are evenly distributed and consistent cell numbers are used. Although in these experiments consistent cell numbers were used (see Methods section), some variability might still take place due to pipetting or human errors. Taken together, the variability in both transfection efficiency and co-culture conditions can greatly influence receptor signalling outcome. Alternative methods that can potentially reduce the issues associated with the variability in co-

culture conditions involve using plate-bound ligands, which can be thoroughly quantified and controlled.

Having plate-bound ligands in place of transiently transfected sender cells would also reduce the flaws of the experimental design in the dose response experiments. The dose response experiments were carried out by transiently transfecting wild-type MetBo2 cells with varying quantities of the ligand-coding plasmids. However, this pipeline does not ensure the proportional increase in the ligand expression among the different cell populations, as transfection efficiency is dependent on the quantity of the input plasmid material. Therefore, normalisation of the transfection reactions with a standard non-coding plasmid (e.g., pcDNA3.1) should be conducted. This would ensure all the titers receive an equal amount of total DNA and result in more consistent transfection, unaffected by varying quantities of the input DNA.

Another useful addition to the characterisation of receptor activity and its dependence on ligand availability would be using competing anti-CD19, anti-CD206 and anti-F4/80 antibodies. To be more precise, ligand-specific antibodies could be used to block interaction between synNotch ECD and its cognate ligands, as it would allow to investigate the level of ligand-independent activation.

Another flaw in the experimental design involves fluctuations in protein expression due to metabolic burden. Living cells are dynamic systems that can be greatly influenced by the introduction of exogenous genetic circuits[128]. In the synNotch system, such circuits consist of an inducible reporter cassette and constitutively active puromycin resistance, receptor and H2B-TagBFP cassettes. Direct and indirect interactions between these elements will be subject to mutual fluctuations in expression due to limited metabolic resources of the host cells. For example, induced mCherry expression can potentially negatively impact expression of all other three elements and thus result in lower expression of the receptor and blue fluorescence post-induction. Since H2B-TagBFP is used to gate the relevant cell populations during flow cytometry analysis, this could result in lower numbers of gated events and thus skew the quantitative results.

5.3.2 The challenges of applying synNotch receptors for cell-cell contact monitoring *in vivo*

synNotch reactivity to multiple immune cell populations in the mouse spleen extract reveals significant challenges for the application of the synNotch system *in vivo*. In particular, this will potentially result in a high number of synNotch cells, activated by incorrect interaction partners (false positives) and thus no possibility to discriminate the precise interacting partners at the tumour sites. For example, while being targeted at $CD206^+$ macrophages, αCD206-synNotch cells will report activation signal upon contact with B cells ($CD19^+$), which are also abundant at primary tumour and metastatic sites[10]. An additional level of complexity is introduced by the fact that reporter cells will likely get activated by multiple other immune cells shortly after injection while circulating in the bloodstream and before establishing primary and metastatic tumours in mice.

One way of minimising the detection of false positives would be to evaluate the longevity of synNotch activation. Knowing the duration of fluorescent signal following receptor activation will allow for more precise temporal discrimination between false positive activation and ligand-specific activation. To be more precise, it could make it possible to determine the timeline for when the unspecific activation which happened prior to tumour establishment should decrease and when one can start tracking the contact reporting following injection of engineered cells. Because the response duration is highly dependent on the degradation rate of mCherry, adding degradation domains to the mCherry in the reporter cassette could greatly improve not only the signal-to-noise ratio of the whole system *in vitro*, but also potentially allow for better discrimination between positives and false positives *in vivo*, having the spatiotemporal knowledge of tumour growth and migration dynamics (e.g., having an estimation of how soon injected cells establish primary breast tumours and metastasise into the bone tissue). Alternatively, immunodeficient mice can be used, particularly T and B cell-deficient strains, which would at least partially reduce contact events with irrelevant cell types[129].

Unexpected findings were the lack of co-staining between anti-CD19 and anti-F4/80 small antibody domains with their ligand-positive immune cell populations. This can suggest suboptimal experimental conditions, in particular, during the data acquisition step. For example, the spectral overlap on all five antibody fluorophores made it extremely laborious to set up the flow cytometry workflow using multiple iterations of compensation procedures. Therefore, it would be preferential to review the antibody panel for this experiment by introducing more spectrally distant antibody variants.

Unfortunately, none of the orthogonal synNotch extracellular small antibody domains (such as αGFP scFV), were used in this experiment, however, having such control could bring more insight into the extent of the reduced specificity of the synNotch ECD. Additionally, CD19 and CD206 constructs, as well as the respective synNotch receptors, contain either HA and/or myc tags in their architectures, which can be contributing factors to receptor and ECD cross-specificity. Therefore, removing the tags and re-testing both the receptors and ECDs under the same conditions could provide more insight into the problem of receptor cross-specificity.

Additionally, secreted small antibody domains produced in HEK293FT cells as mNeonGreen fusions were harvested from cell culture supernatant and used directly on pre-stained spleen extracts. Although this methodology yielded positive results when validating expression of ligands on transiently transfected sender cells, purification and binding affinity evaluation is required to fully validate the use of in-house produced fluorescent binders for both quantitative and qualitative research.

5.4 Conclusions

In this chapter, αCD19-synNotch and αCD206-synNotch monoclonal cell populations were assessed for receptor activation with corresponding ligands displayed on sender cells. Despite significant levels of activation detected in co-cultures with $CD19^+$ and $CD206^+$ cells, receptors also demonstrated cross-reactivity with other immune cell surface markers. Although there are ways to minimise the

negative impact of such receptor behaviour *in vivo*, this remains a major caveat for effective receptor-reporter system implementation *in vivo*. Future efforts must be aimed at increasing receptor specificity though the development of more specific binding domains.

Chapter 6

synFP: synNotch receptors based on dimerisation-dependent fluorescent proteins

Outline

In this chapter, a novel development of the synthetic Notch system will be introduced. This new synthetic Notch variant is based on dimerisation-dependent fluorescent proteins (ddFPs), which are incorporated into the intracellular signal transduction module. The new synthetic Notch variant is therefore referred to as synFP.

The main steps discussed in this chapter are:

a) Design and development of a new reporter cell line for the αCD19-synFP receptor (MetBo-RANLS);
b) Development of a monoclonal αCD19-synFP receptor cell line;
c) Isolation of αCD19-synFP clone candidates by testing against MetBo2 $CD19^+$ cells;

6.1 Introduction

6.1.1 The utility of fluorescent proteins in biological research

Fluorescent proteins (FPs) are exceptionally commonly used in biotechnology, cell biology and synthetic biology research due to their wide profile of applications. These include visualisation of cellular components, protein localisation, intracellular enzymatic reactions as well as reporters in engineered genetic circuits, where they are capable of providing both qualitative and quantitative information. The availability of FPs in different spectral or structural (monomer vs dimer) configurations have made them useful tools in protein fusion tagging and multi-panel immunochemistry.

FPs have been exploited as valuable assets in biosensing applications. Besides the common use of FPs as reporter proteins, advancements in fluorescent microscopy techniques allowed visualising molecular interactions inside the cells, for example by using Fluorescence Resonance Energy Transfer (FRET) microscopy[130]. The technique is based on the energy transfer between an excited fluorophore (donor) to an acceptor fluorophore within 3-6 nm radius. This technique allows spatial visualisation of interacting protein partners as well as provides information on their subcellular localisation. Furthermore, developments such as photoconvertible[131–133] or photoswitchable[134] FPs further expanded the FP applications portfolio in biosensing, as well as helped overcome certain challenges of using FPs in biological research (e.g., photobleaching)[135].

6.1.2 Dimerisation-dependent fluorescent proteins

Using split FPs has greatly aided in studying protein-protein interactions[135,136]. However, conventional methods using split FPs often result in irreversible reconstitution. On one hand, irreversibility allows for imaging of transient

interactions and low affinity partners, but it also restricts investigating dynamic changes in protein-protein interaction within a cell[137].

Alternatively, Alford et al. developed a new generation of split FPs called dimerisation-dependent fluorescent proteins (ddFPs)[138], which allow reversible and interchangeable tagging of protein partners. In particular, a ddFP system has two dimerising domains – A and B. Domain A is a dimly fluorescent monomer, which, when complemented by domain B, upon dimerisation, leads to reconstitution of full fluorescence (Fig. 6.1A). Initially, a red ddFP was engineered by mutating a monomer of dTomato (H162K and A164R; domain A) and a dTomato-derived B partner that complemented domain A mutations. The group later expanded the ddFP portfolio by developing green and yellow ddFPs[139].

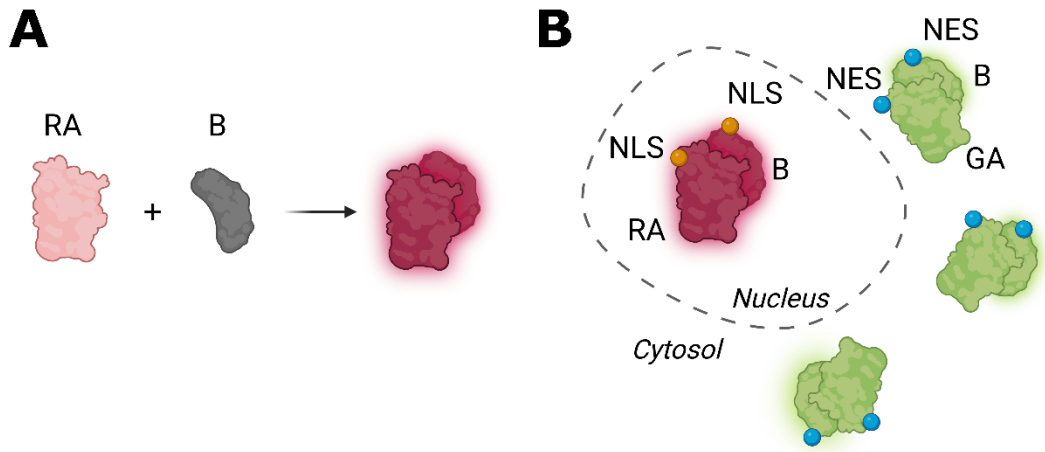

Figure 6.1. Dimerisation-dependent fluorescent proteins. *(A) General schematic representation of ddFPs. (B) Fusion with nuclear localisation or nuclear exclusion sequences can aid in compartmentalised visualisation of protein-protein partners as well as in achieving better signal separation in biosensor applications. NLS – nuclear localisation sequence. NES – nuclear exclusion sequence.*

The applications of ddFPs in biosensing have been successfully demonstrated in both *E. coli* and mammalian cells[75,138,139]. For example, in order to demonstrate the utility of ddFPs in detecting protein-protein interactions, the authors chose a common protein-protein interaction model: rapamycin-dependent interaction of FK506-binding protein (FKBP) and the FKBP-rapamycin-binding

domain (FRB). This system was used as proof-of-concept platform, where A and B domains of a red ddFP were fused to the C-termini of FKBP an FRB and expressed in *E. coli*. Addition of rapamycin resulted in a dose-dependent increase in red fluorescence[138]. Similarly, in mammalian cells, the system demonstrated successful $Ca2^{+}$-dependent dimerisation between calmodulin and M13 peptide, proving that ddFP-based systems can also be used as cellular biosensors[138].

The ddFP capacity in biosensing has also been demonstrated in detection of cell apoptosis and, in particular, caspase-3 protease activity sensing. In this proof-of-concept experiment, A and B domains were fused via the caspase-3 substrate and fluorescence intensity was monitored following addition of apoptosis-inducing factors[138,139]. The reduction in red fluorescence in case of red ddFP not only proved the system to be a reliable biosensing system, but also demonstrated low affinity between A and B domains since no reconstitution was observed following cleavage with protease[138]. However, green and yellow ddFPs demonstrated higher affinity, which limits their suitability for this application[139].

It was later discovered that a single B domain can interchangeably bind and reconstitute fluorescence in red (RA) and green (GA) ddFP variants[75]. Additionally, when fused to nuclear localisation or nuclear exclusion sequences (NLS or NES, respectively), dimerisation can be visualised in different subcellular compartments (Fig. 6.1B). For example, the caspase-3 activity sensor was implemented by fusing RA-NES and B-NLS domains with caspase-3 substrate and co-expressing this fusion with a separate GA-NLS constructs[75]. This way, upon caspase-3 activity, the change from cytoplasmic red fluorescence to nuclear green fluorescence was observed due to the translocation of B-NLS domain into the nucleus.

Altogether, ddFPs provide new opportunities for the development of biosensors for protein-protein interactions or intracellular signalling activity. Although it is important to note that due to varying affinity between the different monomers (K_d) and protein expression levels withing a cell, ddFPs may present discrepancies in quantitative comparison analysis[75].

6.1.3 Incorporation of ddFPs in the synNotch system

The main advantage of using ddFPs in biosensing systems is the simplicity in genetic circuit level design. In particular, while a lot of biosensing systems rely on expression of reporter proteins, ddFPs (and split FPs in general) allow to omit the transcriptional activation step. Due to this reason, it was speculated that incorporating ddFPs in the synNotch system could lead to more rapid cell-cell contact detection.

6.1.4 Design considerations for synFP platform

Previous synNotch receptor-reporter system designs involved using Gal4-UAS reporter system for cell-cell contact detection. In order to implement ddFPs in the system design, Gal4VP64 transcriptional activator at the C-terminal of the receptor construct and its release by cleavage upon receptor activation could be substituted with B-NLS domain, while RA-NLS could be expressed in the cell nucleus (Fig. 6.2A).

Following the strategy described in the chapter 4 of this thesis, the RA-NLS cassette was integrated in ROSA26 safe harbour in MetBo2 cells for stable long-term maintenance. Subsequently, ddFP-based anti-CD19 synNotch (further referred to as αCD19-synFP) was integrated into genomic DNA using the PiggyBac system. The schematic overview of the intended designs is presented in figure 6.2.

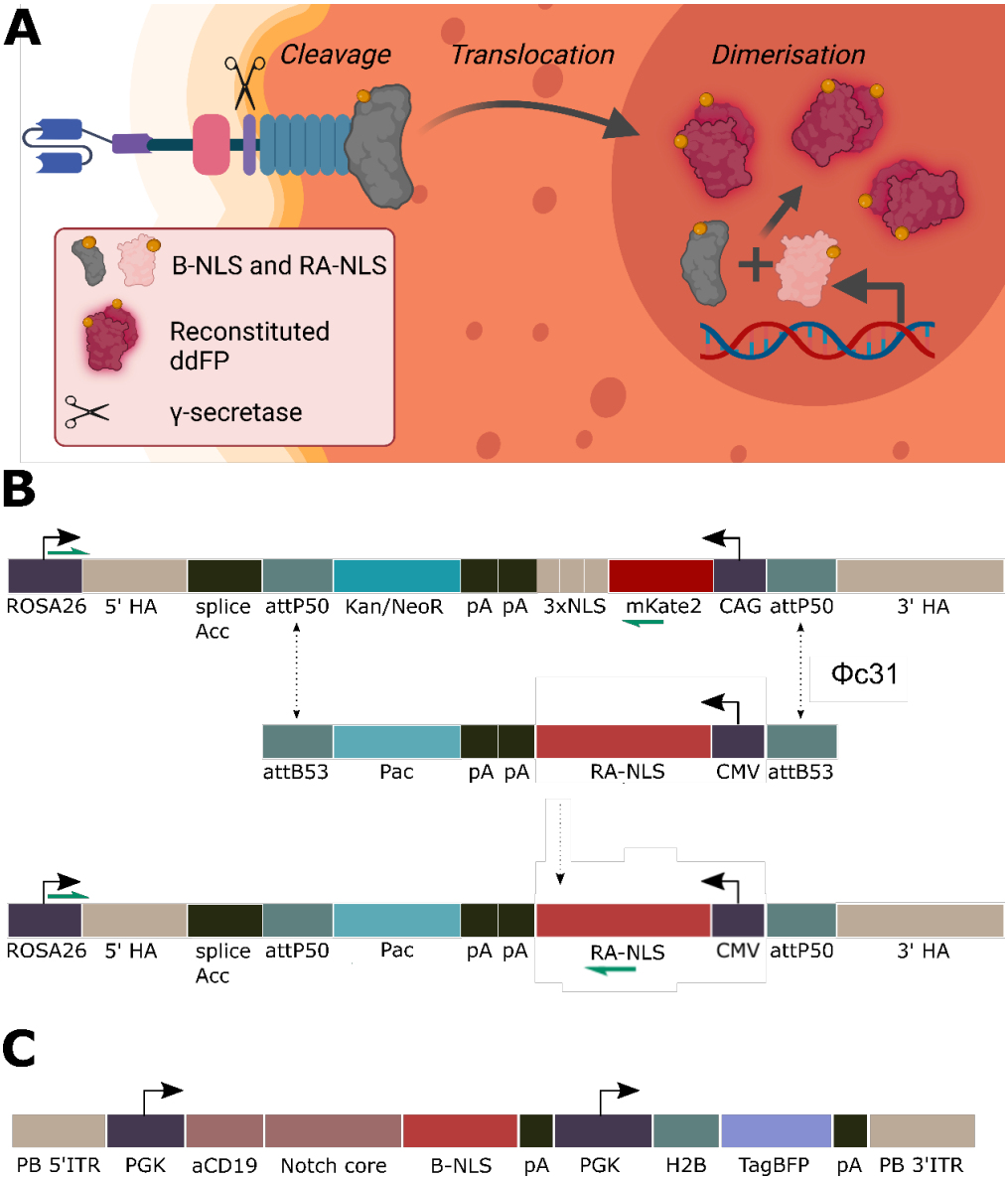

Figure 6.2. Schematic representation of construct design for synFP system. *(A) General representation of synFP system. Upon receptor activation, cleavage by γ-secretase releases the B-NLS monomer at the intracellular receptor domain. The nuclear localisation sequence (NLS) prompts the translocation of B-NLS to the nucleus, where is dimerises with a constitutively expressed RA-NLS counterpart and results in a fluorescent response. (B) A schematic representation of recombinase-mediated cassette exchange (RMCE) of RA-NLS cassette into ROSA26 landing pad. (C) A schematic representation of the αCD19-synFP receptor design. HA – homology arms. Kan/NeoR – Kanamycin/Neomycin (G418) resistance gene. pA – polyadenylation sequence. NLS – nuclear localisation sequence. CAG – Cytomegalvirus immediate enhancer/β-actin promoter. Pac – puromycin acetylase (puromycin resistance gene).*

6.2 Results

6.2.1 MetBo2-RANLS cells exhibit low fluorescence when transfected with B-NLS

In order to integrate the RANLS cassette into MetBo2 genome, RMCE was performed on the MetBo2^{RMCE} cell line. Following puromycin selection and cell sorting, monoclonal populations of MetBo2-RANLS cells were isolated. Despite the significant increase in red fluorescence that was observed among the clones after transient transfection with a plasmid carrying B-NLS, using flow cytometry (Fig. 6.3A), no RFP signal could be detected with fluorescent microscopy (data not shown). Nevertheless, clone 4 was selected for further experiments since it exhibited the highest increase in red fluorescence upon transfection with B-NLS. Correct genomic integration was confirmed by PCR of genomic DNA (Fig. 6.3B).

In the αCD19-synFP design, following cleavage with γ-secretase, B-NLS is speculated to have a VLLSRKR residue at the N-terminus. In order to investigate whether this might result in lower dimerisation efficiency, and, consequently, to the reduced fluorescence capacity, a *VLLSRKR*-B-NLS construct was engineered and tested on MetBo2-RANLS cells. No effect on red fluorescence intensity was observed when MetBo2-RANLS cells were transfected with a B-NLS or a *VLLSRKR*-B-NLS coding plasmid, indicating that a VLLSRKR residue at the N-terminus of B-NLS does not have a significant effect on ddFP reconstitution (Fig. 6.3C).

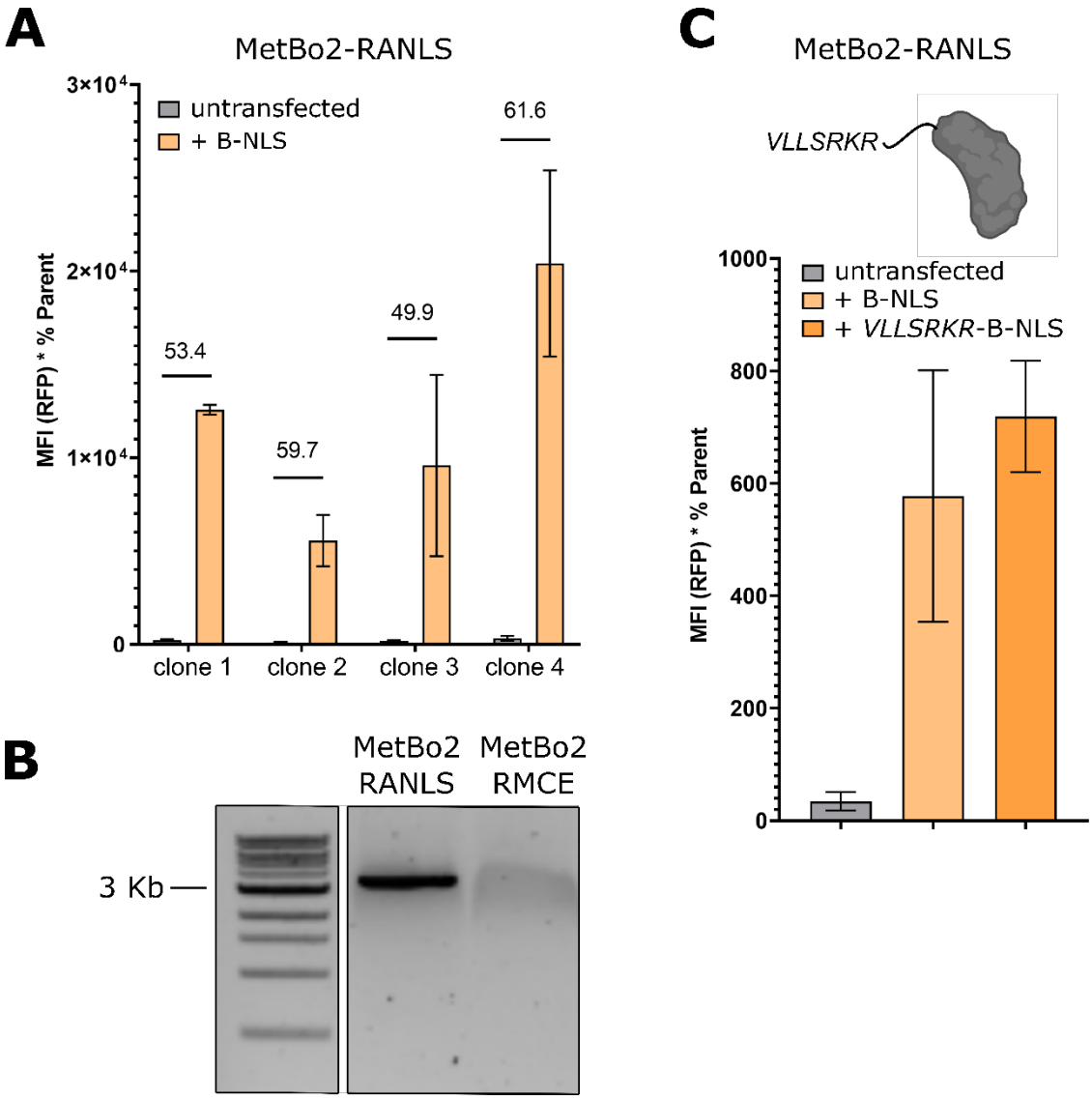

Figure 6.3. Development of MetBo2-RANLS cell line. *(A) Four monoclonal MetBo2-RANLS populations were isolated, which exhibited a significant increase in red fluorescence upon transfection with a B-NLS counterpart. (B) Correct integration into ROSA26 locus was confirmed by PCR (3634 bp). (C) VLLSRKR residue post-cleavage with γ-secretase does not have a significant effect on ddFP dimerisation.*

6.2.2 Assessing αCD19-synFP activity *in vitro*

Following receptor integration using the PiggyBac system, three αCD19-synFP clones were screened for activation with $CD19^+$ cells. All three clones exhibited an increase in red fluorescence, 2.9, 2.8, and 2.0-fold, respectively (Fig. 6.4). Interestingly, two isolated clones exhibited comparable increase in red fluorescence upon co-culture with $CD206^+$ cells. Nevertheless, clone 2, demonstrated specificity to $CD19^+$ cells. Unfortunately, due to time constrains, αCD19-synFP wasn't tested against $F4/80^+$ cells.

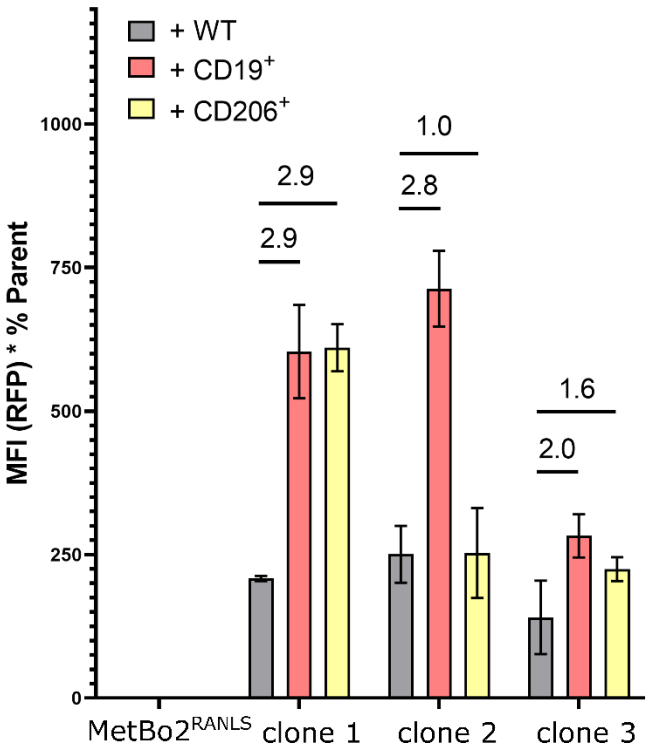

Figure 6.4. Evaluation of αCD19-synFP activity. *Three αCD19-synFP clones demonstrated a low-fold activation when presented to MetBo2 $CD19^+$ cells. Clone 1 and clone 3 demonstrated non-specific activation in response to $CD206^+$ clones, while clone 2 did not.*

6.3 Discussion

In this chapter, some progress has been made in order to establish a new synthetic Notch receptor variant, which employs ddFPs as a cell-cell contact reporter system. Although a successful αCD19-synFP clone, specific to $CD19^+$ cells was isolated, further characterisation is required to fully determine its applications capacity.

6.3.1 Low efficiency of MetBo2-RANLS may be due to low RA-NLS expression

In the first part of this chapter, a cell line harbouring RA-NLS was developed by targeted integration into the ROSA26 locus. Interestingly, when MetBo2-RANLS clones were isolated, all of them exhibited relatively low red fluorescence when transfected with a B-NLS complement. Unlike in the case of the MetBo2-UAS cell line described in chapter 4, increase in fluorescence in MetBo2-RANLS cells was observed only using flow cytometry and was undetectable by fluorescent microscopy.

It is speculated that one of the possible reasons for low fluorescence might be associated with a low number of expressed RA-NLS proteins. As was discussed in chapter 4, targeted integration in ROSA26 safe harbour typically results in a single copy integration. Although MetBo2-UAS exhibited an unequivocal fluorescent response, it is possible that the difference lies within the reporter promoter, i.e., whether there is a constitutive or induced expression of a reporter gene. To be more precise, while each RA-NLS monomer requires the binding of a single B-NLS monomer to reconstitute and elicit a fluorescent signal, the UAS reporter element contains five Gal4 binding sites, which results in higher chance of binding and, therefore, higher chance of reporter expression. Therefore, in order to increase ddFP dimerisation capacity, multiple copy integration of the RA-NLS cassette might be required, which can be achieved with the PiggyBac system.

6.3.2 αCD19-synFP exhibits low activation in response to CD19$^+$ cells

In αCD19-synFP, the activation fold increase in response to MetBo2 CD19$^+$ cells was significantly lower than the activation fold of αCD19-synNotch, which renders the ddFP-based system less robust. Although increasing the number of RA-NLS transcripts may help to increase receptor activation fold, it is important to note that introduction of B-NLS at the intracellular domain (ICD) of synNotch introduces the possibility for structural issues, such as incorrect receptor folding, which may also lead to poor receptor activation. Additionally, investigating the correct membrane localisation of synFP receptor is required in order to exclude the possibility of incorrect intracellular localisation being a reason for poor receptor signalling.

Interestingly, two out of three αCD19-synFP clones exhibited activation when presented to MetBo2 CD206$^+$ cells. On the contrary, previously, αCD19-synNotch demonstrated affinity to F4/80 ligand, but not CD206. It is yet to be tested whether αCD19-synFP is reactive to F4/80, but these results, collectively, indicate significant problems in synNotch applicability in selective biosensing.

6.4 Conclusions

In this chapter, a new synthetic Notch receptor variant, αCD19-synFP, based on dimerisation-dependent fluorescent proteins, was developed. αCD19-synFP exhibited a low fold activation when presented to CD19+ cells; however, further characterisation is required to fully assess its activation capacity and ligand specificity. Additionally, improvements such as increasing RA-NLS gene copy numbers, may be required in order to increase receptor fold activation.

The idea behind incorporating ddFPs in the synNotch system was based on the assumption that this will lead to a faster cell-cell contact response. However, in order to confirm this, direct comparison between aCD19-synNotch and αCD19-synFP must be done through time-point experiments.

Chapter 7

Final Discussion

7.1 Overview of the project

Recent advancements in synthetic biology have provided valuable tools for a broad range of applications in therapeutics, diagnostics and biosensing in general. In particular, a lot of effort has been demonstrated in establishing synthetic receptor platforms[45]. Currently the existing toolkit of synthetic receptors provides scaffolds for varying applications, depending on individual system requirements: ligand recognition capacity (i.e., soluble or membrane-tethered), signal transduction pathways (i.e., endogenous or orthogonal), etc. The ability to implement layered circuits of synthetic receptors, sometimes referred to as 'daisy chains', has shown great potential in increasing the specificity of CAR T technology[45].

Despite their evident contribution to the field of applied research, synthetic receptors were also shown to be valuable assets in foundational research. For example, particular synthetic Notch receptor versions (synNQ and SNTGV) uncovered new insights in neuronal wiring[81,82]. Although to this day the number of such synthetic receptor applications is limited, their potential in aiding cell biology research is undeniable.

The work presented in this thesis aimed to expand the pool of examples of how synthetic receptor systems can serve foundational research, and, in particular, in the field of cancer immunology. Cancer growth and progression has been shown to be largely influenced by a plethora of interactions between malignant cells and immune cells. Although the immune system is inherently designed to target and eliminate tumour cells, the latter can evolve immune escape mechanisms and reprogram immune cells to a more cancer-inducing state[10].

Some mechanisms have been studied in detail. For example, it has been established that tumours recruit T_{reg} cells through secreted tumour-associated cytokine gradients, such as CCL1, CCL17, CCL22, CCL28 and CXCL9/10/11[140]. Once activated, T_{reg} cells perform a vast array of immune suppressing functions: consumption of pro-inflammatory IL-2, direct killing of antigen-presenting cells, inhibition of immune checkpoint mechanisms leading to inhibition of pro-inflammatory T cells, metabolic modulation of dendritic cells, etc[140].

However, the project described in this thesis concentrated on the effect of macrophages on tumour growth and progression. To this day, extensive effort has been made in investigating the mechanisms by which macrophages contribute to propagation of malignant cells. It is known that macrophages are recruited to TME by particular chemokines (CSF-1, MIPs, IL-4, IL-6, IL-10, IL-13[141]), VEGF and CCL2[28–30], and polarise towards anti-inflammatory state, which contributes to successful cancer propagation. However, there are no sufficient omics data on which activated intracellular processes in cancer cells grant them the host immune system.

Therefore, this thesis aimed at implementing an approach that may potentially fill the knowledge gap in this area. By engineering cancer cells with synthetic receptors and, subsequently, establishing tumours *in vivo*, cell-cell contacts between tumour and macrophage cells can be monitored. Eventually, by separating cells that reported contacts from cells that did not, one could study the changes that occurred in cells at the omics level.

7.2 System design and potential further improvements

In the intended system design, the synthetic receptor scaffold was a synNotch receptor. So far, synNotch efficiency was demonstrated in a multitude of applications, both alone, in logic gates or in tandem with CAR T cell receptors, demonstrating high receptor activation and programmability capacity[41–44,66,67,69,71,72,80,85]. In this project, synNotch was reengineered with novel macrophage specific extracellular domains (anti-F4/80 scFV and anti-CD206 VHH), while the intracellular domain – Gal4VP64 – induced mCherry following receptor activation.

In chapter 3, the efforts were focused on (i) learning how the synNotch receptor system must be operated and (ii) establishing basis for future experimental pipeline. In order to achieve this, the original receptor scaffold – anti-CD19-synNotch-Gal4VP64 (αCD19-synNotch) – was used for proof-of-concept purposes.

It was demonstrated that synNotch implementation in transient systems is futile since it leads to high background activation levels from leaky reporter promoters, and thus low activation levels upon contact with ligand-presenting cells. Additionally, the experiments revealed that the use of immune cells in co-cultures may lead to receptor-independent expression of the reporter, potentially due to intrinsic interactions between immune cells and synNotch cells.

7.2.1 Reducing synNotch background activation levels

Despite the consequent decision to exclusively implement the synNotch system in clonal cell populations, additional efforts could have improved synNotch signalling. These efforts involve applying recent advancements in synNotch optimisation to reduce background activation levels. For example, Yang et al. developed a new synNotch receptor version – esNotch – which demonstrated a 14.6-fold reduction in ligand-independent receptor activation[83]. This has been achieved by adding a RAM7 domain sequence (QHGQLWF) to the C terminus of the synNotch core domain (Fig. 7.1). The assumption that such transmembrane domain extension will improve synNotch signal-to-noise ratio was made on the basis of reports that γ-secretase requires a precise transmembrane domain positioning in order to carry out the cleavage. In particular, RAM sequence at the C terminus of endogenous Notch greatly contributes to proper receptor folding. Although introducing transmembrane domain extensions has been proposed before[66], later reports indicated failure to reproduce those results[83].

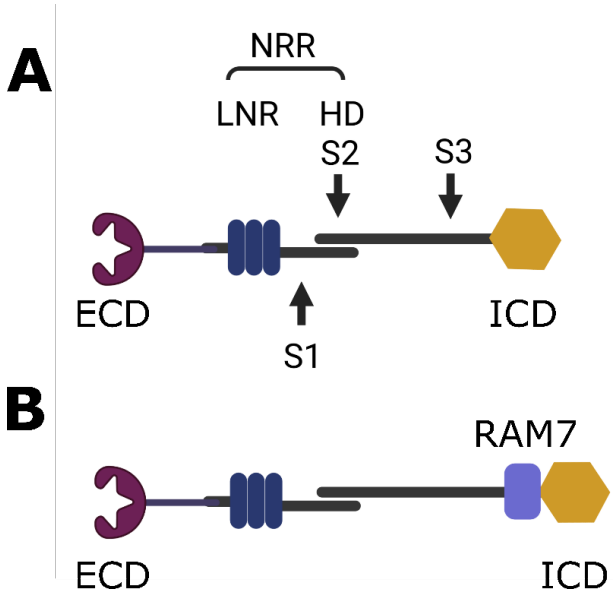

Figure 7.1. Schematic representation of esNotch[83]***.*** *(A) synNotch and (B) esNotch receptor architectures. A RAM7 domain was added to the C terminus of Notch minimal core domain. NRR – Notch regulatory region. LNR – Long terminal repeats. HD – Heterodimerisation domain. ECD – Extracellular domain. ICD – Intracellular domain. S1, S2 and S3 correspond to Notch cleavage sites.*

Additionally, implementing approaches aimed at reducing synNotch ligand-independent signalling could potentially decrease unspecific receptor signalling, as with αCD19-synNotch against F4/80^{+} cells, or αCD19-synFP against CD206^{+} cells. However, unspecific αCD206-synNotch activation was likely due to suboptimal ECD choice, as confirmed by co-staining of immune cell populations.

Another approach to reducing the background activity of the synNotch receptor involves re-engineering of the circuit into an inducible system. To be more precise, expressing the synNotch receptors under inducible promoters, or in the post-transcriptional inducible systems (e.g., aptazymes) could help overcome not only the problems associated with the high background activation of the receptors, but also with the early unspecific activation of the receptors immediately post-injection.

7.2.2 Irreproducible receptor activation presents challenges for standardised receptor characterisation

The lack of standardised system for synthetic receptor characterisation has been addressed before by Manhas et al., who have recently proposed a set of essential quantitative performance metrics for evaluating and describing synthetic receptors[45]. However, such characterisation might be inherently subjective due to variability in receptor expression levels, complexity of underlying genetic circuits and subsequent metabolic load, and many other factors that contribute to changes in gene expression and cellular metabolism.

In chapter 5, an inability to reproduce consistent synNotch activation fold changes over multiple generations were observed. Although as it was discussed previously, discrepancies in experimental conditions will present an even greater challenge for further characterisation attempts of newly developed synNotch, as well as its application in living systems. Therefore, characterisation of synthetic receptors might need to be more extensive and multifaceted, while considering changes of gene expression levels over cell generations. Moreover, such instability is a major caveat in applying synthetic receptors to quantitative research, limiting its use to on/off response acquisition. Therefore, in order to minimise the variability emerging from within the cell's receptor-reporter system and to ensure the stability of the system over generations, careful consideration of the genomic integration strategies must be considered, both in regards to genomic location and methods of integration.

7.2.3 synFP requires further improvements in the system design

Chapter 6 was aimed at developing a novel synthetic Notch receptor variant that would exhibit a faster fluorescent response to sender cells. Using ddFPs in place of a Gal4-UAS promoter/reporter system would skip the transcription and translation steps of a reporter gene expression and, hence, report cell-cell contact in a shorter time.

Unfortunately, due to time constrains and contamination issues post-cell sorting, not much progress was done in pursuing this avenue. Although a functional αCD19-synFP clone was isolated, it still requires further characterisation, assessment for specificity and direct comparison with αCD19-synNotch in regards to response time. Additionally, incorporating more copies of RA-NLS could allow to get a more obvious readout of fluorescent response upon binding between the extracellular domain and the epitope of interest and increase the signal to noise ratio of the system.

7.2.4 Permanent recording of cell-cell contacts

One of the future prospects in synthetic Notch receptor engineering to monitor intercellular interactions include permanent recording of cell-cell contacts. One of the ways to achieve this is through incorporation of a Cre-loxP system at the signal transduction module: the Cre recombinase as the ICD and a reporter protein cassette flanked by loxP-sites in the genomic DNA. This way, upon target molecule recognition, the translocation of Cre to the nucleus would irreversibly flip the reporter cassette to a correct orientation, resulting in a fluorescent response (Fig. 7.2A). Synthetic Notch-Cre (synCRE) system could provide permanent recording of cell-cell contacts, and thus allow not only identifying contact partners after contact happened but also track the migration and long-term behaviour of macrophage-contacted tumour cells.

However, based on the results presented in this thesis, implementing synCRE system is extremely challenging due to several factors. First of all, Cre-mediated cassette flipping is an irreversible process; therefore, in order for the system to function robustly no background activation must be present. The presence of irreversible background activation will make the process of clonal selection and isolation extremely tedious and iterative. Secondly, receptor cross-reactivity with irrelevant ligands would result in permanent recording of a contact, leading to unidentifiable false positives. Alternatively, a split-Cre approach could enable the use of synCRE in AND logic gates, by eliciting a fluorescent response only upon recognition of two distinct ligands (Fig. 7.2B). However, this does not

completely eliminate the possibility of leakiness and non-specific receptor activation. This assumption is supported by work described by previous research attempting to incorporate split Cas9 into the synNotch system, which resulted in high and irreversible background activation[80]. However, if proven functional, the synCRE system could be a valuable addition to the existing toolkit of synthetic Notch receptors.

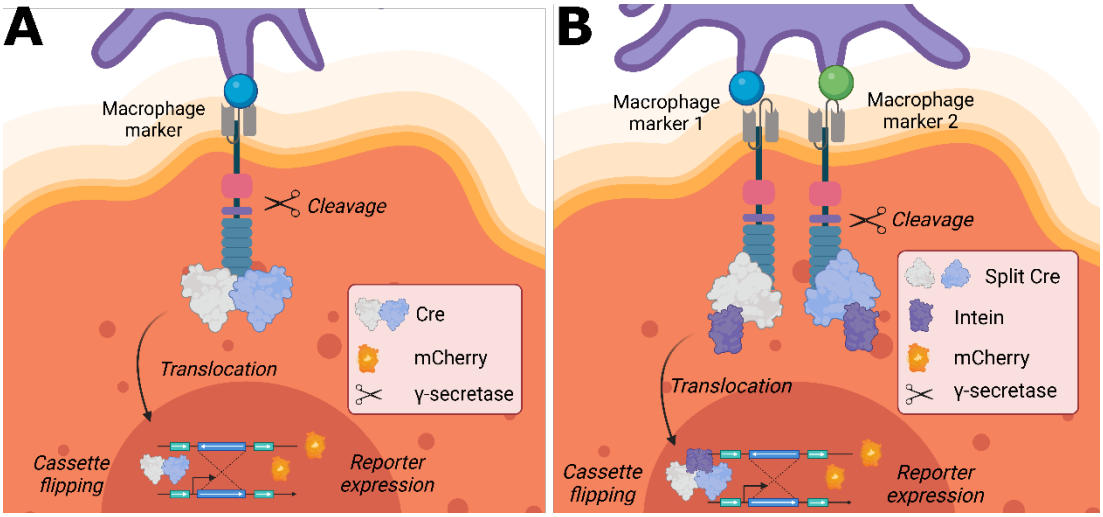

Figure 7.2. Potential incorporation of Cre-loxP system in the synthetic Notch system. *(A) Upon ligand recognition by the receptor, cleaved Cre recombinase translocates into the nucleus and flips the reporter cassette into the correct orientation, resulting in a constitutive expression of a reporter protein (mCherry). (B) By using split-Cre (intein-mediated split), synCRE system could be implemented in AND logic gates to report contacts with cells, positive for two particular surface markers.*

7.3 Future application prospects for the developed synNotch system *in vivo*

Implementing any engineered genetic circuits *in vivo* introduces additional factors that may influence the performance of a receptor-reporter system. Such factors include the increased complexity of biological environments in terms of neighbouring cells and soluble factors, that can greatly affect physiological conditions and, therefore, cell metabolism and intracellular signalling. A widespread

concern in regards to implementing synthetic receptor systems *in vivo* (as well as *in vitro*) is the fact that it introduces forced cell-cell adhesion between neighbouring cells[82]. This, in turn, may affect migration and relative position of host endogenous cells, and thus introduce artificial perturbations to the whole system.

On the other hand, it is important to note the possibility that not all interactions between cancer and immune cells will simultaneously engage in the synNotch-mediated signalling. To be more precise, macrophages could still contact cancer cells through endogenous interactions partners (e.g., CCL2-CCR2 pair), but not through the synNotch system. This could lead to the faulty isolation of the interacting and non-interacting cancer cell populations, and, subsequently, to the acquisition of the unrepresentative omics data. One of the ways to control for this is to deplete cancer cells of the known endogenous macrophage interaction surface partners, and hence inhibit their ability to respond to the macrophage contact. This could allow to obtain reliable negative control data from the population of cancer cells, unaffected by macrophage conditioning. *In vitro*, this can be achieved by using antibodies, specific to macrophage interacting surface markers, which could act as interaction blockers.

Another concern for using the synNotch cells *in vivo* is the possibility that introducing foreign epitopes into a healthy mouse model will likely cause an immune reaction and result in the clearance of synNotch cells. In order to reduce this possibility, screening for low immunogenic synNotch cells might be required. Alternatively, immunodeficient mouse models can be used, particularly B cell/T cell deficient strains. Such approach was used in several publications, where mice with various levels of immunodeficiency were used to demonstrate synNotch effectiveness in targeting cancer cells[42,69,71,72].

Lastly, cross-reactivity of synNotch receptors to irrelevant epitopes is another obstacle to *in vivo* research. In particular, it might result in false positive contact reporting at the tumour site. However, an equally important concern is receptor activation at the early stages of injection, as well as primary tumour and metastasis establishment by the cells present in the bloodstream (B cells, T cells, leukocyte subpopulations, etc.). This problem might be minimised by performing receptor activation persistence assays and further optimisation of the system, by,

for example, introducing degradation tags[142] to the reporter protein to reduce the time span of the activated state and allow the signal to drop to background levels at the tumour site. Alternatively, but equally important is to develop more specific extracellular domains for the surface markers of interest, which could be done through conventional techniques such as phage display, or in conjunction with computational protein engineering work.

7.4 Conclusions

In this thesis, advancements towards establishing a synthetic receptor-based cell-cell contact monitoring tool were described. As a result, two novel synthetic Notch receptors were developed: αCD206-synNotch and αCD19-synFP. Although αCD206-synNotch demonstrated high cross-reactivity with $CD19^+$ ligand, the work described here provides useful insights into the intricacies of synthetic Notch receptor development platforms. Further work should include the optimisation and increasing specificity of αCD206-synNotch, as well as further characterisation of αCD19-synFP.

References

1. The History of Cancer | First Cancer Diagnosis. https://www.cancer.org/treatment/understanding-your-diagnosis/history-of-cancer.html.
2. WHO. WHO Fact Sheets: Cancer. https://www.who.int/news-room/fact-sheets/detail/cancer (2022).
3. Siegel, R. L., Miller, K. D., Fuchs, H. E. & Jemal, A. Cancer Statistics, 2021. *CA Cancer J Clin* **71**, 7–33 (2021).
4. Cancer - Screening and early detection. https://www.who.int/europe/news-room/fact-sheets/item/cancer-screening-and-early-detection-of-cancer.
5. Pashayan, N. & Pharoah, P. D. P. The challenge of early detection in cancer. *Science* vol. 368 589–590 Preprint at https://doi.org/10.1126/science.aaz2078 (2020).
6. Bauml, J. M. *et al.* Pembrolizumab after Completion of Locally Ablative Therapy for Oligometastatic Non-Small Cell Lung Cancer: A Phase 2 Trial. *JAMA Oncol* **5**, 1283–1290 (2019).
7. Esposito, M., Ganesan, S. & Kang, Y. Emerging strategies for treating metastasis. *Nature Cancer* vol. 2 258–270 Preprint at https://doi.org/10.1038/s43018-021-00181-0 (2021).
8. Gobin, E. *et al.* A pan-cancer perspective of matrix metalloproteases (MMP) gene expression profile and their diagnostic/prognostic potential. *BMC Cancer* **19**, 581 (2019).
9. Targeting tumours - pre pub | The Economist. https://www.economist.com/technology-quarterly/2017-09-16/treating-cancer.
10. Kitamura, T., Qian, B.-Z. & Pollard, J. W. Immune cell promotion of metastasis. *Nat Rev Immunol* **15**, 73–86 (2015).
11. Sherman, M. H. *et al.* Stromal cues regulate the pancreatic cancer epigenome and metabolome. *Proceedings of the National Academy of Sciences* **114**, 1129 LP – 1134 (2017).
12. Gouirand, V., Guillaumond, F. & Vasseur, S. Influence of the Tumor Microenvironment on Cancer Cells Metabolic Reprogramming . *Frontiers in Oncology* vol. 8 117 Preprint at https://www.frontiersin.org/article/10.3389/fonc.2018.00117 (2018).
13. Prehn, R. T. The immune reaction as a stimulator of tumor growth. *Science (1979)* **176**, 170–171 (1972).

14. Billingham, R. E., Brent, L. & Medawar, P. B. ‘Actively acquired tolerance’ of foreign cells. *Nature* **172**, 603–606 (1953).

15. Coussens, L. M. & Werb, Z. Inflammation and cancer. *Nature* vol. 420 860–867 Preprint at https://doi.org/10.1038/nature01322 (2002).

16. Qian, B.-Z. & Pollard, J. W. Macrophage diversity enhances tumor progression and metastasis. *Cell* **141**, 39–51 (2010).

17. Martinez, F. O. & Gordon, S. The M1 and M2 paradigm of macrophage activation: Time for reassessment. *F1000Prime Rep* **6**, (2014).

18. Lin, Y., Xu, J. & Lan, H. Tumor-associated macrophages in tumor metastasis: Biological roles and clinical therapeutic applications. *Journal of Hematology and Oncology* vol. 12 1–16 Preprint at https://doi.org/10.1186/s13045-019-0760-3 (2019).

19. Roszer, T. Understanding the mysterious M2 macrophage through activation markers and effector mechanisms. *Mediators of Inflammation* vol. 2015 Preprint at https://doi.org/10.1155/2015/816460 (2015).

20. van Dyken, S. J. & Locksley, R. M. Interleukin-4-and interleukin-13-mediated alternatively activated macrophages: Roles in homeostasis and disease. *Annual Review of Immunology* vol. 31 317–343 Preprint at https://doi.org/10.1146/annurev-immunol-032712-095906 (2013).

21. Kuang, D.-M. *et al.* Activated monocytes in peritumoral stroma of hepatocellular carcinoma foster immune privilege and disease progression through PD-L1. *J Exp Med* **206**, 1327 LP – 1337 (2009).

22. Curiel, T. J. *et al.* Specific recruitment of regulatory T cells in ovarian carcinoma fosters immune privilege and predicts reduced survival. *Nat Med* **10**, 942 (2004).

23. Lin, E. Y. *et al.* Macrophages Regulate the Angiogenic Switch in a Mouse Model of Breast Cancer. *Cancer Res* **66**, 11238 LP – 11246 (2006).

24. DeNardo, D. G. *et al.* CD4+ T Cells Regulate Pulmonary Metastasis of Mammary Carcinomas by Enhancing Protumor Properties of Macrophages. *Cancer Cell* **16**, 91–102 (2009).

25. Ma, R. Y., Black, A. & Qian, B. Z. Macrophage diversity in cancer revisited in the era of single-cell omics. *Trends in Immunology* vol. 43 546–563 Preprint at https://doi.org/10.1016/j.it.2022.04.008 (2022).

26. Kimura, Y. *et al.* The innate immune receptor Dectin-2 mediates the phagocytosis of cancer cells by Kupffer cells for the suppression of liver metastasis. *Proc Natl Acad Sci U S A* **113**, 14097–14102 (2016).

27. Garrido-Martin, E. M. *et al.* M1 hot tumor-associated macrophages boost tissue-resident memory T cells infiltration and survival in human lung cancer. *J Immunother Cancer* **8**, (2020).

28. Pathria, P., Louis, T. L. & Varner, J. A. Targeting Tumor-Associated Macrophages in Cancer. *Trends Immunol* **40**, 310–327 (2019).

29. Kitamura, T. *et al.* CCL2-induced chemokine cascade promotes breast cancer metastasis by enhancing retention of metastasis-associated macrophages. *J Exp Med* **212**, 1043–1059 (2015).

30. Cai, Z. *et al.* Monocyte Chemotactic Protein 1 Promotes Lung Cancer–Induced Bone Resorptive Lesions In Vivo. *Neoplasia* **11**, 228–236 (2009).

31. Lin, E. Y., Nguyen, A. v., Russell, R. G. & Pollard, J. W. Colony-stimulating factor 1 promotes progression of mammary tumors to malignancy. *Journal of Experimental Medicine* **193**, 727–739 (2001).

32. Abraham, D. *et al.* Stromal cell-derived CSF-1 blockade prolongs xenograft survival of CSF-1-negative neuroblastoma. *Int J Cancer* **126**, 1339–1352 (2010).

33. Aharinejad, S., Sioud, M., Lucas, T. & Abraham, D. Targeting stromal-cancer cell interactions with siRNAs. *Methods in molecular biology (Clifton, N.J.)* vol. 487 243–266 Preprint at https://doi.org/10.1007/978-1-60327-547-7_12 (2009).

34. Bechtel, T. J., Reyes-Robles, T., Fadeyi, O. O. & Oslund, R. C. Strategies for monitoring cell–cell interactions. *Nature Chemical Biology* vol. 17 641–652 Preprint at https://doi.org/10.1038/s41589-021-00790-x (2021).

35. Bagheri, Y., Ali, A. A. & You, M. Current Methods for Detecting Cell Membrane Transient Interactions. *Frontiers in Chemistry* vol. 8 1074 Preprint at https://doi.org/10.3389/fchem.2020.603259 (2020).

36. Yang, B. A., Westerhof, T. M., Sabin, K., Merajver, S. D. & Aguilar, C. A. Engineered Tools to Study Intercellular Communication. *Advanced Science* **8**, 2002825 (2021).

37. Groves, J. T. & Dustin, M. L. Supported planar bilayers in studies on immune cell adhesion and communication. *Journal of Immunological Methods* vol. 278 19–32 Preprint at https://doi.org/10.1016/S0022-1759(03)00193-5 (2003).

38. Purwada, A. *et al.* Ex vivo engineered immune organoids for controlled germinal center reactions. *Biomaterials* **63**, 24–34 (2015).

39. Bhatia, S. N. & Ingber, D. E. Microfluidic organs-on-chips. *Nature Biotechnology* vol. 32 760–772 Preprint at https://doi.org/10.1038/nbt.2989 (2014).

40. Nishida-Aoki, N. & Gujral, T. S. Review Emerging approaches to study cell–cell interactions in tumor microenvironment. *Oncotarget* vol. 10 785–797 Preprint at https://doi.org/10.18632/oncotarget.26585 (2019).

41. Toda, S., Blauch, L. R., Tang, S. K. Y., Morsut, L. & Lim, W. A. Programming self-organizing multicellular structures with synthetic cell-cell signaling. *Science (1979)* (2018).

42. Roybal, K. T. *et al.* Engineering T Cells with Customized Therapeutic Response Programs Using Synthetic Notch Receptors. *Cell* **167**, 419-432.e16 (2016).

43. Roybal, K. T. *et al.* Precision Tumor Recognition by T Cells with Combinatorial Antigen-Sensing Circuits. *Cell* **164**, 770–779 (2016).

44. Cho, J. H. *et al.* Engineering Axl specific CAR and SynNotch receptor for cancer therapy. *Sci Rep* **8**, 3846 (2018).

45. Manhas, J., Edelstein, H. I., Leonard, J. N. & Morsut, L. The evolution of synthetic receptor systems. *Nature Chemical Biology* vol. 18 244–255 Preprint at https://doi.org/10.1038/s41589-021-00926-z (2022).

46. Grupp, S. A. *et al.* Chimeric Antigen Receptor–Modified T Cells for Acute Lymphoid Leukemia. *New England Journal of Medicine* **368**, 1509–1518 (2013).

47. Kalos, M. *et al.* T Cells with Chimeric Antigen Receptors Have Potent Antitumor Effects and Can Establish Memory in Patients with Advanced Leukemia. *Sci Transl Med* **3**, 95ra73 (2011).

48. Kochenderfer, J. N. & Rosenberg, S. A. Treating B-cell cancer with T cells expressing anti-CD19 chimeric antigen receptors. *Nat Rev Clin Oncol* **10**, 267–276 (2013).

49. Prasad, V. Tisagenlecleucel — the first approved CAR-T-cell therapy: implications for payers and policy makers. *Nat Rev Clin Oncol* **15**, 11 (2017).

50. KYMRIAH (tisagenlecleucel) | FDA. https://www.fda.gov/vaccines-blood-biologics/cellular-gene-therapy-products/kymriah-tisagenlecleucel.

51. CARVYKTI | FDA. https://www.fda.gov/vaccines-blood-biologics/carvykti.

52. ABECMA (idecabtagene vicleucel) | FDA. https://www.fda.gov/vaccines-blood-biologics/abecma-idecabtagene-vicleucel.

53. BREYANZI (lisocabtagene maraleucel) | FDA. https://www.fda.gov/vaccines-blood-biologics/cellular-gene-therapy-products/breyanzi-lisocabtagene-maraleucel.

54. TECARTUS (brexucabtagene autoleucel) | FDA. https://www.fda.gov/vaccines-blood-biologics/cellular-gene-therapy-products/tecartus-brexucabtagene-autoleucel.

55. YESCARTA (axicabtagene ciloleucel) | FDA. https://www.fda.gov/vaccines-blood-biologics/cellular-gene-therapy-products/yescarta-axicabtagene-ciloleucel.

56. Scheller, L., Strittmatter, T., Fuchs, D., Bojar, D. & Fussenegger, M. Generalized extracellular molecule sensor platform for programming cellular behavior article. *Nat Chem Biol* **14**, 723–729 (2018).

57. Kipniss, N. H. *et al.* Engineering cell sensing and responses using a GPCR-coupled CRISPR-Cas system. *Nat Commun* **8**, 1–10 (2017).

58. Barnea, G. *et al.* The genetic design of signaling cascades to record receptor activation. *Proceedings of the National Academy of Sciences* **105**, 64–69 (2008).

59. Baeumler, T. A., Ahmed, A. A. & Fulga, T. A. Engineering Synthetic Signaling Pathways with Programmable dCas9-Based Chimeric Receptors. *Cell Rep* **20**, 2639–2653 (2017).

60. Morsut, L. *et al.* Engineering Customized Cell Sensing and Response Behaviors Using Synthetic Notch Receptors. *Cell* **164**, 780–791 (2016).

61. Fleming, R. J. Structural conservation of Notch receptors and ligands. *Semin Cell Dev Biol* **9**, 599–607 (1998).

62. Parks, A. L., Klueg, K. M., Stout, J. R. & Muskavitch, M. A. Ligand endocytosis drives receptor dissociation and activation in the Notch pathway. *Development* **127**, 1373 LP – 1385 (2000).

63. Bray, S. J. Notch signalling: A simple pathway becomes complex. *Nat Rev Mol Cell Biol* **7**, 678–689 (2006).

64. Struhl, G. & Adachi, A. Nuclear Access and Action of Notch In Vivo. *Cell* **93**, 649–660 (1998).

65. Lecourtois, M. & Schweisguth, F. Indirect evidence for Delta-dependent intracellular processing of Notch in Drosophila embryos. *Current Biology* **8**, 771–775 (1998).

66. Morsut, L. *et al.* Engineering Customized Cell Sensing and Response Behaviors Using Synthetic Notch Receptors. *Cell* **164**, 780–791 (2016).

67. Xia, M., Chen, J., Meng, G., Shen, H. & Dong, J. CXCL10 encoding synNotch T cells enhance anti-tumor immune responses without systemic side effect. *Biochem Biophys Res Commun* **534**, 765–772 (2021).

68. Wang, Z. *et al.* Using apelin-based synthetic Notch receptors to detect angiogenesis and treat solid tumors. *Nat Commun* **11**, 1–13 (2020).

69. Luo, H. *et al.* Target-Dependent Expression of IL12 by synNotch Receptor-Engineered NK92 Cells Increases the Antitumor Activities of CAR-T Cells. *Front Oncol* **9**, (2019).

70. Srivastava, S. *et al.* Logic-Gated ROR1 Chimeric Antigen Receptor Expression Rescues T Cell-Mediated Toxicity to Normal Tissues and Enables Selective Tumor Targeting. *Cancer Cell* **35**, 489-503.e8 (2019).

71. Choe, J. H. *et al.* SynNotch-CAR T cells overcome challenges of specificity, heterogeneity, and persistence in treating glioblastoma. *Sci Transl Med* **13**, (2021).

72. Hyrenius-Wittsten, A. *et al.* SynNotch CAR circuits enhance solid tumor recognition and promote persistent antitumor activity in mouse models. *Sci Transl Med* **13**, (2021).

73. Tague, E. P., Dotson, H. L., Tunney, S. N., Sloas, D. C. & Ngo, J. T. Chemogenetic control of gene expression and cell signaling with antiviral drugs. *Nat Methods* **15**, 519–522 (2018).

74. Vaghela, R., Arkudas, A., Horch, R. E. & Hessenauer, M. Actually Seeing What Is Going on – Intravital Microscopy in Tissue Engineering. *Frontiers in Bioengineering and Biotechnology* vol. 9 93 Preprint at https://doi.org/10.3389/fbioe.2021.627462 (2021).

75. Ding, Y. *et al.* Ratiometric biosensors based on dimerization-dependent fluorescent protein exchange. *Nat Methods* **12**, 195–198 (2015).

76. Malaguti, M. *et al.* SyNPL: Synthetic Notch pluripotent cell lines to monitor and manipulate cell interactions in vitro and in vivo . *Development* **149**, (2022).

77. Martella, A., Matjusaitis, M., Auxillos, J., Pollard, S. M. & Cai, Y. EMMA: An Extensible Mammalian Modular Assembly Toolkit for the Rapid Design and Production of Diverse Expression Vectors. *ACS Synth Biol* **6**, 1380–1392 (2017).

78. Ma, R. Y. *et al.* Monocyte-derived macrophages promote breast cancer bone metastasis outgrowth. *Journal of Experimental Medicine* **217**, (2020).

79. Thomas, P. & Smart, T. G. HEK293 cell line: A vehicle for the expression of recombinant proteins. *J Pharmacol Toxicol Methods* **51**, 187–200 (2005).

80. Huang, H. *et al.* Cell-cell contact-induced gene editing/activation in mammalian cells using a synNotch-CRISPR/Cas9 system. *Protein and*

Cell vol. 11 299–303 Preprint at https://doi.org/10.1007/s13238-020-00690-1 (2020).

81. Huang, T.-H., Velho, T. & Lois, C. Monitoring cell-cell contacts in vivo in transgenic animals. *Development* **143**, 4073–4084 (2016).

82. He, L., Huang, J. & Perrimon, N. Development of an optimized synthetic Notch receptor as an in vivo cell–cell contact sensor. *Proc Natl Acad Sci U S A* **114**, 5467–5472 (2017).

83. Yang, Z. jie, Yu, Z. yan, Cai, Y. ming, Du, R. rong & Cai, L. Engineering of an enhanced synthetic Notch receptor by reducing ligand-independent activation. *Commun Biol* **3**, 1–7 (2020).

84. Kojima, R., Scheller, L. & Fussenegger, M. Nonimmune cells equipped with T-cell-receptor-like signaling for cancer cell ablation. *Nat Chem Biol* **14**, 42–49 (2018).

85. Toda, S. *et al.* Engineering synthetic morphogen systems that can program multicellular patterning. *Science (1979)* **370**, 327–331 (2020).

86. Efimov, G. A. *et al.* Cell-type-restricted anti-cytokine therapy: TNF inhibition from one pathogenic source. *Proc Natl Acad Sci U S A* **113**, 3006–3011 (2016).

87. WO2014140376A1 - Anti-macrophage mannose receptor single variable domains for use in cardiovascular diseases - Google Patents. https://patents.google.com/patent/WO2014140376A1/en.

88. de Brito Monteiro, L. *et al.* M-CSF- and L929-derived macrophages present distinct metabolic profiles with similar inflammatory outcomes. *Immunobiology* **225**, (2020).

89. Cohen, C. J., Lock, W. M. & Mager, D. L. Endogenous retroviral LTRs as promoters for human genes: A critical assessment. *Gene* vol. 448 105–114 Preprint at https://doi.org/10.1016/j.gene.2009.06.020 (2009).

90. O'Brien, L. E., Zegers, M. M. P. & Mostov, K. E. Building epithelial architecture: Insights from three-dimensional culture models. *Nature Reviews Molecular Cell Biology* vol. 3 531–537 Preprint at https://doi.org/10.1038/nrm859 (2002).

91. Abraham, R. T. & Weiss, A. Jurkat T cells and development of the T-cell receptor signalling paradigm. *Nature Reviews Immunology* vol. 4 301–308 Preprint at https://doi.org/10.1038/nri1330 (2004).

92. Theerakittayakorn, K. & Bunprasert, T. Differentiation Capacity of Mouse L929 Fibroblastic Cell Line Compare With Human Dermal Fibroblast. *International Journal of Medical and Health Sciences* **5**, 51–54 (2011).

93. Ooi, A., Wong, A., Esau, L., Lemtiri-Chlieh, F. & Gehring, C. A Guide to Transient Expression of Membrane Proteins in HEK-293 Cells for Functional Characterization. *Front Physiol* **7**, 300 (2016).

94. Chaudhary, S. *et al.* Efficient expression screening of human membrane proteins in transiently transfected Human Embryonic Kidney 293S cells. *Methods* **55**, 273–280 (2011).

95. Tang, R. *et al.* A versatile system to record cell-cell interactions. *Elife* **9**, 1 (2020).

96. Heap, R. E. *et al.* Proteomics characterisation of the L929 cell supernatant and its role in BMDM differentiation. *Life Sci Alliance* **4**, (2021).

97. Cui, S., Reichner, J. S., Mateo, R. B. & Albina, J. E. Activated murine macrophages induce apoptosis in tumor cells through nitric oxide-dependent or -independent mechanisms. *Cancer Res* **54**, 2462–7 (1994).

98. Nascimento, F. R. F., Gomes, E. A., Russo, M. & Lepique, A. P. Interferon Regulatory Factor (IRF)-1 Is a Master Regulator of the Cross Talk between Macrophages and L929 Fibrosarcoma Cells for Nitric Oxide Dependent Tumoricidal Activity. *PLoS One* **10**, e0117782 (2015).

99. Filley, A. C., Henriquez, M. & Dey, M. CART immunotherapy: Development, success, and translation to malignant gliomas and other solid tumors. *Frontiers in Oncology* vol. 8 Preprint at https://doi.org/10.3389/fonc.2018.00453 (2018).

100. E., O., Subkhankulova, T. & Tolmachov, T. Silencing of Transgene Expression: A Gene Therapy Perspective. in *Gene Therapy - Tools and Potential Applications* (InTech, 2013). doi:10.5772/53379.

101. DiAndreth, B., Wauford, N., Hu, E., Palacios, S. & Weiss, R. PERSIST platform provides programmable RNA regulation using CRISPR endoRNases. *Nat Commun* **13**, 1–11 (2022).

102. Sadelain, M., Papapetrou, E. P. & Bushman, F. D. Safe harbours for the integration of new DNA in the human genome. *Nature Reviews Cancer* vol. 12 51–58 Preprint at https://doi.org/10.1038/nrc3179 (2012).

103. Hsu, C. C. *et al.* Targeted methylation of CMV and E1A viral promoters. *Biochem Biophys Res Commun* **402**, 228–234 (2010).

104. Yang, Y., Mariati, Chusainow, J. & Yap, M. G. S. DNA methylation contributes to loss in productivity of monoclonal antibody-producing CHO cell lines. *J Biotechnol* **147**, 180–185 (2010).

105. Jeziorska, D. M. *et al.* DNA methylation of intragenic CpG islands depends on their transcriptional activity during differentiation and disease. *Proc Natl Acad Sci U S A* **114**, E7526–E7535 (2017).

106. Smith, J. R. *et al.* Robust, Persistent Transgene Expression in Human Embryonic Stem Cells Is Achieved with AAVS1-Targeted Integration. *Stem Cells* **26**, 496–504 (2008).

107. Aznauryan, E. *et al.* Discovery and validation of human genomic safe harbor sites for gene and cell therapies. *Cell Reports Methods* **2**, 100154 (2022).

108. Friedrich, G. & Soriano, P. Promoter traps in embryonic stem cells: A genetic screen to identify and mutate developmental genes in mice. *Genes Dev* **5**, 1513–1523 (1991).

109. Browning, J. *et al.* Highly efficient CRISPR-targeting of the murine Hipp11 intergenic region supports inducible human transgene expression. *Mol Biol Rep* **47**, 1491–1498 (2020).

110. Papapetrou, E. P. & Schambach, A. Gene insertion into genomic safe harbors for human gene therapy. *Molecular Therapy* vol. 24 678–684 Preprint at https://doi.org/10.1038/mt.2016.38 (2016).

111. Gaj, T., Gersbach, C. A. & Barbas, C. F. ZFN, TALEN, and CRISPR/Cas-based methods for genome engineering. *Trends in Biotechnology* vol. 31 397–405 Preprint at https://doi.org/10.1016/j.tibtech.2013.04.004 (2013).

112. Turan, S., Zehe, C., Kuehle, J., Qiao, J. & Bode, J. Recombinase-mediated cassette exchange (RMCE) - A rapidly-expanding toolbox for targeted genomic modifications. *Gene* vol. 515 1–27 Preprint at https://doi.org/10.1016/j.gene.2012.11.016 (2013).

113. Plasterk, R. H. A., Izsvák, Z. & Ivics, Z. Resident aliens the Tc1/mariner superfamily of transposable elements. *Trends in Genetics* vol. 15 326–332 Preprint at https://doi.org/10.1016/S0168-9525(99)01777-1 (1999).

114. Ivics, Z. & Izsvák, Z. Sleeping Beauty Transposition . *Microbiol Spectr* **3**, (2015).

115. Ding, S. *et al.* Efficient transposition of the piggyBac (PB) transposon in mammalian cells and mice. *Cell* **122**, 473–483 (2005).

116. Ciuffi, A. Mechanisms Governing Lentivirus Integration Site Selection. *Curr Gene Ther* **8**, 419–429 (2008).

117. Irion, S. *et al.* Identification and targeting of the ROSA26 locus in human embryonic stem cells. *Nat Biotechnol* **25**, 1477–1482 (2007).

118. Feschotte, C. & Pritham, E. J. DNA transposons and the evolution of eukaryotic genomes. *Annual Review of Genetics* vol. 41 331–368

Preprint at https://doi.org/10.1146/annurev.genet.40.110405.090448 (2007).

119. Kazazian, H. H. Mobile Elements: Drivers of Genome Evolution. *Science* vol. 303 1626–1632 Preprint at https://doi.org/10.1126/science.1089670 (2004).

120. Kazazian, H. H. Mobile Elements: Drivers of Genome Evolution. *Science* vol. 303 1626–1632 Preprint at https://doi.org/10.1126/science.1089670 (2004).

121. Li, M. A. *et al.* Mobilization of giant piggyBac transposons in the mouse genome. *Nucleic Acids Res* **39**, (2011).

122. Li, X. *et al.* PiggyBac transposase tools for genome engineering. *Proc Natl Acad Sci U S A* **110**, E2279–E2287 (2013).

123. Yusa, K., Zhou, L., Li, M. A., Bradley, A. & Craig, N. L. A hyperactive piggyBac transposase for mammalian applications. *Proc Natl Acad Sci U S A* **108**, 1531–1536 (2011).

124. Chu, V. T. *et al.* Efficient generation of Rosa26 knock-in mice using CRISPR/Cas9 in C57BL/6 zygotes. *BMC Biotechnol* **16**, 4 (2016).

125. Głowacka, K. *et al.* An evaluation of new and established methods to determine T-DNA copy number and homozygosity in transgenic plants. *Plant Cell Environ* **39**, 908–917 (2016).

126. Palavesam, A., Esnault, C. & O'Brochta, D. A. Post-Integration Silencing of piggyBac Transposable Elements in Aedes aegypti. *PLoS One* **8**, (2013).

127. Mossine, V. v., Waters, J. K., Hannink, M. & Mawhinney, T. P. piggyBac Transposon plus Insulators Overcome Epigenetic Silencing to Provide for Stable Signaling Pathway Reporter Cell Lines. *PLoS One* **8**, e85494 (2013).

128. Frei, T. *et al.* Characterization and mitigation of gene expression burden in mammalian cells. *Nat Commun* **11**, 1–14 (2020).

129. Mian, S. A., Anjos-Afonso, F. & Bonnet, D. Advances in Human Immune System Mouse Models for Studying Human Hematopoiesis and Cancer Immunotherapy. *Frontiers in Immunology* vol. 11 3753 Preprint at https://doi.org/10.3389/fimmu.2020.619236 (2021).

130. Sekar, R. B. & Periasamy, A. Fluorescence resonance energy transfer (FRET) microscopy imaging of live cell protein localizations. *Journal of Cell Biology* vol. 160 629–633 Preprint at https://doi.org/10.1083/jcb.200210140 (2003).

131. Baker, S. M., Buckheit, R. W. & Falk, M. M. Green-to-red photoconvertible fluorescent proteins: Tracking cell and protein

dynamics on standard wide-field mercury arc-based microscopes. *BMC Cell Biol* **11**, 15 (2010).

132. Wiedenmann, J. *et al.* EosFP, a fluorescent marker protein with UV-inducible green-to-red fluorescence conversion. *Proc Natl Acad Sci U S A* **101**, 15905–15910 (2004).

133. Gurskaya, N. G. *et al.* Engineering of a monomeric green-to-red photoactivatable fluorescent protein induced by blue light. *Nat Biotechnol* **24**, 461–465 (2006).

134. Subach, F. v. *et al.* Red fluorescent protein with reversibly photoswitchable absorbance for photochromic FRET. *Chem Biol* **17**, 745–755 (2010).

135. Wu, B., Piatkevich, K. D., Lionnet, T., Singer, R. H. & Verkhusha, V. v. Modern fluorescent proteins and imaging technologies to study gene expression, nuclear localization, and dynamics. *Current Opinion in Cell Biology* vol. 23 310–317 Preprint at https://doi.org/10.1016/j.ceb.2010.12.004 (2011).

136. Romei, M. G. & Boxer, S. G. Split Green Fluorescent Proteins: Scope, Limitations, and Outlook. *Annual Review of Biophysics* vol. 48 19–44 Preprint at https://doi.org/10.1146/annurev-biophys-051013-022846 (2019).

137. Pedelacq, J. D. & Cabantous, S. Development and applications of superfolder and split fluorescent protein detection systems in biology. *Int J Mol Sci* **20**, (2019).

138. Alford, S. C., Abdelfattah, A. S., Ding, Y. & Campbell, R. E. A fluorogenic red fluorescent protein heterodimer. *Chem Biol* **19**, 353–360 (2012).

139. Alford, S. C., Ding, Y., Simmen, T. & Campbell, R. E. Dimerization-Dependent Green and Yellow Fluorescent Proteins. *ACS Synth Biol* **1**, 569–575 (2012).

140. Ohue, Y. & Nishikawa, H. Regulatory T (Treg) cells in cancer: Can Treg cells be a new therapeutic target? *Cancer Science* vol. 110 2080–2089 Preprint at https://doi.org/10.1111/cas.14069 (2019).

141. Mortezaee, K. & Majidpoor, J. Roles for macrophage-polarizing interleukins in cancer immunity and immunotherapy. *Cellular Oncology* vol. 45 333–353 Preprint at https://doi.org/10.1007/s13402-022-00667-8 (2022).

142. Rogers, S., Wells, R. & Rechsteiner, M. Amino acid sequences common to rapidly degraded proteins: The PEST hypothesis. *Science (1979)* **234**, 364–368 (1986).